2009

Pulsed sprays for better contact between liquid and fluidized solids

Rana Sabouni

PULSED SPRAYS FOR BETTER CONTACT BETWEEN LIQUID AND FLUIDIZED SOLIDS

(Spine title: Effects of Spray Nozzle Pulsations on Jet Bed Interaction)

(Thesis format: Integrated Article)

by

Rana Sabouni

Graduate Program
in
Engineering Science
Department of Chemical and Biochemical Engineering

A thesis submitted in partial fulfillment
of the requirements for the degree of
Master of Engineering Science

The School of Graduate and Postdoctoral Studies
The University of Western Ontario
London, Ontario, Canada

THE UNIVERSITY OF WESTERN ONTARIO
SCHOOL OF GRADUATE AND POSTDOCTORAL STUDIES

CERTIFICATE OF EXAMINATION

Joint-Supervisor

Dr. Cedric Briens

Joint-Supervisor

Dr. Franco Berruti

Examiners

Dr. Lars Rehmann

Dr. Katherine Albion

Dr. Kamran Siddiqui

The thesis by

Rana Sabouni

entitled:
PULSED SPRAYS FOR BETTER CONTACT BETWEEN LIQUID AND FLUIDIZED SOLIDS

is accepted in partial fulfillment of the
requirements for the degree of

Master of Engineering Science

Date_____

Chair of the Thesis Examination Board

ABSTRACT

Many industrial applications, such as fluid catalytic cracking, fluid coking, and gas phase polymerization, use liquid injection into fluidized beds of solid particles.. Therefore, it is of crucial importance to study the mechanism of liquid injection into fluidized beds in order to ensure the best possible distribution of the feed, maximizing the yield of valuable products while minimizing the formation of undesired agglomerates, and, thus, preventing mass and heat transfer limitations.

The objective of this Thesis are: to investigate the potentially beneficial effects of fluctuations on the liquid feed distribution on the particles in the fluidized bed at various operating conditions by imposing fluctuations of well-defined frequency and amplitude on the liquid flow upstream of a spray nozzle; to study the effect of creating natural pulsations on the liquid feed distribution with non-mechanical methods over different operating conditions; and, finally, to compare different spray nozzles geometries under pulsating flow conditions. To achieve these objectives several experiments were conducted in a laboratory-scale fluidized bed filled with silica sand and fluidized with air. Thesis results illustrated that nozzle pulsations significantly improved the spray nozzle performance and the liquid distribution under the different studied operating conditions.

Key words: pulsations, fluidized bed, spray nozzle, nozzle performance index, gas flow rate, liquid flow rate, nozzle geometry and jet penetration.

DEDICATION

To:

My dear husband

Dr. Anas Abou Shaar

My parents

Dr. Abdul Rahim Sabouni and Ms. Maissaa Baroudi

My beloved son

Sami Abou Shaar

CO-AUTHORSHIP

The journal articles written from the present work are listed below, and the individual contributions of all the members are indicated.

Chapter 2

Article Title: Enhancement of the liquid feed distribution in gas solid fluidized beds by nozzle pulsations (induced by a solenoid valve)
Authors: Rana Sabouni, Aidan Leach, Cedric Briens, Franco Berruti
Article Status: To be submitted for possible publication in AIChE J
This work was supervised be C. Briens and F. Berruti. Various drafts of the paper were reviewed by C. Briens and F. Berruti. All the experiments and data analysis were conducted by R. Sabouni. R. Sabouni wrote the manuscript. A. Leach wrote the Labview program, and developed the electrical circuit for the pulsations process.

Chapter 3

Article Title: Enhancement of the liquid feed distribution in gas solid fluidized beds by non mechanically induced nozzle pulsations
Authors: Rana Sabouni, Cedric Briens, Franco Berruti
Article Status: To be submitted for possible publication in Powder Technology
R. Sabouni conducted all the experiments, analyzed the data and wrote the manuscript for this paper. This work was supervised be C. Briens and F. Berruti. Various drafts of the paper were reviewed by C. Briens and F. Berruti.

Chapter 4

Article Title: Comparison of the flow pulsations on the performance of various liquid gas injections nozzles in gas-solid fluidized bed.
Authors: Rana Sabouni, Cedric Briens, Franco Berruti
Article Status: To be submitted for possible publication in Canadian Journal of Chemical Engineering
R. Sabouni conducted all the experiments, analyzed the data and wrote the manuscript for this paper. This work was supervised be C. Briens and F. Berruti. Various drafts of the paper were reviewed by C. Briens and F. Berruti.

Appendix A

Article Title: Use of pulsations to enhance the distribution of liquid injected into fluidized particles with commercial-scale nozzles
Authors: Aidan Leach, Rana Sabouni, Cedric Briens, Franco Berruti
Article Status: To be submitted for possible publication in Chemical Engineering and Processing –Process Intensification
This work was supervised be C. Briens and F. Berruti. Various drafts of the paper were reviewed by C. Briens and F. Berruti. All the experiments and data analysis were conducted by A. Leach. A. Leach wrote the manuscript. The small scale experiments were conducted by R. Sabouni.

ACKNOWLEDGMENTS

Many people supported me during the completion of this thesis with criticism, helpful assistance and references. This thesis would have never been possible without them.

I am greatly thankful to both my supervisors Dr. Cedric Briens and Dr. Franco Berruti, for their guidance, insights, thoughtful suggestions and continuous support during the course of this research.

I would like to express my sincere thanks for their financial support to Syncrude Canada Ltd., and the Natural Science and Engineering Research Council (NSERC) of Canada. Also I would like to acknowledge the assistance of the Engineering Stores and the University Machine Services (UMS) at the University of Western Ontario. In addition, I would like to express my appreciation to my friends, colleagues, secretaries and personnel in the Department of Chemical and Biochemical Engineering and the University of Western Ontario without whom this work would not have been possible.

Furthermore, I would like to express my gratitude to my mother Mrs. Maissaa Baroudi and my father Dr. Abdul-Rahim Sabouni for their love, support, encouragement and all their sacrifices. Also, I would like to thank my father in law and mother in law. Finally I would like to express my deepest thanks to my husband Dr. Anas for his love and persistent support, and to my beloved son Sami.

TABLE OF CONTENTS

CERTIFICATE OF EXAMINATION ii
ABSTRACT iii
DEDICATION iv
CO-AUTHORSHIP v
ACKNOWLEDGMENTS vii
TABLE OF CONTENTS viii
LIST OF FIGURES xi
LIST OF SYMBOLS xvi

1 Introduction 1
1.1 Introduction: 1
1.2 Industrial application of gas-liquid injections into gas-solid fluidized beds: 1
1.3 Recent experimental studies about liquid jets in fluidized beds: a review 7
1.4 Research Objectives: 14
1.5 References 16

2 Enhancement of the Liquid Feed Distribution in Gas-Solid Fluidized Beds by Nozzle Pulsations (induced by solenoid valve) 19
2.1 Introduction: 19
2.2 Apparatus: 22
2.3 Experimental Procedure: 27
2.4 Result and Discussion: 30
2.4.1 Effect of Frequency 30
2.4.2 Optimizing the Pulsation Amplitude 35
2.4.3 Other Conditions 36
2.4.3.1 Effect of liquid flow rate 36
2.4.3.2 Effect of nozzle geometry 37
2.4.3.3 Effect of atomization gas properties 38
2.5 Conclusions: 39
2.6 References: 39

3 Enhancement of the Liquid Feed Distribution in Gas Solid Fluidized Beds by Non-Mechanically Induced Nozzle Pulsations. 42
3.1 Introduction: 42
3.2 Apparatus: 45
3.3 Experimental Procedure: 50
3.4 Result and discussion 53
3.4.1 Effect of liquid flowrate 53
3.4.2 Effect of gas restriction 56
3.4.3 Effect of liquid restriction 58
3.4.4 Relation between gas, liquid flowrates and predicted jet penetration 60
3.5 Conclusions: 61
3.6 References: 62

4 Comparison of the Impact of Flow Pulsations on the Performance of the Various Liquid Gas Injections Nozzles in Gas-Solid Fluidized Bed 64
4.1 Introduction: 64
4.2 Apparatus: 67
4.3 Experimental Procedures: 73
4.4 Results and discussion: 76
4.4.1 Liquid flowrate 76
4.4.2 Gas orifice restriction 80
4.4.3 Air to liquid ratio (ALR) 85
4.5 Conclusions: 89
4.6 References: 90

5 Conclusions and Recommendations 92
5.1 Conclusions: 92
5.2 Recommendations: 94
5.3 References: 97

APPENDIX A 98

A. Use of pulsations to enhance the distribution of liquid injected into fluidized particles with commercial scale nozzles. 98

A.1 Introduction 98

A.2 Experimental Apparatus 101

A.1.1 Probes and Data Acquisition 103

A.1.2 Active Conductance Technique 104

A.1.3 Solenoid Valve 106

A.1.4 Sampling Port 107

A.3 Experimental Procedure 108

A.3.1 Agglomerate Sampling 109

A.3.2 Micro-agglomerate and Macro-agglomerate Calculations 110

A.4 Results 113

A.4.1 Effect of Pulsation Amplitude 118

A.4.2 Effect of Pulsation Frequency 124

A.4.3 Effect of Different Pre-mixers 127

A.5 Conclusions 129

A.6 References 130

VITA 132

LIST OF FIGURES

Figure 1.1: schematic diagram for fluid coking process. (House et al., 2004) 4

Figure 2.1: Schematic Diagram of Experimental Apparatus 24

Figure 2.2: Internal Geometry of Type I Nozzle and Type II Nozzle 24

Figure 2.3: Circuit Diagram of used in the experiments. 26

Figure 2.4: Schematic Diagram of Conductive Probe. 27

Figure 2.5: Conductance method, 1 Hz, Fully open needle valve, Type I Nozzle D=1.66 mm, F_L=0.022 kg/s, 1 mm restriction orifice, P_L=25 psi, P_g=30 psi, 1.7 ALR%, V_{air}=14 $cm^3$29

Figure 2.6: Liquid flowrate and gas flowrate as function of time, 0 Hz, Fully open needle valve, , Type I Nozzle D=1.66 mm, F_L=0.022 (kg/s), 1 mm restriction orifice, P_L=30 Psi, P_g=30 Psi, 1.7 ALR%, Air, V_{air}=14 cm^3 30

Figure 2.7: Liquid flowrate and gas flowrate as function of time, 1 Hz, Fully open needle valve, , Type I Nozzle D=1.66 mm, F_L=0.022 (kg/s), 1 mm restriction orifice, P_L=25 Psi, P_g=30 Psi, 1.7 ALR%, Air, V_{air}=14 cm^3 31

Figure 2.8: Effect of frequency on NPI, Fully Open needle valve, Type I Nozzle D=1.66 mm, 1.7% ALR, F_L=0.022 kg/s, Air, V_{air}=14 cm^3, 1 mm orifice restriction, 95% Confidence intervals 32

Figure 2.9: Effect of Frequency on NPI, Fully Open needle valve, Type I Nozzle D=1.66 mm, F_L=0.022 kg/s, Air, V_{air}=14 cm^3, 1 mm orifice restriction, standard deviation error bar33

Figure 2.10: predicted jet penetration for both no imposed pulsation and imposed pulsation effect., F_L= 0.022 kg/s, 1.7% ALR , Fully open needle valve, Type I Nozzle D=1.66 mm, 1 mm restriction, Air, V_{air}=14 cm^3 34

Figure 2.11: Effect of changing ALR % on NPI, Fully Open Needle Valve, F_L=0.022 (kg/s), Type I Nozzle D=1.66 mm, Air, V_{air}=14 cm^3, 1 mm Restriction Orifice 35

Figure 2.12: Effect of changing air line volume on NPI,1 Hz, Fully open needle valve, Type I Nozzle D=1.66 mm, F_L=0.022 (kg/s), 1 mm restriction orifice, 1.7%ALR, Air, V_{air}=14 cm^3 36

Figure 2.13: Effect of Liquid Flowrate on NPI, Fully open needle valve, Type I Nozzle D=1.66 mm, 1.7% ALR, Air, V_{air}=14 cm^3, standard deviation error bar 37

Figure 2.14: Effect of Nozzle Geometry on NPI, fully open needle valve, F_L=0.022 kg/s, 1.7%, V_{air}=14 cm^3 38

Figure 2.15: Effect of Gas Properties on NPI, fully open needle valve, TEB nozzle D=1.6 mm, V_{air}=14 cm^3 39

Figure 3.1: Schematic Diagram of Experimental Apparatus. 45
Figure 3.2: Internal Geometry of Type I Nozzle. 46
Figure 3.3: Circuit Diagram of used in the experiments. 49
Figure 3.4: Schematic Diagram of Conductive Probe. 50
Figure 3.5:Conductance method, non-mechanically pulsating flow, Fully open needle valve, Type I Nozzle D=1.66 mm, F_L=0.027 kg/s, 1 mm gas restriction orifice, 1.2 ALR% 53
Figure 3.6: Visually stable, 1.2% ALR, F_L=0.027 cm3, Type I spray nozzle D=1.66 mm, 1 mm gas orifice restriction, fully open needle valve. 54
Figure 3.7: Non-mechanically pulsating flow, 1.2% ALR, F_L=0.027 cm3, Type I spray nozzle D=1.66 mm, 1 mm gas orifice restriction, fully open needle valve 54
Figure 3.8: NPI vs. Liquid flow rate, 1.2% ALR, 1 mm gas orifice restriction, Fully Open needle valve, Type I Nozzle D=1.66 mm, standard deviation error bar 55
Figure 3.9: Jet penetration for visually stable and non-mechanically induced pulsating flows, fully open needle valve, F_L=0.027 kg/s, 1 mm gas orifice restriction 56
Figure 3.10: NPI vs. gas restriction, 1.2% ALR, F_L= 0.027 kg/s, fully open needle valve, Type I spray nozzle D=1.66 mm 57
Figure 3.11: Jet penetration vs visually stable flow and non-mechanically pulsating flow, 0.7 mm gas orifice restriction, 1.2% ALR, F_L= 0.027 kg/s, fully open needle valve, type I spray nozzle D=1.66 mm 57
Figure 3.12: NPI vs. liquid restriction, 1.2% ALR, 1 mm gas orifice restriction, type I spray nozzle D=1.66 mm 59
Figure 3.13: jet penetration for visually stable and non-mechanically pulsating flow, one rotation close needle valve, type I spray nozzle D=1.66 mm, 1.2% ALR 59
Figure 3.14: Relationship between instantaneous liquid flow rate and jet penetration for non-mechanically pulsating flow, fully open needle valve, Type I spray nozzle D=1.66 mm, 1.2% ALR, F_L=0.027 kg/s 60
Figure 3.15: Relationship between instantaneous gas flow rate and jet penetration for non-mechanically pulsating flow, fully open needle valve, Type I spray nozzle D=1.66 mm, 1.2% ALR, F_L=0.027 kg/s 61

Figure 3.16: Relationship between instantaneous liquid flow rate and jet penetration for imposed pulsation using solenoid valve, fully open needle valve, Type I spray nozzle D=1.66 mm, 1.7% ALR, F_L=0.027 kg/s 61

Figure 4.1: Schematic Diagram of Experimental Apparatus..... 68
Figure 4.2: Schematic Diagram of Conductive Probe..... 69
Figure 4.3: Circuit Diagram used in the experiments. 70
Figure 4.4: Internal Geometry of Type I Nozzle and Type II Nozzle..... 72
Figure 4.5: Internal geometry of commercial nozzles (BETE Fog Nozzle Co.): hollow cone (XA AD 200, top) and vertical fanjet (XA PF 200, bottom). 73
Figure 4.6: Conductance method, 1 Hz, Fully open needle valve, Type I Nozzle D=1.66 mm, F_L=0.022 kg/s, 1 mm restriction orifice, 1.7 ALR%..... 76
Figure 4.7: Effect of Liquid flowrate, F_L= 0.019 kg/s, fully open needle valve, 1.7% ALR, 1 mm gas orifice restriction. Standard deviation error bars..... 77
Figure 4.8: Effect of Liquid flowrate, F_L= 0.022 kg/s, fully open needle valve, 1.7% ALR, 1 mm gas orifice restriction. Standard deviation error bars..... 78
Figure 4.9: Effect of Liquid flowrate, F_L= 0.026 kg/s, fully open needle valve, 1.7% ALR, 1 mm gas orifice restriction, standard deviation error bars. 78
Figure 4.10: NPI with pulsations/ NPI without pulsations vs. liquid flow rate, 1.7%ALR, 1 mm gas orifice restriction, and standard deviation error bars. 79
Figure 4.11: instantaneous gas and liquid flowrate for both Type II and Vertical fanjet air atomized nozzles, 1.7%, F_L=0.022kg/s, 1mm gas restriction 80
Figure 4.12: Effect of gas orifice restriction, 0.7 mm gas orifice restriction, fully open needle valve, F_L= 0.022 kg/s, 1.7% ALR..... 81
Figure 4.13: Effect of gas orifice restriction, 1 mm gas orifice restriction, fully open needle valve, F_L= 0.022 kg/s, 1.7% ALR..... 82
Figure 4.14: Effect of gas orifice restriction, 1.2 mm gas orifice restriction, fully open needle valve, F_L= 0.022 kg/s, 1.7% ALR..... 82
Figure 4.15: $NPI_{\text{with pulsations}}$ / $NPI_{\text{without pulsations}}$ vs. gas orifice restriction. 1.7% ALR, F_L= 0.022 kg/s. 83
Figure 4.16: Instantaneous gas and liquid flowrate for both Type II and Vertical fanjet air atomized nozzles,1.7%, F_L=0.022kg/s, 1.2 mm gas restriction 84

Figure 4.17: Effect of Air to Liquid ratio, F_L= 0.022 kg/s, fully open needle valve, 1.5% ALR, 1 mm gas orifice restriction 85
Figure 4.18: Effect of Air to Liquid ratio, F_L= 0.022 kg/s, fully open needle valve, 1.7% ALR, 1 mm gas orifice restriction 86
Figure 4.19: Effect of Air to Liquid ratio, F_L= 0.022 kg/s, fully open needle valve, 2.5% ALR, 1 mm gas orifice restriction 86
Figure 4.20: $NPI_{\text{with pulsations}}$ / $NPI_{\text{without pulsations}}$ vs. ALR%, F_L= 0.022 kg/s, 1 mm gas orifice restriction 88
Figure 4.21: Instantaneous gas and liquid flowrate for both Type II and Vertical fanjet air atomized nozzles, 2.5%, FL=0.022kg/s, 1mm gas restriction 89

Figure A.1: Schematic diagram of experimental apparatus 102
Figure A.2: Dimensions of experimental apparatus (top view) with placement of conductance probe in grey 102
Figure A.3: Placement and corresponding circuit for the conductance probe. 104
Figure A.4: Diagram of the nozzle used in this study 105
Figure A.5: Circuit diagram of solenoid valve-based pulsation technique 107
Figure A.6: Liquid and Gas Flowrates during Injection with 2 Hz Pulsations with the BFC Pre-mixer and a volume of 12.5 mL between Solenoid Valve and Restriction Orifice 113
Figure A.7: Liquid and Gas Flowrates during Injection with 2 Hz Pulsations in Type I Nozzle with BFC Pre-mixer and a volume of 500 mL between Solenoid Valve and Restriction Orifice 115
Figure A.8: Gas-to-Liquid Ratios (GLR) at various spacing volumes between the solenoid valve and the sonic nozzle. 2 Hz Pulsations in Type I Nozzle with BFC Pre-mixer, average (GLR) of 0.8 wt% 116
Figure A.9: The effect of changing the volume between the solenoid valve and restriction orifice on the amplitude of the nozzle pulsations. 2 Hz Pulsations in Type I Nozzle with BFC Pre-mixer, average (GLR) of 0.8 wt% 117
Figure A.10: Conductance Probe signal, including defluidization and refluidization (drying) zones. 118

Figure A.11: Effect of changing the amplitude of the nozzle pulsation on the nozzle performance. 2 Hz Pulsations in Type I Nozzle with BFC Pre-mixer, average (GLR) of 0.8 wt%. 119
Figure A.12: Correlation between free moisture content in fluidized bed and NPI. R2 = 0.8032. 121
Figure A.13: Micro Agglomerate (Equation 3) Content of Bed after 10 minutes of refluidization. 2 Hz Pulsations in Type I Nozzle with BFC Pre-mixer, average (GLR) of 0.8 wt%. 122
Figure A.14: Macro Agglomerate (Equation 4) Content of Bed after 10 minutes of refluidization. 2 Hz Pulsations in Type I Nozzle with BFC Pre-mixer, average (GLR) of 0.8 wt%. 123
Figure A.15: Comparison Amplitude Tests in Small and Large Scale units. Type I nozzle and BFC pre-mixer used in both cases, with an average (GLR) ratio of 0.8%. Scaling Factor of 8 between large and small scale nozzles 124
Figure A.16: The Effect of Pulsation Frequency on Nozzle Performance. Average (GLR) Ratio of 0.8 wt%, Pulsation Amplitude of 0.6 wt% (GLR). 125
Figure A.17: Agglomeration occurring after 10 minutes refluidization, with various pulsation frequencies. Average (GLR) ratio of 0.8 wt%, pulsation amplitude of 0.6 wt% (GLR).126
Figure A.18: A comparison of the effect of pulsation frequency on small and large-scale fluidized beds. Type I nozzle and BFC pre-mixer, average (GLR) of 0.8 wt% used.. 127
Figure A.19: Comparison of BFC and Venturi Pre-mixers. Type I Nozzle, 12.5 mL dead volume, 0.8% Average (GLR), 2 Hz Pulsation Frequency 128

LIST OF SYMBOLS

ALR	Air-to-Liquid Ratio (mass)
d_{sm}	Sauter mean diameter of droplets (μm)
GLR	gas-to-liquid mass ratio (wt %)
G_{bed}	electrical conductance of fluidized bed (mS)
i	electrical current travelling through probe/bed (A)
L/S	liquid-to-solid ratio in bed (wt %)
$(L/S)_{free\ moisture}$	amount of free moisture present in fluidized bed (wt%)
$(L/S)_{macro}$	amount of macro agglomerates present in fluidized bed (wt%)
$(L/S)_{micro}$	amount of micro agglomerates present in fluidized bed (wt%)
L_v	predicted jet penetration for visually stable flow (m)
L_p	predicted jet penetration for pulsating flow (m)
m_L	mass of liquid in the bed (kg)
NPI	Nozzle Performance Index (-)
P_g	Pressure of upstream restriction orifice (Psi)
P_L	Pressure of the upstream needle valve (Psi)
R_{bed}	electrical resistance of fluidized bed (Ω)
R_m	resistance of resistor (kΩ)
t	elapsed time of test
t_{av}	mean time between avalanches (s)
V_1	voltage measured across function generator (V)

V_2	voltage measured across resistor (V)
V_g	voltage of the air pressure transducer (V)
V_{BFC}	voltage of the BFC pressure transducer (V)
V_L	voltage of the liquid pressure transducer (V)
Γ_{bed}	electrical conductance of fluidized bed (mS)
ρ_B	bed density (kg/m^3)

Chapter 1

INTRODUCTION

1.1 Introduction:

The research work presented in this thesis has been carried out to investigate the interaction between a gas-liquid feed jet and a gas-solid fluidized bed of solid particles, or jet-bed interaction (JBI). The thesis uses the "integrated article" format.

In this chapter, section 1.2 illustrates various industrial applications where liquids are injected into gas-solid fluidized beds. Section 1.3 reviews the recent experimental studies about gas-liquid jets in fluidized beds. Finally section 1.4 presents the objectives of this thesis.

1.2 Industrial application of gas-liquid injections into gas-solid fluidized beds:

Many industrial applications involve the use of liquid injection into a bed of fluidized particles such as: (a) physical operations, like agglomerates, drying, and coating of particles; (b) chemical processes, like those employed in the food industries, slurries, wetting, pharmaceutical, agriculture; and (c) several petrochemical processes, like fluid catalytic cracking, gas-phase polymerization and fluid coking.

Most of the above mentioned processes use the method of liquid injection through spray nozzles into gas-solid fluidized bed. This method has the following main advantages:

good mixing of the solids with spray atomized liquid droplets, and improved heat removal for highly exothermic reactions.

In the following paragraphs some of the industrial applications of gas-liquid injections into a fluidized bed with solid particles are discussed.

Wet granulation is one of the best known methods used in pharmaceutical industry to manufacture tablets. In a wet granulator, the solid particles are agglomerated due to the inter-particle bonds established by using liquid binders, which are sprayed onto the surface of the solid particles. There are several parameters that affect the quality of the final product of the tablets, such as granule size distribution and moisture content. Both of these parameters depend on the liquid-solid contact in the wet granulator (Rantanen et al., 2000), where increasing the liquid binder content of the granules causes a rise in granule size (Kristensen and Schaefer, 1987).

Tablet coating in fluidized beds, is another example of a pharmaceutical operation where injected liquid is sprayed into the surface of solid particles (tablets) for coating. The amount of injected liquid plays an important role in the quality of the final product, where the amount of liquid sprayed can affect the gas and solids flows and could potentially lead to uncontrollable particle agglomerations and poor gas-solid contact (Passos and Mujumdar, 2000). Accordingly, there is a limited amount of liquid injected above which the agglomerate cannot be controlled, and may lead to excessively big agglomerates and bed defluidization (Becher and Schlünder, 1998).

Liquid injection in fluidized beds is used in petrochemical processes, such as fluid coking, fluid catalytic cracking, and gas-phase polymerization. In these processes, the proper injection of liquid and its distribution on fluidized particles have a significant influence on product yields, selectivity and, overall productivity. For example, for gas-phase polymerization, there are many advantages of using liquid injection instead of gaseous injection, including cost reduction of the external heat exchanger required to evaporate the liquid, because liquid evaporates in the interior of the fluidized bed, and efficient heat removal and mixing occur for highly exothermic reactants (Bruhns and Werther, 2005).

Fluid coking is a continuous process used for upgrading heavy low grade feedstock, such as bitumen and residual petroleum, to lighter, more valuable products, such as gas oil, or naphtha. In the late 1940's and 1950's, there was a strong encouragement to develop a continuous process to convert heavy vacuum residua into lighter products. Exxon research and Development Company was the first research group to study and develop the fluid coking process. Later the Lummus Company developed contact coking, using the moving bed principle (McKetta and Cunningham, 1979). In 1954, the first commercial fluid coker started operation.

A fluid coking plant consists of two main pieces of equipments, the reactor, or coking vessel, and the burner, or heater vessel, as shown in Figure 1.1. Residual feedstocks, preheated to 260-370°C, are sprayed as liquid through several nozzles installed at different axial locations along the circumference of the reactor. It was originally thought that the liquid feed is distributed as a thin oil film on the hot coke particles, which are at a

temperature of 480-565°C in the reactor (Lee and Lee, 2005). It has since been discovered that most of the injected liquid forms agglomerates with the coke particles (Ariyapadi et al., 2003). The heavy components in the liquid film or in the agglomerates are cracked into vapors. The coke particles flow down from the spray region to the bottom section (stripper) of the reactor. In this section, the coke particles are steam stripped to remove adsorbed and interstitial hydrocarbons and then the coke flows into a riser that leads to the burner where part of the coke is combusted. Some of the reheated coke particles are recycled back to the reactor to provide the required heat for cracking, and the remaining excess coke is a waste material, which must be either stored or discarded. Finally, the flue gases from the burner pass through cyclones and discharge to the stack.

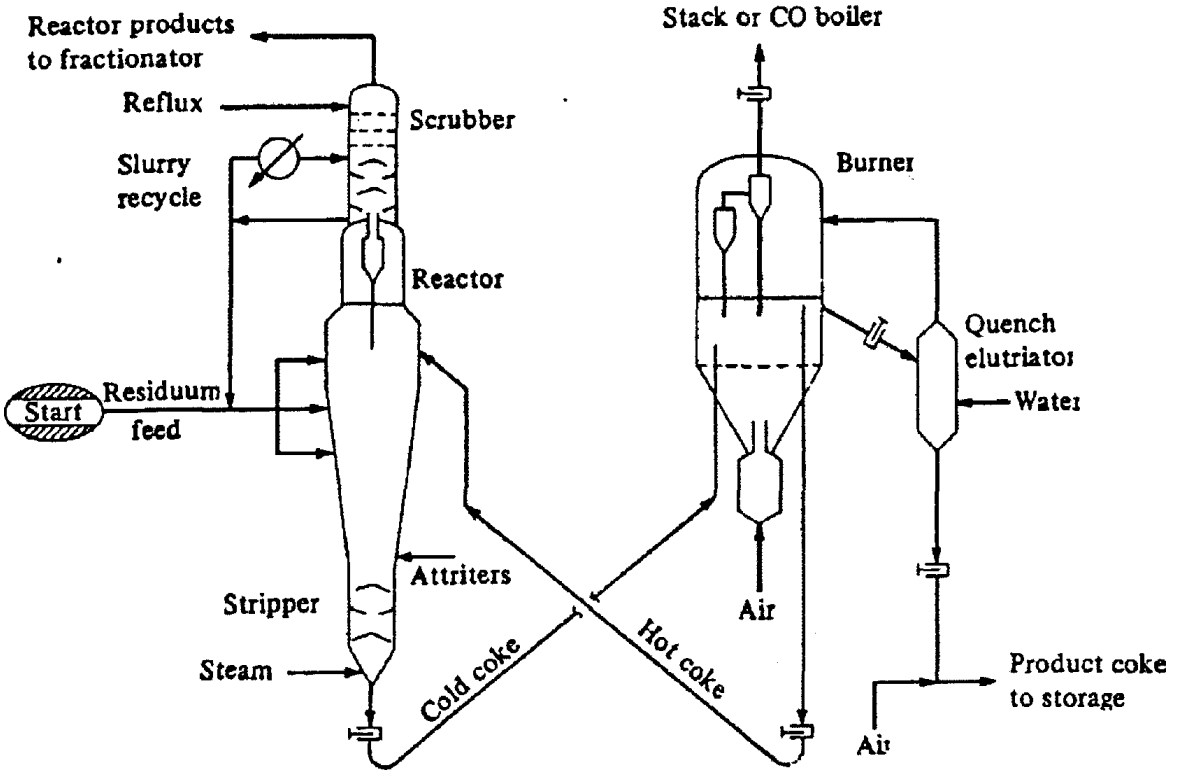

Figure 1.1: schematic diagram for fluid coking process. (House et al., 2004)

Since the fluid coking process requires contact between liquid and solid phases, it is essential to have good and uniform contact between liquid droplets and solid particles to maximize mass and heat transfer, since the cracking reaction is endothermic. Most of the injected liquid feed creates liquid droplets that interact with the fluidized solids forming liquid-solid agglomerates (Ariyapadi et al., 2003). These agglomerates introduce a significant resistance to heat transfer from the bulk of the fluidized bed to the reacting liquid, inside the agglomerates. This poor heat transfer reduces liquid yields and reactor operability (Felli et al., 2000). To minimize all these problems, rapid and fast vaporization of liquid should occur by contacting the solid particles quickly and uniformly. This could be achieved either by using spray nozzles that form a thin film on the surface of each particle (Gray et al., 2001) or, more practically, that form agglomerates that are drier, (House et al., 2004). Agglomerates that are drier are weaker and break up more easily in the fluidized bed, although their survivability is also affected by fluidized bed hydrodynamics and material properties (McDougall et al., 2004). Heat and mass transfer are influenced by agglomerates formation and survivability and, if the fluidized bed mixing is not intense enough, agglomerates survive for a relatively long time. As a consequence, a portion of the injected liquid becomes trapped within such agglomerates, and its conversion is negatively affected by mass and heat transfer limitations (House et al., 2004).

Fluid catalytic cracking (FCC) is another key example where liquid injection is employed. It is widely used to convert relatively heavy hydrocarbons to lighter, more valuable products, such as gasoline, by cracking over a catalyst at temperatures of around 500-550°C. An FCC unit has three main sections: the reactor/regenerator, the main fractionator, and the gas recovery section (Wilson, 1997). In the reactor/regenerator section,

the hot feed is injected at the base of the riser where it contacts the hot catalyst particles that are recycled from the regenerator. The feed is immediately vaporized thanks to the heat brought by the hot catalyst and both the catalyst and oil vapors travel upward along the riser while cracking reactions occur. At the top of the riser, a riser termination device is employed to rapidly separate spent catalyst from the product vapors. The product vapors then flow to the freeboard of the stripper vessel where they mix with the steam and hydrocarbon products rising from the spent catalyst stripper, before flowing to a recovery train. The residual material left on the catalyst, primarily in the form of coke co-product, is burned off in the regenerator.

Liquid injection plays an essential role in FCC process since it has been found to greatly affect the yield of valuable products. Chen (2006) indicates that, the feed injection at the riser of the FCC process can be improved to reduce the thermal cracking reactions that are the primary source of dry gas, and to maximize the catalytic cracking reactions, which provide more desirable products. These improvements can be employed by controlling the feed atomization, feed distribution and mixing with the catalyst. Feed atomization can be improved by using special nozzles, designed to produce fine droplets for fast vaporization (Avidan, 1992; Murphy 1992). However, Newton (1998) found that, those very small droplets can also be undesirable, because they tend to over crack producing dry gas instead of more valuable condensable vapors. For better feed distribution, multiple nozzles at a single riser elevation can be used (Murphy, 1992). Finally, the mixing with the catalyst can be enhanced to achieve a uniform rapid riser temperature as quickly as possible by using new feed nozzle designs (Chen & Dewitz, 1998; Chen et al., 1999) that create a sudden expansion of the two-phase at the nozzle exit.

In addition, the feed injection angle can also enhance the mixing or the feed with the catalysts (Chen, 2006).

1.3 Recent experimental studies about liquid jets in fluidized beds: a review

This section discusses a review of some of the recent experimental studies dealing with liquid injection into gas-solid fluidized beds. This review mainly focuses on the fluid coking operation, where the cracking of heavy hydrocarbons feedstock first occurs in the liquid phase.

Ariyapadi et al. (2003), Bruhns and Werther (2005) and Weber et al. (2006) found that liquid sprayed into gas-solid fluidized beds forms liquid-solid agglomerates. Ariyapadi et al. (2003) employed digital X-ray imaging to study the horizontal injection of gas-liquid jets into fluidized beds and clearly showed that liquid-solid agglomerates were formed.

Bruhns and Werther (2005) investigated the mechanism of liquid injection into a pilot plant bubbling fluidized bed using water and ethanol at temperature between 120 to 180 °C. Two different bed materials were compared: FCC catalyst and sand. In addition, a number of different measurement techniques were investigated such as fast response thermocouples to measure the local temperatures near the injection nozzle, gas suction probes to measure the gas composition, and capacitance probes for the detection of liquid in the dense gas-solid phase. These authors found that the vapor concentration measured in a bed of FCC catalyst decreases steeply with increasing distance from nozzle exit. On the other hand, the bed of sand behaves differently, where the measured vapor concentration decreased with further distance from the nozzle exit. When using a bed of sand, the

agglomerates are formed near the nozzle exit and those agglomerates are more stable and stick to the tip of the suction probes. However, for a bed of FCC catalyst the agglomerates are less stable and can be broken up more easily. Later, these authors used capacitance probes to confirm the previous findings. They found that there is no instantaneous liquid evaporation at the exit of the nozzle even for the highly volatile liquids (ethanol). This confirms that agglomerates formed at the exit of the nozzle. Moreover, these authors, obtained interesting result when they located the capacitance probes further from the nozzle exit. At this new location, the agglomerates decayed and mixed into the bulk of the fluidized bed.

McMillan et al. (2005) investigated the effect of liquid properties, such as liquid viscosity, surface tension and contact angle on the agglomerating tendency of a wet gas-solid fluidized bed. The authors found that liquid with a low contact angle injected into a fluidized bed of 135 μm coke particles would only form agglomerates if the liquid viscosity is high. However, the liquid always forms agglomerates when the contact angle is high. However, for 175 and 300 μm glass beads particles, the liquid viscosity has a negligible effect on agglomeration behaviour when the contact angle is high. Moreover the authors concluded that surface tension (ranging from 0.021 and 0.029 N/m) has no effect on agglomerates formation. Finally the authors found that, agglomerates formation with different liquids is independent of the fluidization gas velocity when the liquid spray is almost perfect.

McMillan et al. (2005) studied the injection of cold ethanol into a fluidized bed of heated coke particles via two-phase spray nozzles in order to develop a quick method to

determine the quality of solid-liquid mixing on a short time scale. The authors used fast thermocouples located at different axial positions along the length of the jet downstream of the gas-liquid spray to measure the instantaneous temperature of the liquid spray jet cross section. By measuring the variations of the time-averaged temperatures, the authors created contour plots of the liquid/solid distribution within the cross-sectional area of the jet for two different cases: the free spray jet and the jet when a draft tube is used. Their results show that the draft tube improved the liquid/solid mixing.

Knapper et al. (2003) showed that the quality of the interaction between the gas-liquid jet and the fluidized bed is strongly impacted by the nozzle performance. Portoghese et al. (2005) investigated the use of triboelectric probes to measure solid moisture content in fluidized beds. The liquid was injected into fluidized bed of glass beads under several operating conditions by varying liquid pressure, injection time and superficial gas velocity. The authors found that the bed drying time and the amount of agglomerates formed increase when increasing the mass of injected liquid. Increasing the fluidization gas velocity reduces the amount of agglomerates formed. Finally the authors estimated the fraction of liquid forming agglomerates by fast analysis of the triboelectric signals that provided the bed drying time.

Portoghese et al. (2007) studied the use of a triboelectric probe to characterize the performance of gas atomization nozzles injecting liquid into a gas-solid fluidized bed. The authors introduced the nozzle performance index (NPI) to characterize the efficiency of the contact between spray liquid and the fluidized bed material. Then to validate the triboelectric method, the authors developed another index based on bed temperature

measurements, TI, and compared it to the nozzle performance index (NPI) obtained for the triboelectric probes over a wide range of operating conditions. The authors found that, a strong linear relationship existed between the two performance indices (R^2=0.938). However, the results provided by the triboelectric technique were more reproducible. However, they showed that the triboelectric probes are not the best method for assessing the performance of spray nozzle, because they measure a current generated by the collision of bed particles with the electrode and they are very sensitive to the local bed hydrodynamics. Furthermore, Portoghese et al. (2008) developed another method that is much less sensitive to the local hydrodynamics to evaluate the nozzle performance. This new method is based on the electric conductance of the bed solids after the liquid injection and defluidization of the wetted particles. As a result for their investigation, the Nozzle Performance Index was defined based on the bed electric conductance measured after the liquid injection and bed defluidization.

Leach et al. (2008) developed a rapid and reliable experimental method to evaluate the liquid-solid contact efficiency using the triboelectric probes developed by Portoghese et al. (2007). However, the authors used another technique to measure the probe signal. This technique is based on recording the signals generated by the triboelectric probes during the defluidization instead of the previous method used by Portoghese et al. (2008) where the measurements recorded were taken during fluidization. Later, the authors used the developed technique to investigate the effect of gas-to-liquid ratio (GLR) on the performance of two different nozzles (Type I and Type II). The authors concluded that, increasing the GLR increases the nozzle performance for Type II nozzle; however Type I nozzle showed a lower increase when compared to Type II nozzle. Moreover, using the

new method with defluidization measurements exhibited higher sensitivity to changes in the GLR and lower scatter in the experimental results compared to the fluidization method. Leach et al. (2008) and Portoghese et al. (2008) explained this improvement using the new method. This method is based on defluidizing the bed shortly after the injection of liquid into the fluidized bed of solid particles to ensure the preservation of the liquid-solid distribution produced during the initial interaction between the liquid jet and the fluidized bed. The charges previously accumulated on the particles by the triboelectric probes discharge through high conductivity wet paths among the particles to the grounded electrode.

Leach et al. (2009) compared the performance of various spray nozzles (Type I, Type II, Vertical Fanjet, Hollow Cone and Wide Hollow Cone spray nozzles) in gas solid fluidized bed based on the Nozzle Performance Index (NPI). The Nozzle Performance Index was defined by the authors as the slope of the logarithmic region of the bed conductivity which is measured by the conductance probes developed by Portoghese et al. (2008) over time. Leach et al. (2009) found that the conductance technique successfully characterized the performance of atomizing spray nozzles. Moreover, the authors concluded that the Type II nozzle displayed the best performance among the five different spray nozzles for gas to liquid ratio (GLR) less that 2.5%. Furthermore, a non linear relationship was found between the gas to liquid ratio (GLR) and the quality of the mixing for all the nozzles. Finally these authors determined that the geometry of the spray nozzles has a considerable impact on the jet bed interaction, because of the relationship between the droplet size and jet bed interaction was different for each nozzle.

Ariyapadi et al. (2004) developed a correlation to predict the horizontal jet penetration of gas-liquid spray jets in a gas-solid fluidized beds by combining a theoretical model to predict the momentum flux of two phase sprays with a correlation for gas jets originally proposed by Benjelloun et al. (1995). In addition, Ariyapadi et al. (2004) employed the use of thermocouple to measure the jet penetration experimentally for several spray nozzle geometries, sizes and various jet fluids. Following to what discussed previously the following paragraphs shows the modification of Benjeloun et al. (1995) correlation to predict jet penetration done by Ariyapadi et al. (2004)

$$L_{jet} = \frac{5.52}{g^{0.27}} \frac{1}{(\rho_p - \rho_g)^{0.27}} (\rho_f U_f^{\,2})^{0.27} d^{0.73} \qquad \text{Eq. 1.1}$$

For a single fluid nozzle, the term $\rho_f U_f^2$ in the above equation represents the momentum flux (Mf /Anoz) of the fluid, which is usually based on the nozzle exit conditions.

For a gas-liquid jet, the momentum at the nozzle tip can be expressed as follows:

$$M_f = W_L U_L + W_g U_g \qquad \text{Eq. 1.2a}$$

(or)

$$M_f = W_L U_L \left(1 + \frac{W_g}{W_L} \frac{U_g}{U_L}\right) \qquad \text{Eq. 1.2b}$$

In Equation (2b), Wg and WL refer to the mass flowrates of gas and liquid fed to the nozzle, and Ug and UL are the velocities of the gas and the liquid phases respectively. For most two-phase feed nozzles, the air-to-liquid mass ratio (ALR = Wg/WL) is a key parameter. Moreover, an important aspect in two-phase (gas continuous) flows is the

existence of a mean slip velocity ratio slip velocity (S = Ug/UL) at the nozzle exit. In this regard, Equation (2b) can be rewritten as follows:

$$M_f = W_L U_L (1 + ALR [S])$$

Eq.1.3

The liquid velocity, UL, can be expressed as:

$$UL = WL/ [\rho_L (1-\varepsilon') Anoz] \qquad \text{Eq. 1.4}$$

Here, ρ_L refers to the liquid density and (1- ε') is the average liquid holdup at the nozzle exit. For convenience, a liquid-phase superficial mass velocity can be defined.

$$GL = WL/Anoz \qquad \text{Eq.1.5}$$

From Equations (3), (4), and (5), the momentum flux ($\rho_f U_f^2$) in the original Benjelloun et al. (1995) equation can be replaced and the result is the modified correlation, shown below:

$$L_{jet} = \frac{5.52}{g^{0.27}} \frac{1}{(\rho_p - \rho_g)^{0.27}} \left(\frac{G_L^2 (1 + ALR [S])}{\rho_L (1 - \varepsilon')} \right)^{0.27} d^{0.73}$$

Constants — Bed effects — Nozzle conditions — Scale

Eq.1.6

An inherent advantage in using Equation (6) is the fact that the various effects have been isolated to clearly indicatethe influence on jet penetration. To compute the jet penetration (Ljet), the nozzle size (scale), nozzle operating conditions (at the exit orifice), and the bed properties need to be known. When a two-phase (gas-liquid) jet is considered, evaluating ε' at the nozzle tip becomes much more complex. Hence, a detailed step-wise approach is required as indicated in the following section. The authors found that their predicted values were in good agreement with the experimental data. The previous correlation was applied in the current work to calculate the jet penetration for both stable and pulsating jets.

Berruti et al. (2009) investigated the use of two methods based on either triboelectric probes or a thermal tracer to characterize the jet angle of the jet penetration and, overall, to map the boundaries of gas-liquid jets formed during the air-assisted injection of liquids into gas-solid fluidized beds. In addition, they studied the effects of nozzle geometries and the scale of the fluidized bed on the jet boundaries. Their results showed that jet penetration depth increased by increasing the air to liquid ratio (ALR); however, when using commercial scale nozzles, the depth of the jet penetration decreased with increasing air to liquid ratio (ALR). Finally the authors verified the accuracy of the correlation of Ariyapadi et al. (2004) in predicting the depth of jet penetration and determined a maximum 5% error.

1.4 **Research Objectives:**

This review has clearly shown the importance of achieving good contact between injected liquids and fluidized particles in many industrial processes. It has also shown that traditional approaches, such as changing the nozzle geometry or adjusting operating conditions, have not achieved major improvements in liquid-solid contact, under conditions relevant to the fluid coking process.

The major objective of this thesis is, therefore, to attempt to develop a transformative technology by taking a non-traditional approach. Although flow pulsations in spray nozzles have traditionally been minimized, this thesis investigated whether some specially designed flow pulsations might actually be beneficial.

Therefore several experiments where conducted using laboratory scale fluidized bed in order to investigate the effect of inducing pulsations of well defined amplitude and

frequency on gas-liquid interaction by applying two different types of pulsations: mechanical pulsations using solenoid valve attached to the gas stream and non mechanically induced pulsations. Moreover the mechanical pulsations using solenoid valve are applied to different spray nozzles including two custom made spray nozzles and two commercial spray nozzles. In addition the effect of both types of pulsations are investigated under variety of operating conditions such as liquid flow rate, gas orifice restriction, liquid restriction, and gas properties.

1.5 References

Ariyapadi, S., Berruti, F., Briens, C., McMillan, J. & Zhou, D. 2004, "Horizontal penetration of gas-liquid spray jets in gas-solid fluidized beds", *International Journal of Chemical Reactor Engineering,* vol. 2.

Ariyapadi, S., Holdsworth, D., Norley, C., Berruti, F., & Briens, C. 2003, "Digital X-ray imaging technique to study the horizontal injection of gas-liquid jets into fluidized beds", *International Journal of Chemical Reactor Engineering, 1*(A56).

Avidan, A.A. 1992, "FCC is far from being a mature technology", *Oil and Gas Journal,* vol. 90, no. 20, pp. 59-62, 64.

Becher, R.-. & Schlünder, E.-. 1998, "Fluidized bed granulation - The importance of a drying zone for the particle growth mechanism", *Chemical Engineering and Processing: Process Intensification,* vol. 37, no. 1, pp. 1-6.

Benjelloun, F., Liegeois, R., Vanderschuren, J. 1995, "Penetration length of horizontal gas jets into atmospheric fluidized beds", Proc. Fluidization-VIII, J-F. Large and C. Laguerie Eds., Engineering Foundation, N.Y., 239-246.

Berruti, F., Dawe, M. & Briens, C. 2009, "Study of gas-liquid jet boundaries in a gas-solid fluidized bed", *Powder Technology,* vol. 192, no. 3, pp. 250-259.

Bruhns, S. & Werther, J. 2005 "An investigation of the mechanism of liquid injection into fluidized beds", *AIChE Journal,* vol. 51, no. 3, pp. 766-775.

Chen, Y.-. 2006, "Recent advances in FCC technology", *Powder Technology,* vol. 163, no. 1-2, pp. 2-8.

Chen, Y., Brosten, D., Nielson, J.W. Feed nozzle, U.S. Patent 5,979,799 (1999).

Chen, Y., Dewitz, T.S. Feed nozzle, U.S. Patent 5,794,857 (1998).

Gray, M.R., Le, T., McCaffre, W.C., Berruti, F., Soundararajan, S., Chan, E., Huq, I. & Thorne, C. 2001, "Coupling of mass transfer and reaction in coking of thin films of an Athabasca vacuum residue", *Industrial and Engineering Chemistry Research,* vol. 40, no. 15, pp. 3317-3324.

House, P.K., Saberian, M., Briens, C.L., Berruti, F. & Chan, E. 2004, "Injection of a liquid spray into a fluidized bed: Particle-liquid mixing and impact on fluid coker yields", *Industrial and Engineering Chemistry Research,* vol. 43, no. 18, pp. 5663-5669.

Knapper, B. A., Gray, M. R., Chan, E. W., & Mikula, R. 2003, "Measurement of efficiency of distribution of liquid feed in a gas-solid fluidized bed reactor", *Int. J. Chem. React. Eng., 1*(A35)

Kristensen, H.G. & Schaefer, T. 1987, "Granulation. A review on pharmaceutical wet-granulation", *Drug development and industrial pharmacy,* vol. 13, no. 4-5, pp. 803-872.

Leach, A., Chaplin, G., Briens, C. & Berruti, F. 2009, "Comparison of the performance of liquid-gas injection nozzles in a gas-solid fluidized bed", *Chemical Engineering and Processing: Process Intensification,* vol. 48, no. 3, pp. 780-788.

Leach, A., Portoghese, F., Briens, C. & Berruti, F. 2008, "A new and rapid method for the evaluation of the liquid-solid contact resulting from liquid injection into a fluidized bed", *Powder Technology,* vol. 184, no. 1, pp. 44-51.

Lee, S., & Lee, L. 2005, "*Encyclopaedia of Chemical Processing",* CRC Press.

McDougall, S.L., Saberian, M., Briens, C., Berruti, F. & Chan, E.W. 2004, "Characterization of fluidization quality in fluidized beds of wet particles", *International Journal of Chemical Reactor Engineering,* vol. 2.

McKetta, J. J., & Cunningham, W. A. 1979, "*Encyclopaedia of chemical processing and design*", CRC Press.

McMillan, J., Zhou, D., Ariyapadi, S., Briens, C., Berruti, F. & Chan, E. 2005, "Characterization of the Contact between Liquid Spray Droplets and Particles in a Fluidized Bed", *Industrial & Engineering Chemistry Research,* vol. 44, no. 14, pp. 4931-4939.

Molstedt, B.V. & Moser, J.F. 1958, "Fluid Coking Development: A Mechanically Fluidized Reactor", *Industrial & Engineering Chemistry,* vol. 50, no. 1, pp. 21-23.

Murphy, J.R. 1992, "Evolutionary design changes mark FCC process", *Oil and Gas Journal,* vol. 90, no. 20, pp. 49-56, 58.

Newton, D. 1998, "How BP makes use of its X-ray imaging facility to support developments in fluidized bed processes", *Proceedings of the 1998 AIChE Annual Meeting* (p.220).

Passos, M.L. & Mujumdar, A.S. 2000, "Effect of cohesive forces on fluidized and spouted beds of wet particles", *Powder Technology,* vol. 110, no. 3, pp. 222-238.

Portoghese, F., Berruti, F. & Briens, C. 2005, "Use of triboelectric probes for on-line monitoring of liquid concentration in wet gas–solid fluidized beds", *Chemical Engineering Science,* vol. 60, no. 22, pp. 6043-6048.

Portoghese, F., Ferrante, L., Berruti, F., Briens, C. & Chan, E. 2008, "Effect of injection-nozzle operating parameters on the interaction between a gas-liquid jet and a gas-solid fluidized bed", *Powder Technology,* vol. 184, no. 1, pp. 1-10.

Portoghese, F., Berruti, F., Briens, C. & Chan, E. 2007, "Novel triboelectric method for characterizing the performance of nozzles injecting gas-atomized liquid into a fluidized bed", *Chemical Engineering and Processing: Process Intensification,* vol. 46, no. 10, pp. 924-934.

Rantanen, J., Rasanen, E., Tenhunen, J., Kansakoski, M., Mannermaa, J., Yliruusi, J. 2000, "In-line moisture measurement during granulation with a four-wavelength near infrared sensor: an evaluation of particle size and binder effects", *European Journal of Pharmaceutics and Biopharmaceutics, 50,* 271-276.

V. Felli, S. Ariyapadi, M. Saberian, F. Berruti, C. Briens, "Injection of Liquids in Fluidized Beds: Fundamentals of Particles Agglomeration", Chemical Reaction Engineering VIII Conference, Chemical Reactor Engineering 2000: Novel Reactor Engineering For The New Millennium, June 24-29, 2001, Barga, Italy.

Weber, S., Briens, C., Berruti, F., Chan, E. & Gray, M. 2006, "Agglomerate stability in fluidized beds of glass beads and silica sand", *Powder Technology,* vol. 165, no. 3, pp. 115-127.

Wilson, J. W. 1997, "*Fluid catalytic cracking technology and operations*", Penn Well Books.

Chapter 2

ENHANCEMENT OF THE LIQUID FEED DISTRIBUTION IN GAS-SOLID FLUIDIZED BEDS BY NOZZLE PULSATIONS (INDUCED BY SOLENOID VALVE)

Rana Sabouni [1], Aidan Leach, Cedric Briens[1], Franco Berruti[1]

[1]Institute for Chemical and Fuels from Alternative Resources (ICFAR),
Engineering, University of Western Ontario
London, ON, Canada N6A 5B9

2.1 Introduction:

Many industrial applications use liquid injection into fluidized beds of solid particles, such as fluid catalytic cracking, fluid coking, and gas phase polymerization. In these applications, the reactor yield depends on the effectiveness of the liquid distribution on the bed particles. Therefore, it is of crucial importance to study the mechanism of liquid injection into fluidized beds in order to minimize the formation of undesired agglomerates, and, thus, prevent mass and heat transfer limitations and maximize the yield of valuable product.

In the above processes, liquid feed is injected into the fluidized bed with gas atomization nozzles. Ariyapadi et al. (2003) and Bruhns and Werther (2005) demonstrated that liquid sprayed into a gas-solid fluidized bed typically forms liquid-solid agglomerates. By using X-ray imaging, Ariyapadi et al. (2003) showed that agglomerates formed at the tip of the spray jet cavity. Agglomerate survivability is affected by fluidized bed hydrodynamics and material properties (McDougall et al., 2004; Weber et al., 2006). Heat

and mass transfer are influenced by agglomerates formation and survivability and, if the fluidized bed mixing is not intense enough, agglomerates survive for a relatively long time. As a consequence, a portion of the injected liquid becomes trapped within such agglomerates, and its conversion is negatively affected by mass and heat transfer limitations (House et al., 2004).

Many researchers focused on studying the parameters affecting the interaction between gas-liquid jets and fluidized beds to minimize the formation undesired agglomerates and maximize mass and heat transfer, thus making the unit more efficient and profitable. Knapper et al. (2003) showed that the quality of the interaction between the gas-liquid jet and the fluidized bed is strongly impacted by nozzle performance. Portoghese et al. (2007) studied the use of triboelectric probe to characterize the performance of gas atomization nozzles injecting liquid into a gas-solid fluidized bed. However, triboelectric probes measure the current generated by the collisions of bed particles with the electrodes and are too sensitive to the local bed hydrodynamics. Portoghese et al. (2008a) developed another method that is much less sensitive to the local hydrodynamics to evaluate the nozzle performance. It is based on measuring the electrical conductance of the bed solids after completing the liquid injection and defluidizing the wetted particles. If most of the injected liquid is concentrated in a few agglomerates, most of the bed is dry and the bed conductance is small. Conversely, if the liquid is well distributed on the particles, forming a liquid film on the particles surface that connects all the particles, the bed conductance is large.

Leach et al. (2008) improved both methods from Portoghese et al. (2007, 2008a). Their study showed that increasing the liquid flow rate or reducing the nozzle size enhanced its spraying performance in the fluidized bed. Moreover, House et al. (2008) demonstrated that both the nozzle internal geometry and internals have a strong impact on the quality of the liquid-solid contact.

Ariyapadi et al. (2004) developed a correlation to predict the horizontal jet penetration of gas-liquid sprays jets in a gas-solid fluidized bed by combining both a theoretical model to predict the momentum flux of two phase sprays with a correlation from Benjelloun et al. (1995) for the penetration of gas jets. They found that their correlation predicted values that were in good agreement with the experimental data.

The objective of this study was to impose fluctuations of well-defined frequency and amplitude on the liquid spray, and measure the resulting effect on the interactions between the gas-liquid jet and the fluidized particles and, consequently, on the effectiveness of the liquid feed distribution throughout the bed. Chan et al. (2001) assumed that stable, non-pulsating sprays are required for optimal reactor operation and showed that, in a pilot plant fluid coker, a stable spray provided higher liquid yields and lower sulfur dioxide emissions than a strongly pulsating spray. McDougall et al. (2004) found that a pulsating spray reduced bed fluidity and promoted the formation of agglomerates. The basic assumption of the current study is that, contrarily to those preliminary findings, well-designed spray pulsations may actually enhance the liquid-solid contact, by disrupting the region, near the tip of the jet, where the wet agglomerates form.

2.2 Apparatus:

The experimental apparatus, shown in Figure 2.1, consists of:

1) A fluidized bed with a rectangular cross-section of 1.2 m by 0.15 m. It was filled with 250 kg of silica sand particles with a Sauter mean diameter of 190 μm and an apparent particle density of 2600 kg/m^3 (Group B of the Geldart's powder classification). Air at a superficial gas velocity of 0.24 m/s was used to fluidize the bed.

2) The air stream was supplied from a medical air cylinder, and regulated by a pressure transducer, solenoid valve and 1 mm restriction orifice. A pressure transducer was used to measure the pressure (P_g) upstream of the 1mm restriction orifice. In order to induce pulsations in the liquid spray, a solenoid valve was introduced in the air stream, just upstream of the restriction orifice (Figure 2.1). A 70mm long section of 6.4 mm diameter line between the solenoid valve and the restriction orifice provided a volume that acted as a capacitance, to dampen the gas flow fluctuations induced by the opening and closing of the valve. This solenoid valve was controlled by a function generator using the circuit shown in Figure 2.3. By opening and closing the gas line (because of the opening and closing of the solenoid valve), the gas-to-liquid ratio is no longer held constant, and the fluctuations in gas pressure in the line cause the water flowrate to also change. This induces the pulsations whose effects were investigated in this study. The frequency of pulsation was fast enough that the gas flowrate never decreased to zero, as there was still a release of gas from the region between the solenoid valve and the restriction orifice governing the gas flowrate.

3) The injected liquid stream was de-ionized water. The water tank was pressurized by a nitrogen cylinder and a pressure transducer measured the pressure (P_L) upstream of the needle valve.

4) A pre-mixer for the gas and liquid streams, where the pressure (P_{BFC}) was measured with a pressure transducer.

5) A spray nozzle. Two spray nozzles were used for comparison in this study (Type I nozzle and Type II Nozzle) as illustrated in Figure 2.2. The first one had throat diameter of 1.6 mm. The second one had the same internal geometry as Type I, except for a deviated section located downstream of the second throat. Both types of nozzles were developed by Portoghese et al. (2008a). The spray nozzle was located 0.6 m above the fluidization gas distributor and protruded into the bed for 0.05 m from the wall.

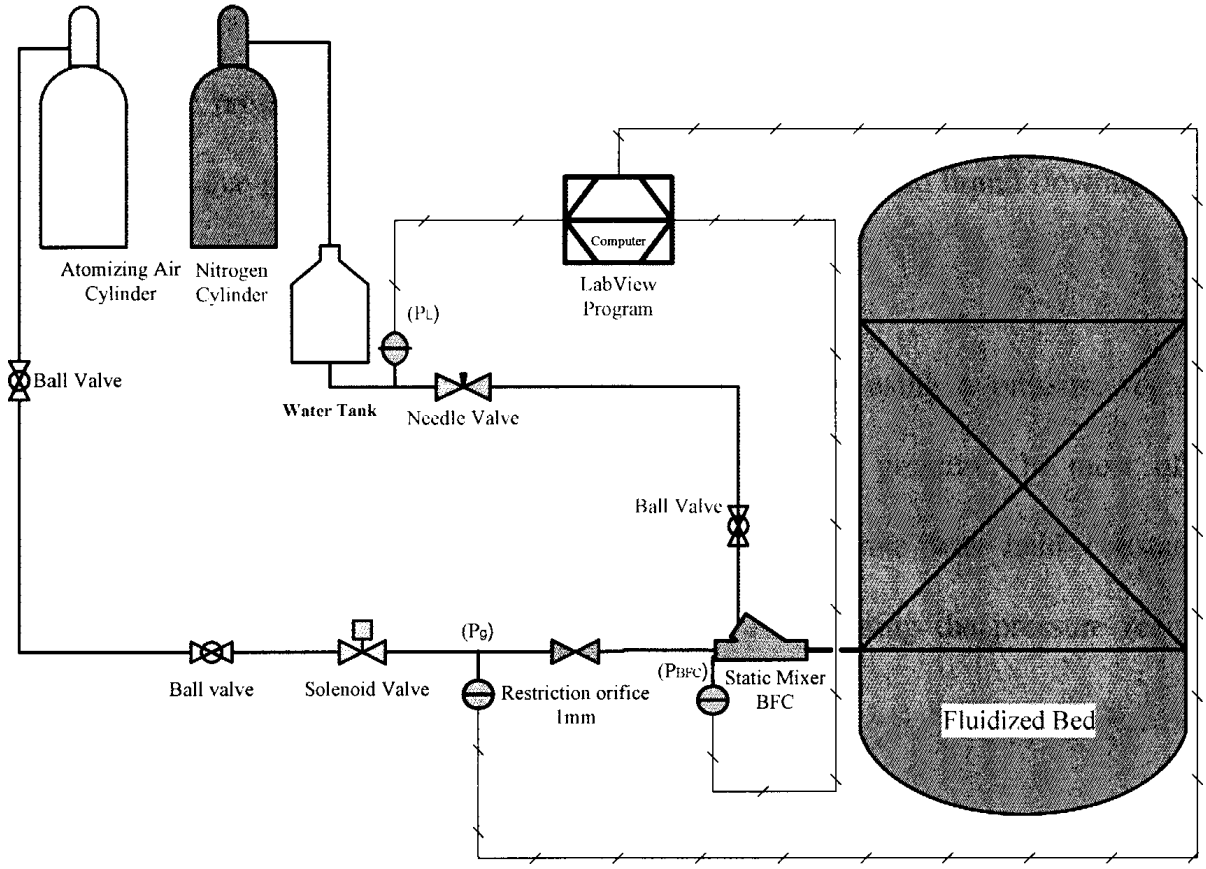

Figure 2.1: Schematic Diagram of Experimental Apparatus.

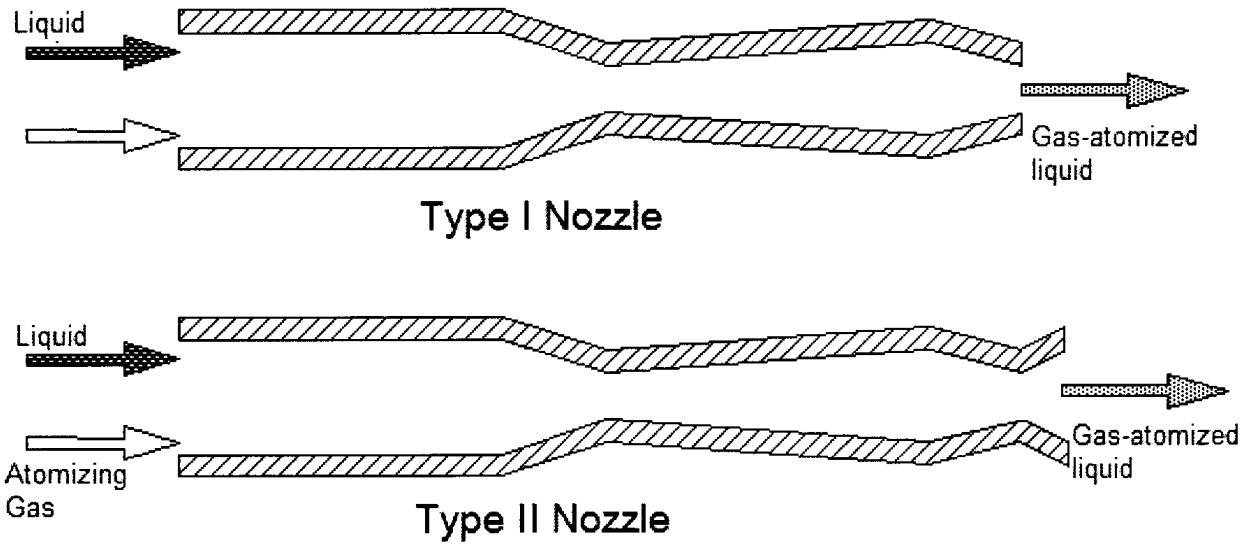

Figure 2.2: Internal Geometry of Type I Nozzle and Type II Nozzle.

All pressure transducers were calibrated and connected to a data acquisition system to measure the pressure drops across the air restriction orifice (P_g-P_{BFC}), and across the liquid needle valve (P_L-P_{BFC}), from which the instantaneous gas and liquid flowrates to the premixer could be determined.

The time-averaged liquid flowrate was controlled by using a pressure regulator placed on the nitrogen cylinder to adjust the liquid tank pressure. In most of the experiments on this study, the time-averaged liquid flowrate was held constant at 0.022 kg/s. The time-averaged air flowrate was controlled using the pressure regulator placed upstream of the restriction orifice.

The temperature of the bed was measured using four thermocouples, placed in the bed to ensure that the bed temperature was 20 degrees Celsius at the start of each injection. All the thermocouples were type J and placed in the bed at heights of 15, 35, 55 and 75 cm above the gas distributor.

A function generator was used to control the solenoid valve frequency (0 Hz to 10 Hz) and to create a sinusoidal waveform with a 6.7 RMS voltage. Figure 2.3 shows the circuit diagram used in the experiments.

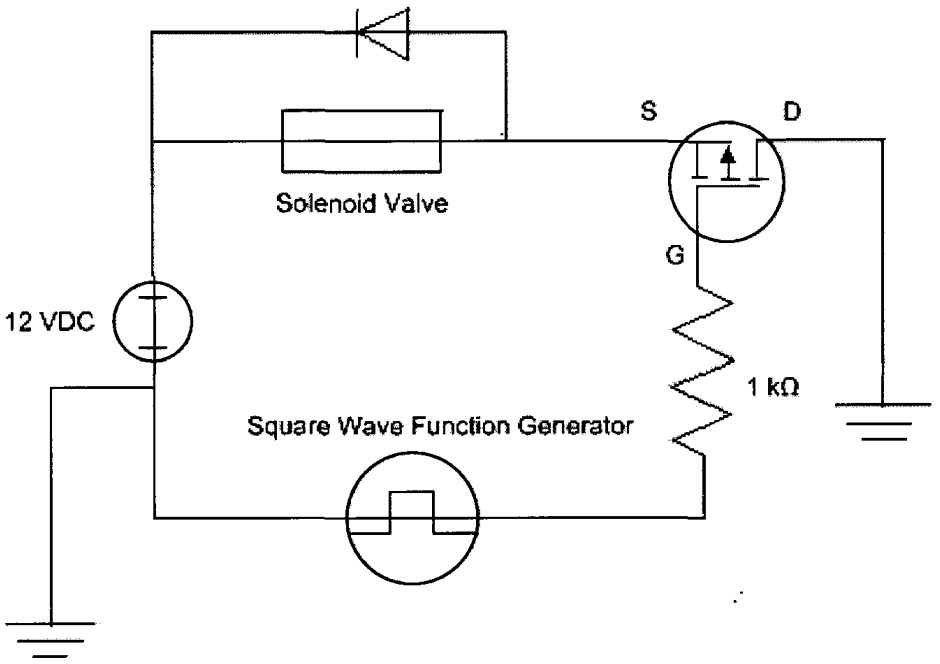

Figure 2.3: Circuit Diagram of used in the experiments.

Based on the previous work of Portoghese et al. (2008a), the bed conductivity can be measured by applying a sinusoidal current to the fluidized bed and measuring the voltage drop across the fluidized bed. This particular technique was also used in the current work. The conductivity of the bed was measured using an electrode which was placed at the centre of the bed, 0.37 cm above the gas distributor. The electrode was made of a stainless steel hollow tube with an outer diameter of 7 mm. It was connected to a 51 kΩ resistor. Figure 2.4 shows the schematic diagram of the electrode circuit. The voltage imposed by the signal generator was used with the voltage measured across the resistor to calculate the bed conductance using Ohm's law:

$$G_{bed} = \frac{1}{R_{bed}} = \frac{1}{R_m} * \left[\frac{V_2}{V_1 - V_2} \right] \tag{2.1}$$

A data acquisition system was used to measure the voltage V_1 imposed by the signal generator, the voltage V_2 across the resistor, and the temperature of the four thermocouples, at a frequency of 1000 Hz.

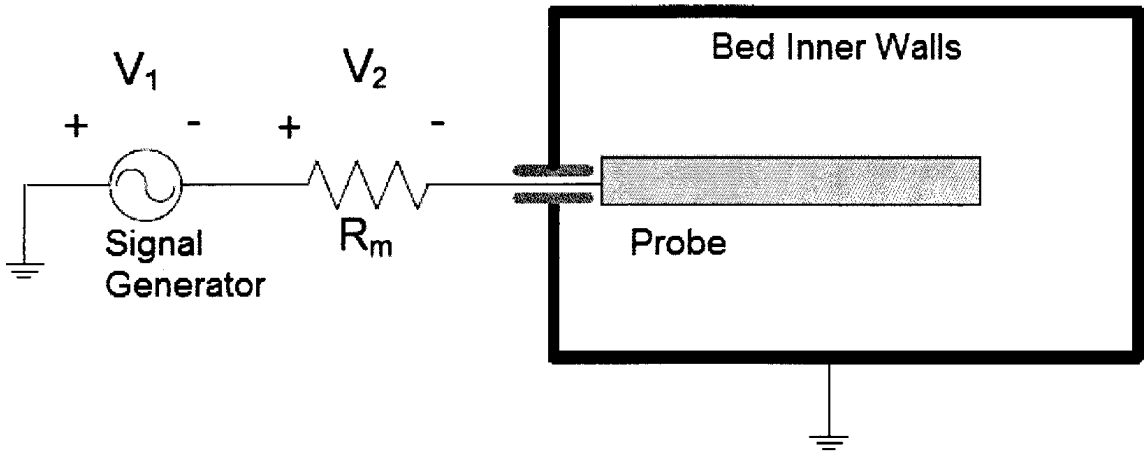

Figure 2.4: Schematic Diagram of Conductive Probe.

2.3 Experimental Procedure:

The objective of the conducted experiments was to study the effects of spray nozzle pulsations on the jet-bed interaction, which was characterized by a Nozzle Performance Index (NPI). The NPI characterized the quality of the interaction between injected liquid and bed solids. (Leach et al., 2008; Portoghese et al., 2008b)

A common experimental procedure was used for all experiments:

1) The fluidization air velocity was set to 0.25 m/s.

2) The needle valve opening was set fully open in all the experiments.

3) At t=0, the data acquisition was started using the LabView program (version 8, National Instruments)

4) Simultaneously, the solenoid valve was switched on and pulsated at the desired frequency for 15 s.

5) At t=10 s, water was injected into the bed through the spray nozzle. The duration of the water injection was 15 s.

6) At t = 25 s, the liquid injection, fluidization air, and solenoid valve were stopped, and the bed was defluidized for 7 minutes. Conductivity measurements were performed during these 7 minutes. The conductance of the fluidized bed solids were measured by the conductance probe during the 7 minutes of defluidizing as developed by Leach et al., (2008) where taking the conductivity measurements during defludiziation gave better results because much noise in the probe signal were found compare to when the bed is fluidized.

7) At t=7 min the bed was refluidized again to dry it by vaporizing the injected water and to ensure that the bed temperature returned to its initial value of 20 ^{0}C before starting a new experiment. In addition, refluidizing the bed caused the agglomerates to break up and, therefore, facilitated the drying.

The injection time was kept constant at 15 seconds in all of the experiments to ensure that the mass of injected liquid was always the same, since the liquid mass flowrate was maintained at 0.022 kg/s. The air to liquid ratio (ALR) was maintained constant for each run. The tests were repeated for different frequencies, using the same conditions. The pressure values for the pre-mixer (P_{BFC}), liquid (P_L), and air (P_g) streams were recorded during each experiment.

As a last step, a plot of bed conductance vs. time was used to estimate the Nozzle Performance Index (NPI), which is defined as the slope of the trend-line of that plot, using a logarithmic scale for time. This method was developed by Leach et al. (2008). A high NPI value means that water diffuses quickly through the defluidized bed, increasing the bed conductance quickly. A high NPI therefore corresponds to a good original distribution of the liquid on the bed particles, just before defluidization. To ignore any irregularities in the start-up of the defluidization, only data subsequent to t = 50 s were used. Figure 2.5 shows an example of the change with time of the conductance of the defluidized bed. In the case corresponding to Figure 2.5, the NPI was 0.8637.

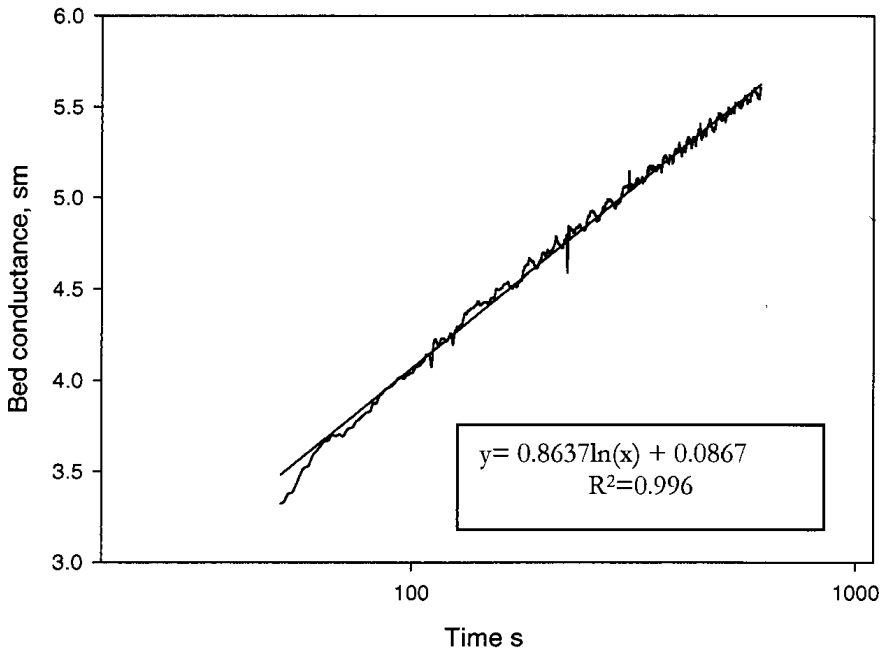

Figure 2.5: Conductance method, 1 Hz, Fully open needle valve, Type I Nozzle D=1.66 mm, F_L=0.022 kg/s, 1 mm restriction orifice, P_L=25 psi, P_g=30 psi, 1.7 ALR%, V_{air}=14 cm^3

2.4 Result and Discussion:

2.4.1 Effect of Frequency

Figures 2.6 and 2.7 show the variations with time of the liquid and gas flowrates for two different operating conditions as follows: the data illustrated in Figures 2.6 and 2.7 have the same liquid flowrate of 0.22 kg/s but different frequencies of 0 Hz and 1 Hz respectively. The jet penetration was calculated using the model from Ariyapadi et al. (2004), using the measured instantaneous liquid and gas flowrates (Figures 2.6 and 2.7).

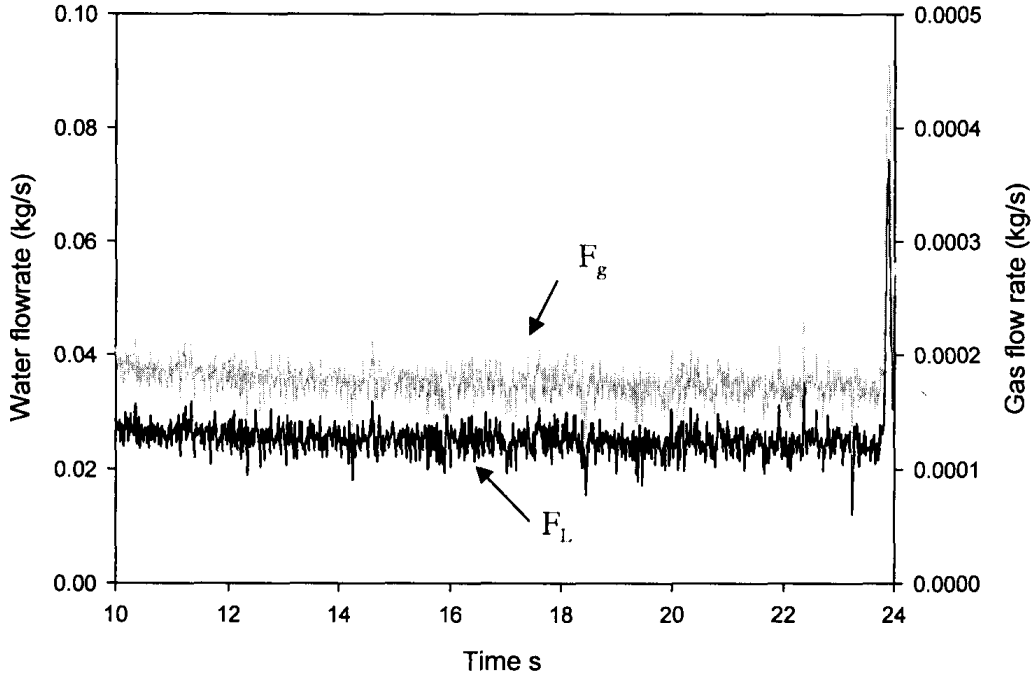

Figure 2.6: Liquid flowrate and gas flowrate as function of time, 0 Hz, Fully open needle valve, , Type I Nozzle D=1.66 mm, F_L=0.022 (kg/s), 1 mm restriction orifice, P_L=30 Psi, P_g=30 Psi, 1.7 ALR%, Air, V_{air}=14 cm^3

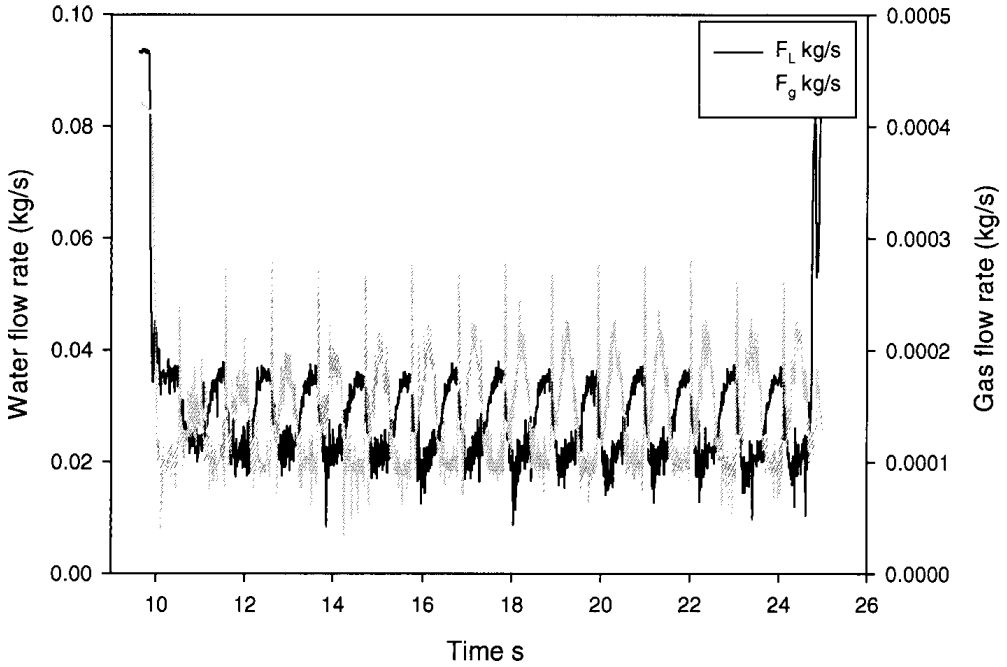

Figure 2.7: Liquid flowrate and gas flowrate as function of time, 1 Hz, Fully open needle valve, , Type I Nozzle D=1.66 mm, F_L=0.022 (kg/s), 1 mm restriction orifice, P_L=25 Psi, P_g=30 Psi, 1.7 ALR%, Air, V_{air}=14 cm^3

Figure 2.8 demonstrates the effect of changing the nozzle fluctuation frequency on the NPI. Each point in the Figure represents an average of three replicates under the same conditions (1.7% ALR and F_L= 0.022 kg/s) and the 95% confidence intervals are shown. It is obvious that there is a huge positive impact of pulsations on the NPI, with pulsations more than doubling the NPI. The detailed explanation for this phenomenon is discussed later in this paper.

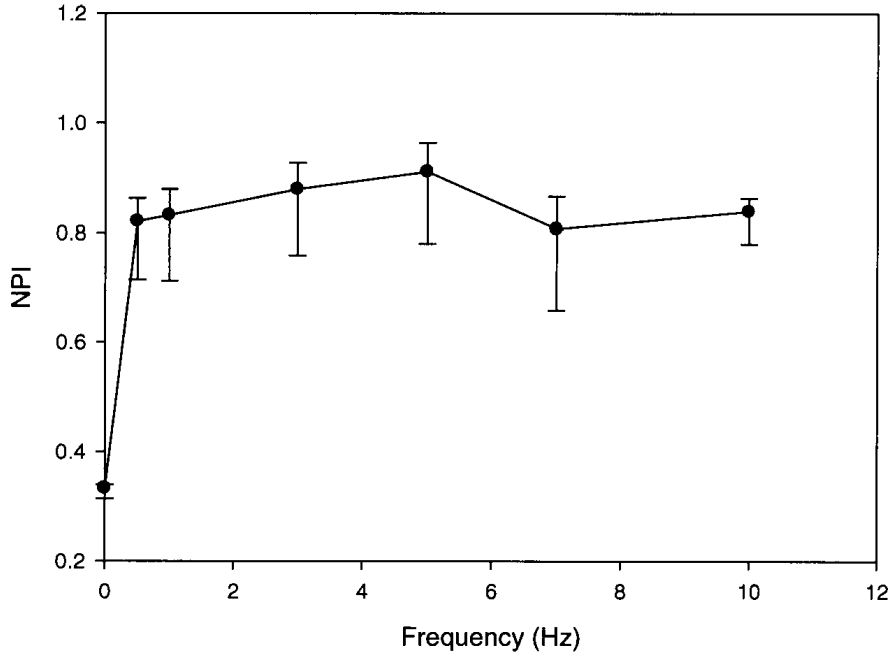

Figure 2.8: Effect of frequency on NPI, Fully Open needle valve, Type I Nozzle D=1.66 mm, 1.7% ALR, F_L=0.022 kg/s, Air, V_{air}=14 cm^3, 1 mm orifice restriction, 95% Confidence intervals

Figure 2.9 shows the effect of changing the ALR on the NPI as a function of frequency of the nozzle pulsations. Each point is obtained from the average of three tests performed under the same operating conditions. Standard deviation error bar was used to show the error for the three different runs. The error bars of Figure 2.9 show that one can not differentiate the effect of frequencies above 1Hz because of the small number of experimental replicates. However, in all cases it is clear that pulsations always improve the NPI.

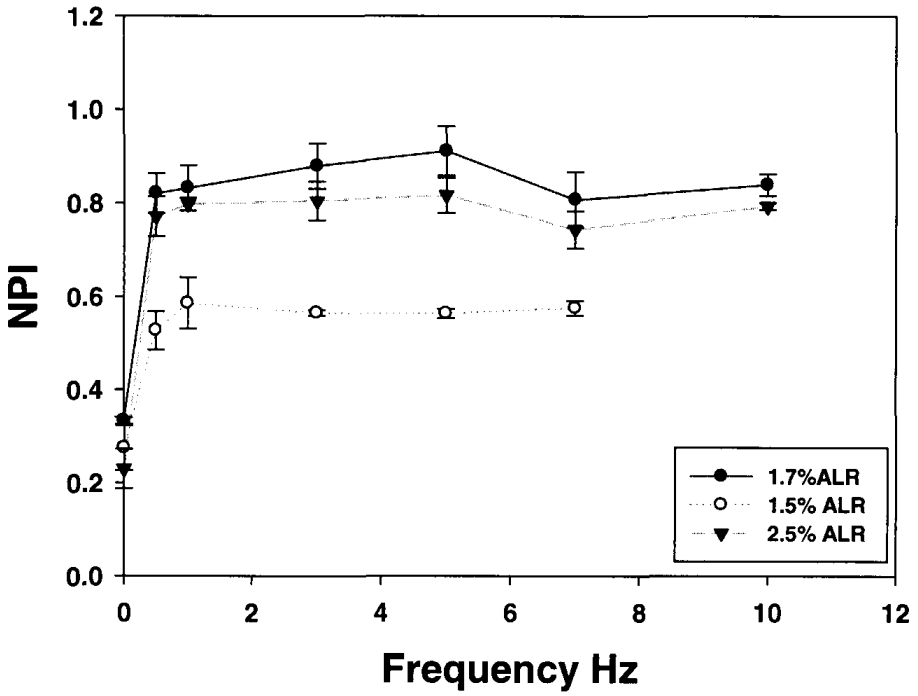

Figure 2.9: Effect of Frequency on NPI, Fully Open needle valve, Type I Nozzle D=1.66 mm, F_L=0.022 kg/s, Air, V_{air}=14 cm^3, 1 mm orifice restriction, standard deviation error bar

Figure 2.10 shows that, as a result of the pulsations, the jet penetration moves rapidly back and forth. Since the wet agglomerates form at the jet tip, this back and forth motion has two impacts: it distributes the liquid over more bed solids than a stable jet and it disrupts the agglomerates. When compared to a stable jet, a pulsating jet thus creates dryier and weaker agglomerates that are more likely to break up, which promotes further dispersion of the liquid on the bed particles.

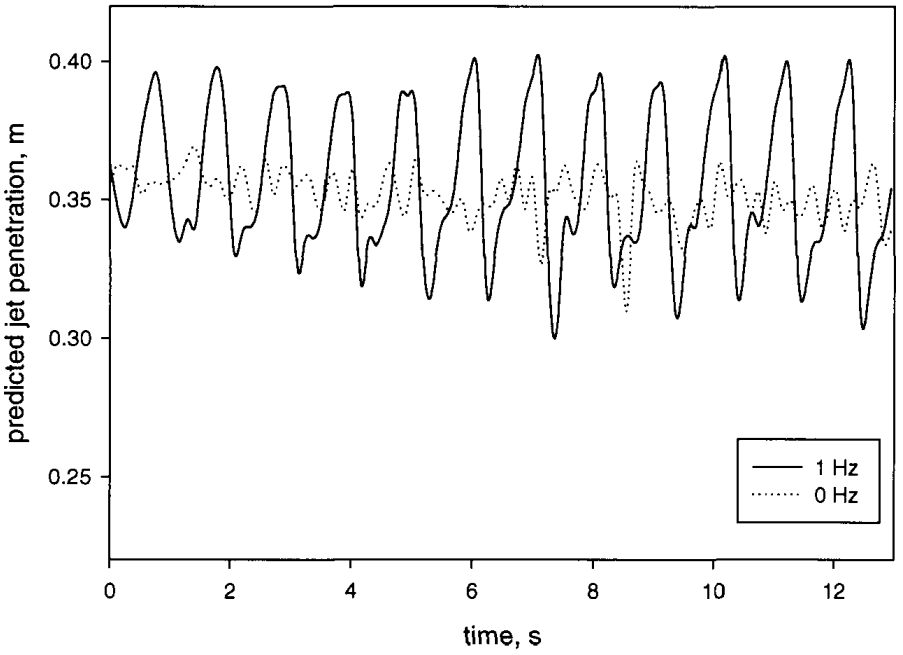

Figure 2.10: predicted jet penetration for both no imposed pulsation and imposed pulsation effect., F_L= 0.022 kg/s, 1.7% ALR , Fully open needle valve, Type I Nozzle D=1.66 mm, 1 mm restriction, Air, V_{air}=14 cm^3

Figure 2.11 illustrates the effect of changing the ALR on the NPI for various solenoid valve frequencies. Each point in the figure is the average of three tests under the same operating conditions. It is clear that the ALR of 1.7% corresponds to the highest NPI values, with and without pulsations. For all ALRs, imposing pulsations greatly improved the NPI.

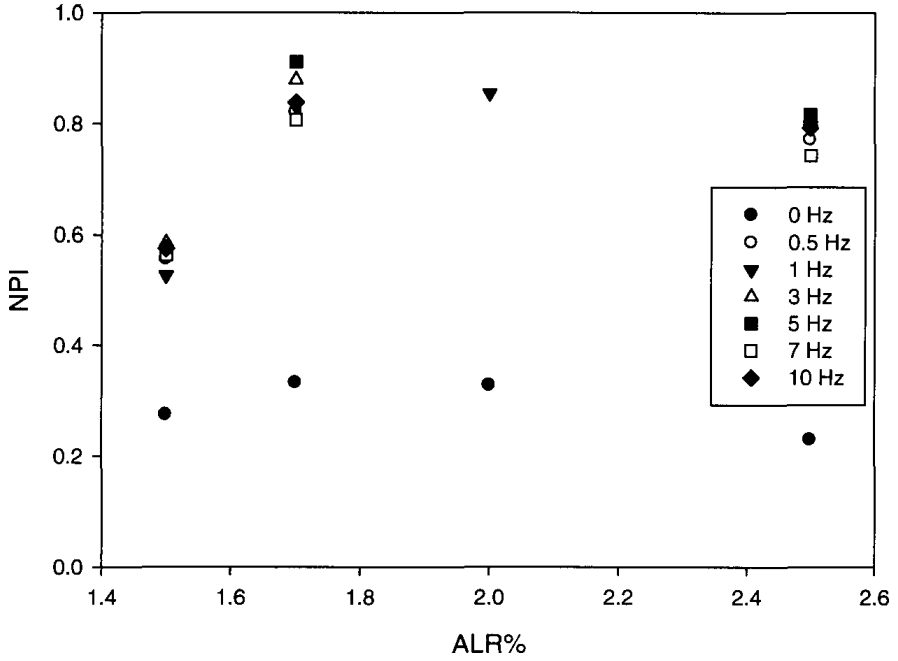

Figure 2.11: Effect of changing ALR % on NPI, Fully Open Needle Valve, F_L=0.022 (kg/s), Type I Nozzle D=1.66 mm, Air, V_{air}=14 cm^3, 1 mm Restriction Orifice

2.4.2 Optimizing the Pulsation Amplitude

The air line volume, between the solenoid valve and the restriction orifice (Figure 2.1) was changed in order to study the effect of pulsation amplitude on the NPI. The average liquid and gas flowrates were held constant. The effects of four different air line volumes are compared in Figure 2.12. To characterize the impact of the air line volume on the pulsations, the instantaneous jet penetration was calculated from the measured instantaneous air and liquid flowrates, using the method from Ariyapadi et al. (2004). In order to attain a better understanding of the effect of these pulsations, the standard deviation of the jet penetration weighted with the instantaneous liquid flow rate was calculated. According to Figure 2.12, there is a linear relationship between the standard

deviation of the jet penetration weighted with the instantaneous liquid flow rate and the NPI, with R^2= 0.9977.

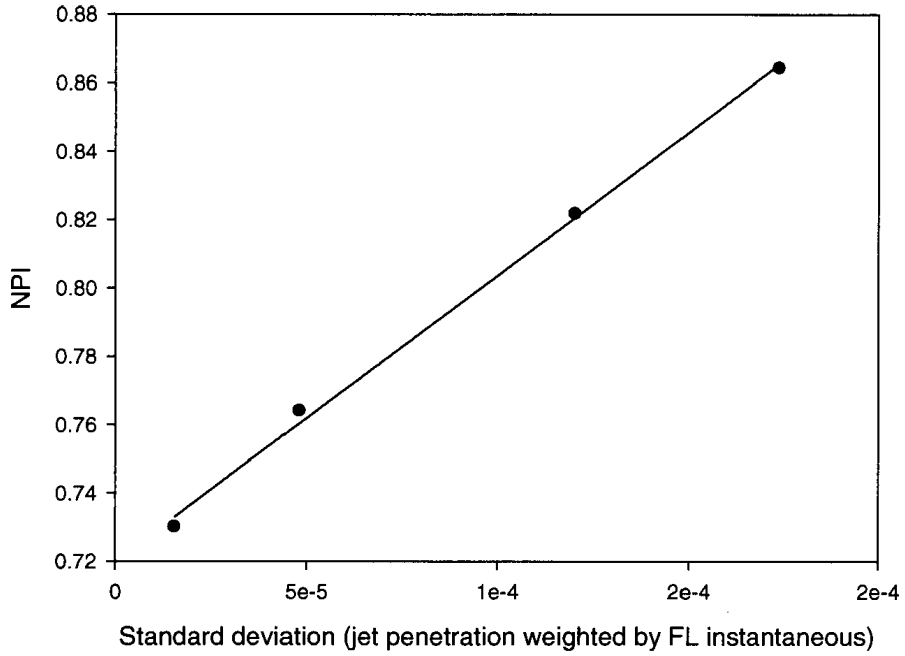

Figure 2.12: Effect of changing air line volume on NPI,1 Hz, Fully open needle valve, Type I Nozzle D=1.66 mm, F_L=0.022 (kg/s), 1 mm restriction orifice, 1.7%ALR, Air, V_{air}=14 cm^3

2.4.3 Other Conditions

The effect of pulsations on the interaction between gas-liquid jet and fluidized bed particles was studied under three different conditions to establish whether pulsations were beneficial over a wide range of conditions.

2.4.3.1 Effect of liquid flow rate

In order to study the effect of changing liquid flowrate on the NPI, six experiments were conducted under different liquid flow rates but at the same ALR (1.7%) and air line volume (14 cm^3). For three different liquid flowrates (0.019, 0.022 and 0.026 kg/s),

experiments were conducted with pulsations of 1 Hz and with no pulsations. The results of these experiments are summarized in Figure 2.13. It is clear that pulsations have a dramatic impact on NPI for all liquid flowrates.

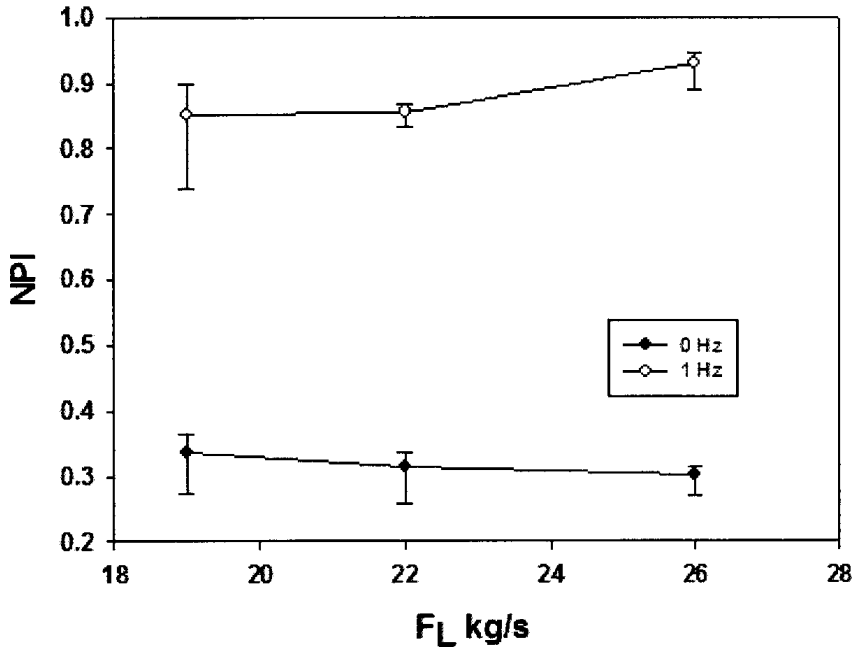

Figure 2.13: Effect of Liquid Flowrate on NPI, Fully open needle valve, Type I Nozzle D=1.66 mm, 1.7% ALR, Air, V_{air}=14 cm^3, standard deviation error bar

2.4.3.2 *Effect of nozzle geometry*

The effect of changing the nozzle geometry on NPI was investigated using both the Type I nozzle and the Type II nozzle. Several experiments were conducted for the two types of spray nozzles at constant liquid flowrate of 0.022kg/s and (ALR) of 1.7%. Figure 2.14 confirms that pulsations are beneficial with different spray nozzle geometries.

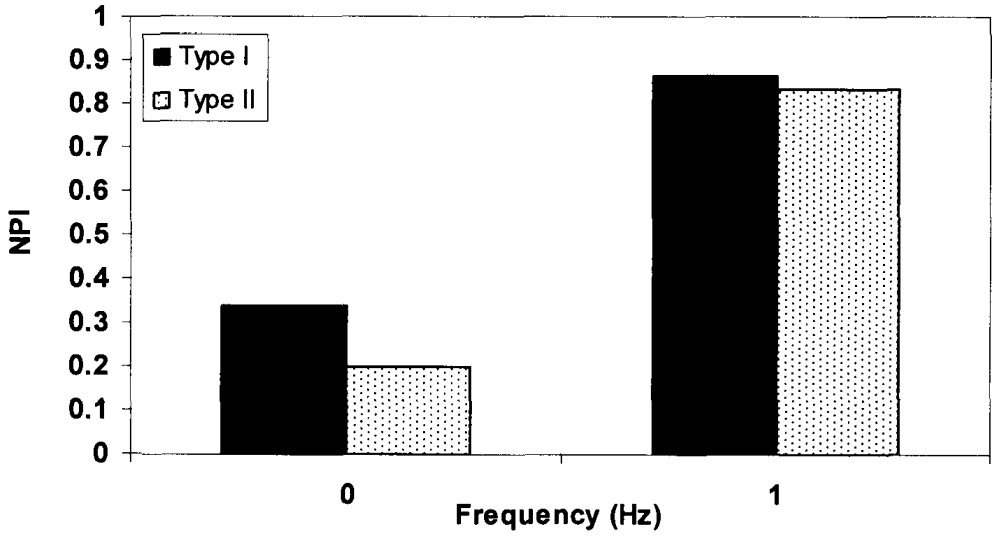

Figure 2.14: Effect of Nozzle Geometry on NPI, fully open needle valve, F_L=0.022 kg/s, 1.7%, V_{air}=14 cm^3

2.4.3.3 *Effect of atomization gas properties*

Two atomization gases were utilized to determine how gas properties affect the impact of pulsations on NPI. These two gases were air and a mixture of 18 mole% helium and 82 mole% nitrogen (this composition of mixed gas was used in the course of experiments because it has the same viscosity of steam at 300°C and to match the density and the speed of sound). Figure 2.15 shows that pulsations greatly improved the NPI with both gas types.

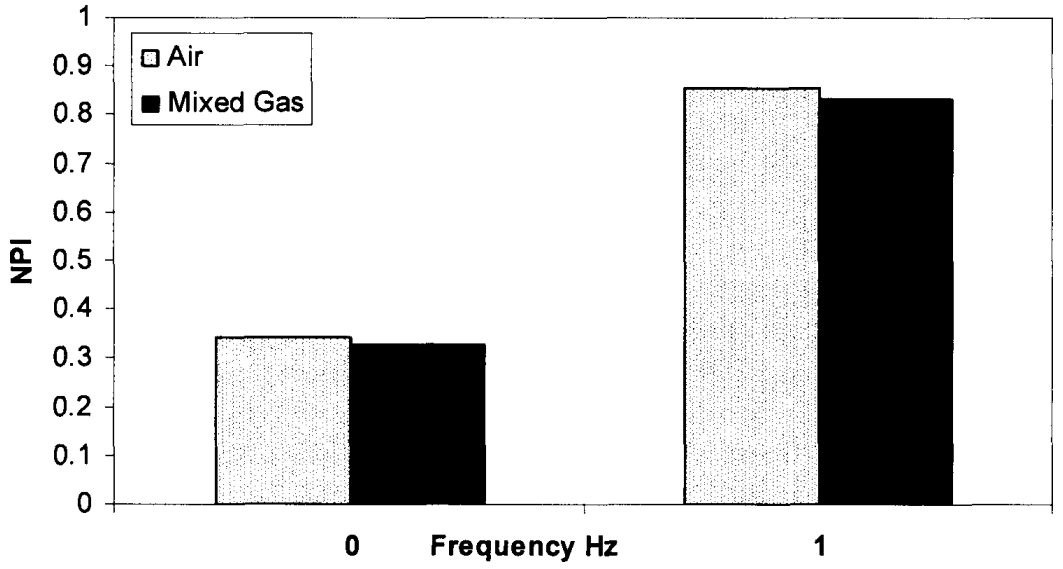

Figure 2.15: Effect of Gas Properties on NPI, fully open needle valve, TEB nozzle D=1.6 mm, V_{air}=14 cm^3

2.5 Conclusions:

This study investigates the effect of imposing fluctuations of well-defined frequency, on the interactions between a gas-liquid spray jet and fluidized particles. It was found that pulsations doubled the value of a nozzle performance index (NPI) for three different air to liquid ratios (ALR). Changing the amplitude of the pulsations showed that the pulsations improve the liquid-particles contact through complex mechanisms that require further investigation. The strong, beneficial effect of pulsations on liquid-particles contact was confirmed over a variety of operating conditions such as different liquid flowrates, gas properties and spray nozzle geometries.

2.6 References:

Ariyapadi, S., Berruti, F., Briens, C., McMillan, J. & Zhou, D. 2004, "Horizontal penetration of gas-liquid spray jets in gas-solid fluidized beds", *International Journal of Chemical Reactor Engineering,* vol. 2.

Ariyapadi, S., Holdsworth, D., Norley, C., Berruti, F., & Briens, C. 2003, "Digital X-ray imaging technique to study the horizontal injection of gas-liquid jets into fluidized beds", *International Journal of Chemical Reactor Engineering, 1*(A56).

Base et. al. 1999. *U.S. Patent No. 6,003,789.* Washington, D.C.: U.S. Patent and Trademark Office.

Benjelloun, F., Liegeois, R., Vanderschuren, J. 1995, "Penetration length of horizontal gas jets into atmospheric fluidized beds", Proc. Fluidization-VIII, J-F. Large and C. Laguerie Eds., Engineering Foundation, N.Y., 239-246.

Bruhns, S. & Werther, J. 2005, "An investigation of the mechanism of liquid injection into fluidized beds", *AICHE Journal,* vol. 51, no. 3, pp. 766-775.

Chan, E. W., Base, T. E., & McCracken, T. 2001, "Design and development of syncrude coker feed nozzles: A coker 2000 initiative", *Syncrude Canada Technical Report,*

House, P. K., Briens, C. L., Berruti, F., & Chan, E. 2008, "Effect of spray nozzle design on liquid-solid contact in fluidized beds", P*owder Technology, 186*(1), 89-98.

House, P.K., Saberian, M., Briens, C.L., Berruti, F. & Chan, E. 2004, "Injection of a liquid spray into a fluidized bed: Particle-liquid mixing and impact on fluid coker yields", *Industrial and Engineering Chemistry Research,* vol. 43, no. 18, pp. 5663-5669.

Knapper, B. A., Gray, M. R., Chan, E. W., & Mikula, R. 2003, "Measurement of efficiency of distribution of liquid feed in a gas-solid fluidized bed reactor", *Int. J. Chem. React. Eng., 1*(A35).

Leach, A., Chaplin, G., Briens, C. & Berruti, F. 2009, "Comparison of the performance of liquid-gas injection nozzles in a gas-solid fluidized bed", *Chemical Engineering and Processing: Process Intensification,* vol. 48, no. 3, pp. 780-788.

Leach, A., Portoghese, F., Briens, C. & Berruti, F. 2008, "A new and rapid method for the evaluation of the liquid-solid contact resulting from liquid injection into a fluidized bed", *Powder Technology,* vol. 184, no. 1, pp. 44-51.

McDougall, S., Saberian, M., Briens, C., Berruti, F. & Chan, E. 2005, "Effect of liquid properties on the agglomerating tendency of a wet gas–solid fluidized bed", *Powder Technology,* vol. 149, no. 2-3, pp. 61-67.

McDougall, S.L., Saberian, M., Briens, C., Berruti, F. & Chan, E.W. 2004, "Characterization of fluidization quality in fluidized beds of wet particles", *International Journal of Chemical Reactor Engineering,* vol. 2.

Portoghese, F., Ferrante, L., Berruti, F., Briens, C. & Chan, E. 2008a, "Effect of injection-nozzle operating parameters on the interaction between a gas-liquid jet and a gas-solid fluidized bed", *Powder Technology,* vol. 184, no. 1, pp. 1-10.

Portoghese, F., House, P., Berruti, F., Briens, C., Adamiak, K. & Chan, E. 2008b, "Electric conductance method to study the contact of injected liquid with fluidized particles", *AICHE Journal,* vol. 54, no. 7, pp. 1770-1781.

Portoghese, F., Berruti, F., Briens, C. & Chan, E. 2007, "Novel triboelectric method for characterizing the performance of nozzles injecting gas-atomized liquid into a fluidized bed", *Chemical Engineering and Processing: Process Intensification,* vol. 46, no. 10, pp. 924-934.

Weber, S., Briens, C., Berruti, F., Chan, E. & Gray, M. 2006, "Agglomerate stability in fluidized beds of glass beads and silica sand", *Powder Technology,* vol. 165, no. 3, pp. 115-127.

Chapter 3

ENHANCEMENT OF THE LIQUID FEED DISTRIBUTION IN GAS SOLID FLUIDIZED BEDS BY NON-MECHANICALLY INDUCED NOZZLE PULSATIONS

Rana Sabouni [1], Cedric Briens[1], Franco Berruti[1]

[1]Institute for Chemical and Fuels from Alternative Resources (ICFAR),
Engineering, University of Western Ontario
London, ON, Canada N6A 5B9

3.1 Introduction:

The injection of liquid feed into gas-solid fluidized beds is employed in many petrochemical industrials, such as fluid catalytic cracking, fluid coking, and gas phase polymerization, and in the pharmaceutical industry for granulation and agglomeration. The mechanism of liquid injection into fluid bed cokers, fluid catalytic crackers and gas-phase polyermization reactors, is critically important in order to minimize the formation of undesired agglomerates, and, thus, prevent mass and heat transfer limitations, which reduce the yields of valuable products.

In fluid coking, most of the injected liquid feed cannot vaporize at the reactor temperature and most of the liquid feed reacts before becoming vapour as found by Leclere et al. (2004) and Gray et al. (2001). Therefore, liquid droplets form agglomerates with the solid fluidized bed particles as demonstrated by Ariyapadi et al. (2003) and Bruhns & Werther (2005). In order to improve the reactor performance and enhance the production of valuable products, it is important to optimize the contact between the fluidized solids and

the injected liquid. This could be achieved by providing better distribution and efficient coating of solid particles with a thin film of liquid feed as concluded by House et al. (2004). However, this is not the case in most industrial reactors, where the injected liquid forms agglomerates and the survivability of these agglomerates is affected by fluidized bed hydrodynamics and agglomerate properties. The weaker and drier agglomerates can be easily broken up to smaller agglomerates, while the wetter and stronger agglomerates are difficult to break up and can survive for a long time if the fluidized bed agitation is not intense enough, causing heat and mass transfer limitations (McDougall et al., 2005; Weber et al., 2006). By using X-ray imaging, Ariyapadi et al. (2003) showed that agglomerates formed at the tip of the spray jet cavity.

Studies have been conducted to investigate the parameters affecting the interaction between gas-liquid jets and fluidized beds aimed at minimizing the undesired agglomerates and maximizing mass and heat transfer, thus making the unit more efficient and profitable. Knapper et al. (2003) showed that the quality of the interaction between the gas-liquid jet and the fluidized bed is strongly impacted by nozzle performance.

Portoghese et al. (2008) investigated the use of conductance probes to evaluate the nozzle performance. The conductance probes were used to measure the electrical conductance of the bed solids after completing the liquid injection and defluidizing the wetted particles. If most of the injected liquid is concentrated in a few agglomerates, most of the bed is dry and the bed conductance is small. Conversely, if the liquid is well distributed on the particles, forming a liquid film on the particles surface that connects all the particles, the bed conductance is large. Leach et al. (2008) improved this method

through the definition of a Nozzle Performance Index (NPI) to rank various nozzles according to their liquid-solid contact performance.

Ariyapadi et al. (2004) developed a correlation to predict the horizontal jet penetration of gas-liquid sprays jets in a gas-solid fluidized beds by combining both a theoretical model to predict the momentum flux of two phase sprays with a correlation originally proposed by Benjelloun et al. (1995) for the penetration of gas jets.

Under some flow conditions, the liquid flow through gas-liquid spray injectors, such as used in the fluid coking process, becomes unstable. Previous studies done by Chan et al. (2001) and McDougall et al. (2004) showed that such unstable, pulsating spray injectors were detrimental. Pulsating sprays reduced the bed fluidity and promoted the formation of agglomerates as found by McDougall et al. (2004). Chan et al. (2001) also found that pulsating flow may reduce the liquid yields and increase sulfur dioxide emissions.

On the other hand, our previous work, described in Chapter 2, determined that imposing liquid flow pulsations with a solenoid valve closing and opening with a frequency of 1 to 10 Hz nearly doubled the Nozzle Performance Index (NPI). However, mechanical means of inducing pulsations, such as solenoid valves, may not be reliable enough for industrial applications. This study, therefore, focuses on the use of non-mechanical means of inducing liquid flow pulsations, i.e. on the choice of geometric and operating parameters leading to the development of non-mechanically induced pulsations in the flow. The liquid flow was split into two streams, one of which was mixed with gas in proportions that induced stable slug flow; the two streams were then recombined just upstream of the spray nozzle.

3.2 Apparatus:

The experimental apparatus used in the current study is shown in Figure 3.1. The experiments were conducted in a fluidized bed with a rectangular cross-section of 1.2 m by 0.15 m. It was filled with 250 kg of silica sand particles with a Sauter mean diameter of 190 μm and an apparent particle density of 2600 kg/m^3 (Group B of the Geldart's powder classification). In addition, it was fluidized by air at a superficial gas velocity of 0.24 m/s. Three parallel sonic nozzles were used to control the fluidization air flowrate. The outgoing air with the entrained particles were sent to two cyclones placed in series to separate the entrained particles from the gas exiting and to return them back into the bed.

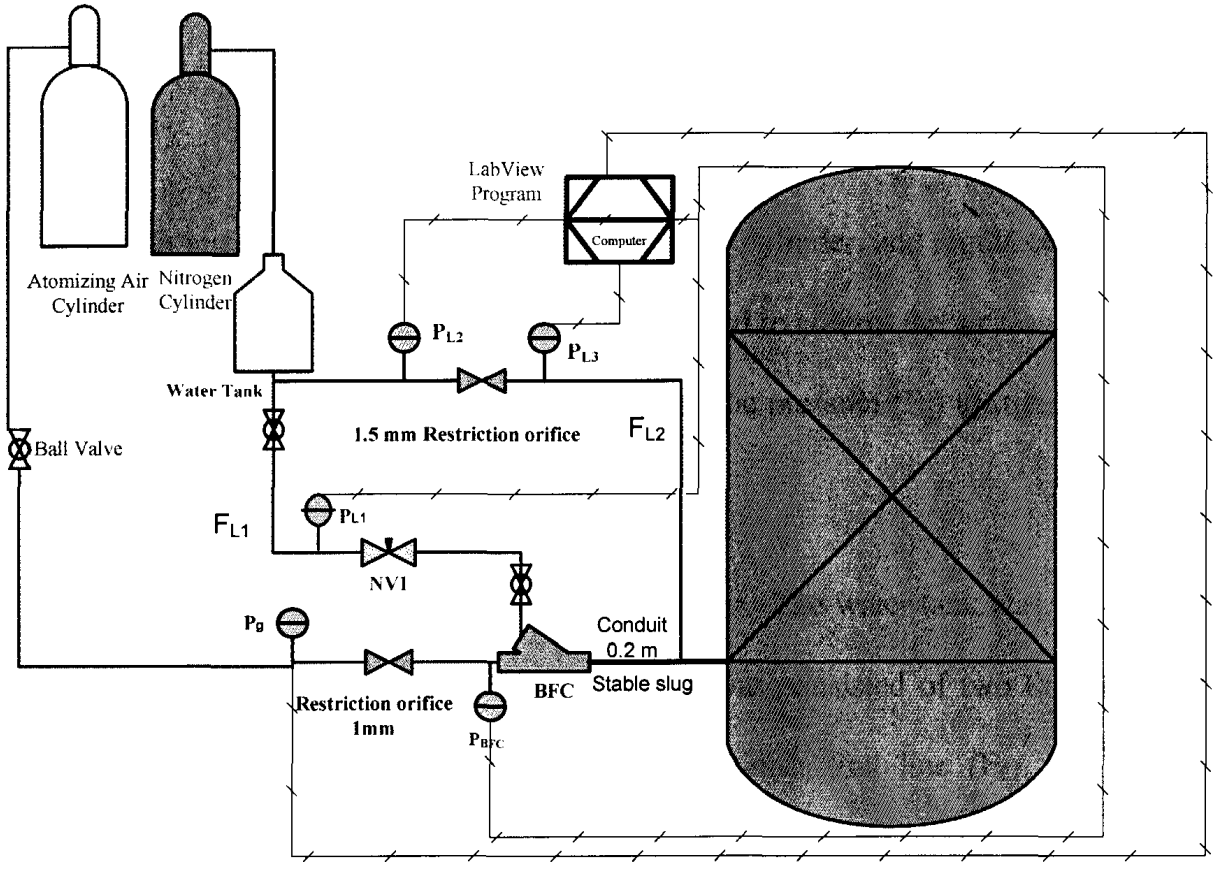

Figure 3.1: Schematic Diagram of Experimental Apparatus.

Both air and water were mixed using a pre-mixer before being injected through the spray nozzle into the fluidized bed. A pressure transducer used to measure the pressure (P_{BFC}) at the pre-mixer level. The Type I atomized air nozzle was used as illustrated in Figure 3.2. The Type I nozzle has a throat diameter of 1.6 mm. For each test, the nozzle was located 0.6 m above the fluidization gas distributor and protruded into the bed for 0.05m from the wall.

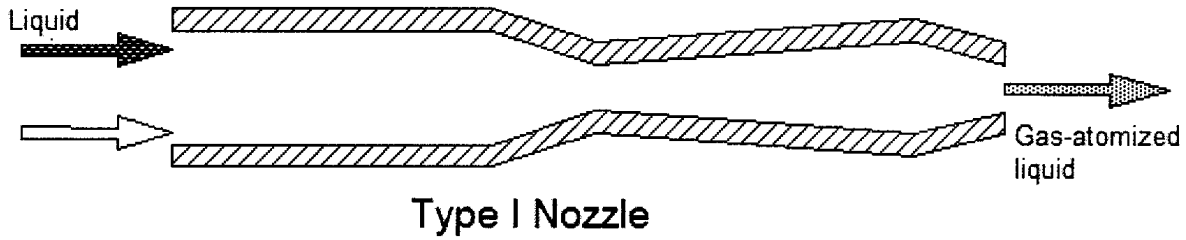

Figure 3.2: Internal Geometry of Type I Nozzle.

The air stream was supplied from a medical air cylinder, and regulated by a pressure regulator. Moreover, 1 mm restriction orifice was used to control the air flowrate on the air stream. A pressure transducer was used to measure the pressure (P_g) upstream of the 1mm restriction orifice (Figure 3.1).

The injected liquid stream was de-ionized water. The water tank was pressurized by an ultra pure nitrogen cylinder. The liquid stream was consisted of two lines in order to create the desired non-mechanically induced pulsations: first line (F_{L1}, 1.2 m length) included a pressure transducer to measure the pressure drop across the needle valve. The needle valve was used to control the liquid flow rate; water from this line was mixed with gas in proportions that create slug flow through the conduit (0.20 m, Figure 3.1) upstream

the spray nozzle with a high ARL%. Lamari et al. (2001) demonstrated that, the two-phase flow regime in the conduit leading up to the nozzle has a significant impact on the stability of the nozzle. Dispersed bubble flow (gas bubbles randomly dispersed in a continuous liquid phase) in the conduit section is thought to produce a stable spray. However, an intermittent or slug flow pattern, which is associated with pressure pulses and severe pressure oscillations, is expected to cause an unstable spray. Poor upstream mixing or an improper gas-to-liquid ratio can also cause pulsing in a nozzle, due to liquid slugs and gas pockets formed in the conduit. In addition, previous studies have used pressure fluctuations measured in a conduit upstream of feed nozzles to characterize the degree of heterogeneity (Ariyapadi et al., 2003) and (Ariyapadi et al., 2005). Heterogeneous two-phase flow regimes such as slug flow are characterized by low frequency, high amplitude pressure fluctuations.

The key feature of this design is to create stable slug flow in the first line, using a gas to liquid ratio that maximizes slug flow. Such slug flow would give poor spraying. To reduce the amplitude of the flow pulsations and reduce the gas to liquid ratio to the desired value (1.2 % ALR), the gas-liquid mix from the first line is combined with additional liquid. Pulsations are then gradually dampened along the line leading to the spray nozzle.

The second water line (F_{L2}) reduced the ALR% to the desired value of (1.2%). It included 1.5 mm gas orifice restriction (to control the liquid flow rate) and two pressure transducers to measure the pressure drop across the orifice restriction. The second water line was combined with stream coming out of the pre-mixer upstream of the spray nozzle (Figure 3.1). The length of this line is 0.95 m.

Several horizontal two phase flow regime maps have been reported in literature. In order to know the type of flow pattern in the conduit, flow map such as the one developed by Taitel & Dukler, 1976 was used in this study to confirm reaching the slug flow regime.

All pressure transducers were calibrated and connected to a data acquisition system to measure the pressure drops across the air restriction orifice (P_g-P_{BFC}), across the liquid needle valve (P_L-P_{BFC}), and across the water orifice restriction ($P_{L2} - P_{L1}$) from which the instantaneous gas and liquid flowrates to the pre-mixer could be determined.

The time-averaged liquid flowrate was controlled by using pressure regulator placed on the nitrogen ultra high pure cylinder to adjust the liquid tank pressure. In most of the experiments of this study, the time-averaged liquid flowrate was held at 0.027 kg/s, except when studying the effect of liquid flowrate experiments. The time-averaged air flowrate was controlled using the pressure regulator placed upstream of the gas restriction orifice and the time averaged air to liquid ration (ALR) was kept constant at 1.2%.

The temperature of the bed was measured using four thermocouples, placed in the bed to ensure that the bed temperature was 20 degree Celsius at the start of each injection. All the thermocouples were type J and placed in the bed at heights of 15, 35, 55 and 75 cm above the gas distributor.

Based on the previous work of Portoghese et al. (2008), the bed conductivity can be measured by applying a sinusoidal current to the fluidized bed and measuring the voltage drop across the fluidized bed, and this technique was used in the current work. A function generator was used to create a sinusoidal waveform with a 6.7 MS voltage. Figure 3.3

shows the circuit diagram used in the experiments. The conductivity of the bed was measured using an electrode which was placed at the centre of the bed, 0.37 cm above the gas distributor. The electrode was made of a stainless steel hollow tube with an outer diameter of 7 mm. It was connected to a 51 kΩ resistor. Figure 3.4 shows the schematic diagram of the electrode circuit. The voltage imposed by the signal generator was used with the voltage measured across the resistor to calculate the bed conductance using Ohm's law:

$$G_{bed} = \frac{1}{R_{bed}} = \frac{1}{R_m} * \left[\frac{V_2}{V_1 - V_2} \right] \tag{3.1}$$

A data acquisition system was used to measure the voltage V_1 imposed by the signal generator, the voltage V_2 across the resistor, and the temperature of the four thermocouples, at a frequency of 100 Hz.

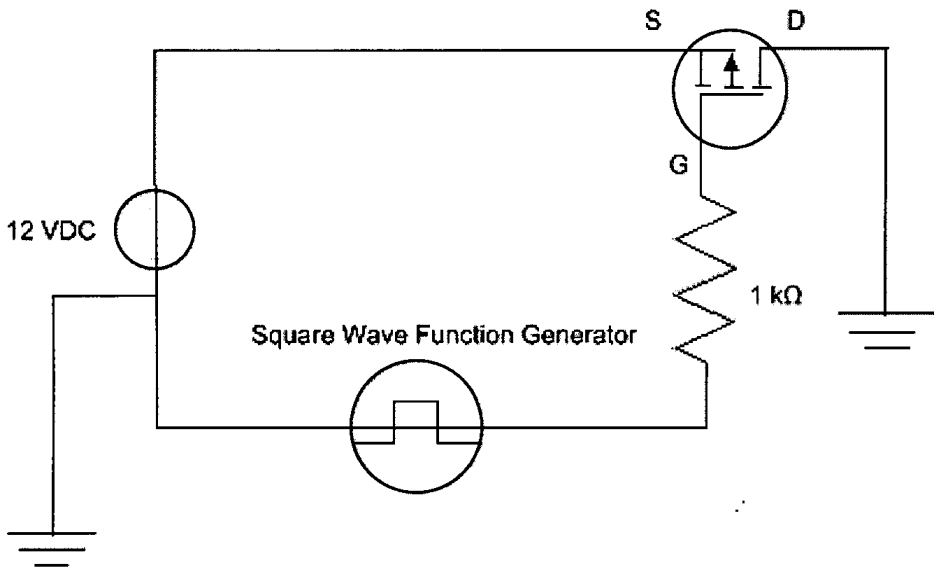

Figure 3.3: Circuit Diagram of used in the experiments.

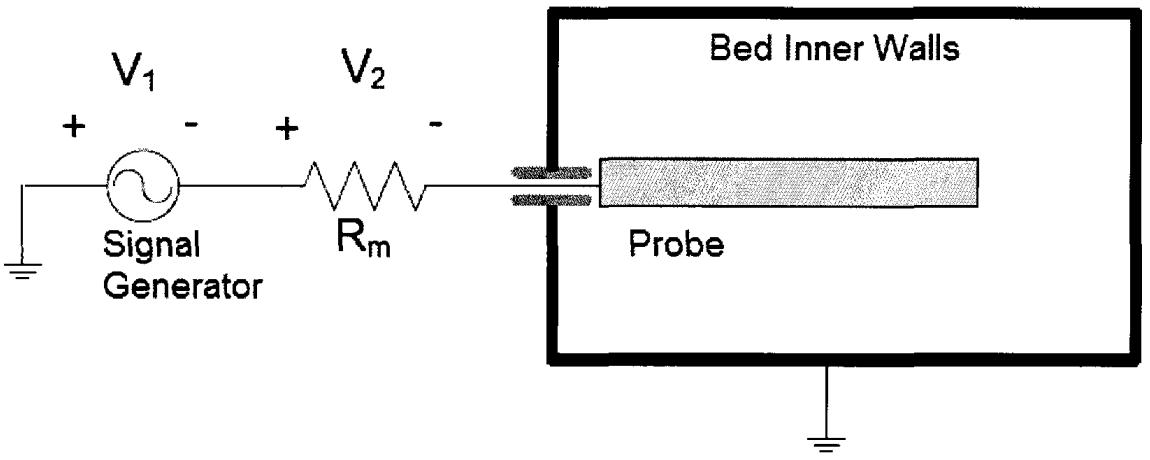

Figure 3.4: Schematic Diagram of Conductive Probe.

3.3 **Experimental Procedure:**

The objective of the conducted experiments was to study the effects of non-mechanically induced pulsations of the spray nozzle on the jet-bed interaction, which was characterized by a Nozzle Performance Index (NPI) (Leach et al., 2008; Portoghese et al., 2008).

The following experimental procedure was used for all experiments:

1) The fluidization air velocity was set to 0.25 m/s.

2) The needle valve opening was set differently depending on the experiments.

3) At t=0, the data acquisition was started using the LabView program (version 8)

4) After 10 s, water was injected into the bed through the spray nozzle. The duration of injection was 15 s.

5) At t = 25s, the liquid injection and fluidization air were stopped, and the bed was defluidized for 7 minutes. The conductance of the fluidized bed solids were measured by the conductance probe technique during the 7 minutes of de-fluidizing as developed by (Leach et al., 2008). The authors found that, the conductance of the bed was low when the bed is dry and defluidized, because silica sand particles don't conduct electricity. However, when these particles were wetted with water the conductity of the bed increases because the water forms high conductance paths and transfer electrical current. Therefore, if the water is well distributed over the solid particles there will be more conductance paths causing higher bed conductance. If the bed maintained fluidized for short time after the injection of water the longer the mixing of the bed will make the larger wetter and heavier liquid solid agglomerates settle away form the electrode region. Therefore, performing the conductivity measurements during the 7 minutes of de-fluidizing.

6) At t=7 min the bed was refluidized again to dry it by vaporizing the water and to bring the bed temperature back to its initial value of 20 ^{o}C before starting a new experiment.

To create the natural pulsations of the water and air flows with a non mechanical method such as a solenoid valve, water and air flowrates were controlled using the air and nitrogen cylinders (Figure 3.1). Several spray trials were performed in open air to adjust conditions to get either the most effective pulsations or a visually stable spray. To have visually stable flow the first liquid line was turned off during the injection and the water flows throw the second water line only.

The time-averaged atomization gas flowrate was maintained constant for all runs. The tests were repeated for visually stable and pulsating flows, which were all operated under the same conditions. The pressure values for the pre-mixer (PBFC), liquid (PL), and air (Pg) streams were recorded during each experiment.

As a last step, a plot of bed conductance vs. time was used to estimate the Nozzle Performance Index (NPI), which is defined as the slope of the trend-line of that plot, using a logarithmic scale for time. This method was developed by Leach et al. (2008). A high NPI value means that water diffuses quickly through the defluidized bed, increasing the bed conductance quickly. A high NPI therefore corresponds to a good original distribution of the liquid on the bed particles, just before defluidization. Figure 3.5 shows an example of the change with time of the conductance of the defluidized bed. To disregard any irregularities in the start-up of the de-fluidization, only data subsequent to t = 50 s were used. In the case corresponding to Figure 3.5, the NPI was 0.6676.

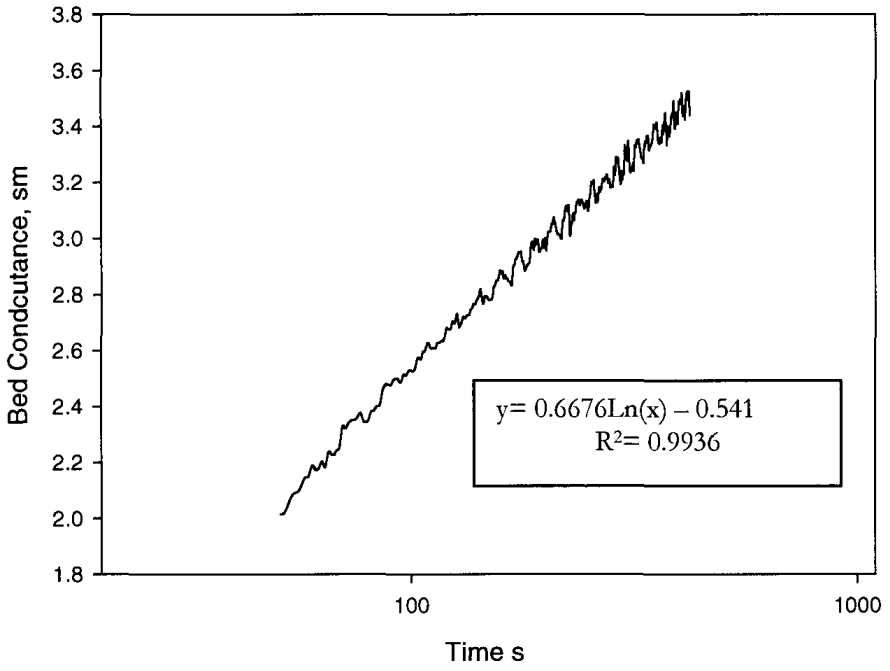

Figure 3.5:Conductance method, non-mechanically pulsating flow, Fully open needle valve, Type I Nozzle D=1.66 mm, F_L=0.027 kg/s, 1 mm gas restriction orifice, 1.2 ALR%

3.4 Result and discussion

3.4.1 Effect of liquid flowrate

Figures 3.6 and 3.7 demonstrate the variations with time of the liquid and gas flow rates for both visually stable and non-mechanically pulsating flows, respectively, at a constant liquid flowrate of 0.027 kg/s. A dramatic difference in the pulsations of the liquid flowrate is very evident from these results.

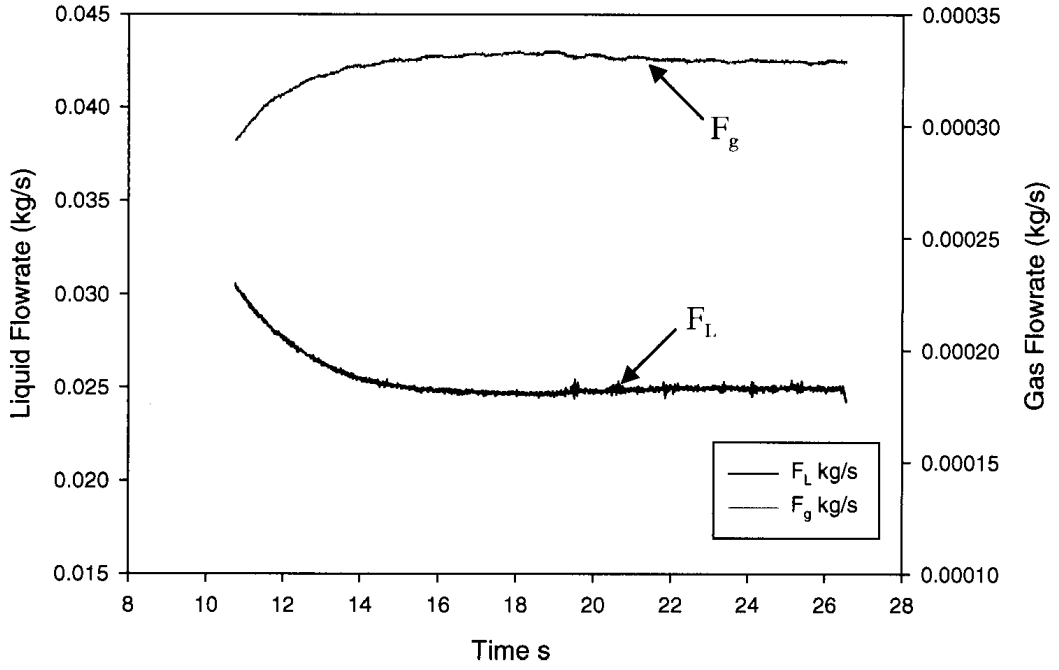

Figure 3.6: Visually stable, 1.2% ALR, F_L=0.027 cm3, Type I spray nozzle D=1.66 mm, 1 mm gas orifice restriction, fully open needle valve.

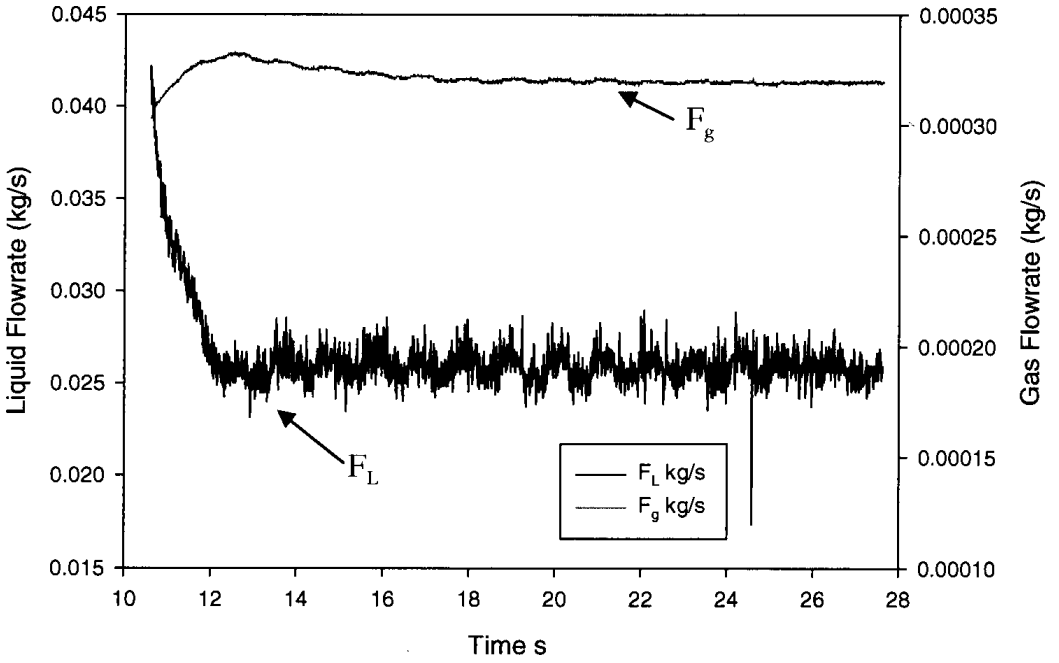

Figure 3.7: Non-mechanically pulsating flow, 1.2% ALR, F_L=0.027 cm3, Type I spray nozzle D=1.66 mm, 1 mm gas orifice restriction, fully open needle valve.

Figure 3.8 demonstrates the effect of changing the liquid flow rate on the NPI for both visually stable and non-mechanically pulsating flows. The liquid flow rate was varied (0.02 kg/s, 0.024 kg/s and 0.027 kg/s), but the air-to-liquid ratio (ALR) was kept constant at 1.2wt%. The impact of pulsations on the NPI is striking. The largest impact of pulsations on the NPI is observed at the 0.027 kg/s liquid flow rate (Figure 3.8).

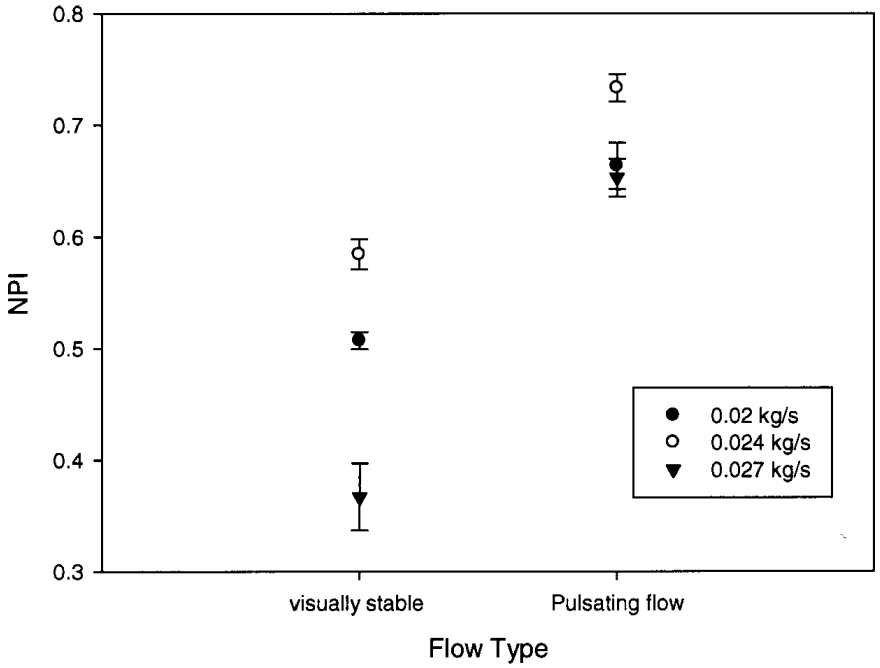

Figure 3.8: NPI vs. Liquid flow rate, 1.2% ALR, 1 mm gas orifice restriction, Fully Open needle valve, Type I Nozzle D=1.66 mm, standard deviation error bar.

Figure 3.9 compares the predicted jet penetrations which were calculated with the model from Ariyapadi et al. (2004) for both visually stable and non-mechanically pulsating flows at a 0.027 kg/s liquid flow rate. As a result of the pulsations, the jet penetration moves rapidly back and forth (Figure 3.9). Since the wet agglomerates form at the jet tip, this back and forth motion has two effects: it involves more bed solids into the wet agglomerates and it disrupts the agglomerates. This means that the wet agglomerates are

smaller, dryier, and more likely to break up, which promotes further dispersion of the liquid on the bed particles.

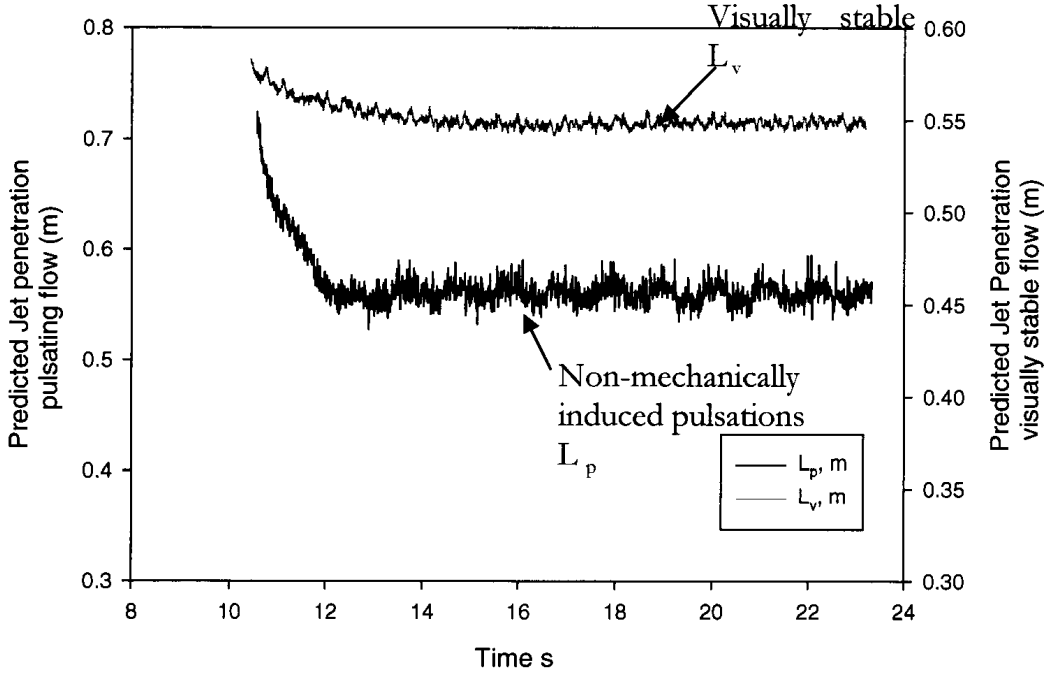

Figure 3.9: Jet penetration for visually stable and non-mechanically induced pulsating flows, fully open needle valve, F_L=0.027 kg/s, 1 mm gas orifice restriction

3.4.2 Effect of gas restriction

To study the effect of the gas restriction on the NPI, several experiments were performed using 0.7 mm, 1 mm, and 1.2 mm restriction orifices in the air line. the gas restriction was used to control the gas flowrate. Figure 3.10 shows the effect of changing gas restriction on NPI at a 0.027 kg/s liquid flow rate and 1.2wt% ALR. The 1 mm orifice restriction allowed for the largest improvement in NPI with pulsating flow (Figure 3.10). The jet penetration of visually stable and pulsating flows is shown in Figure 3.11 for the 0.7 mm orifice restriction. Pulsations affect the jet penetration inside the bed, which improves the NPI when compared to the visually stable jet penetration.

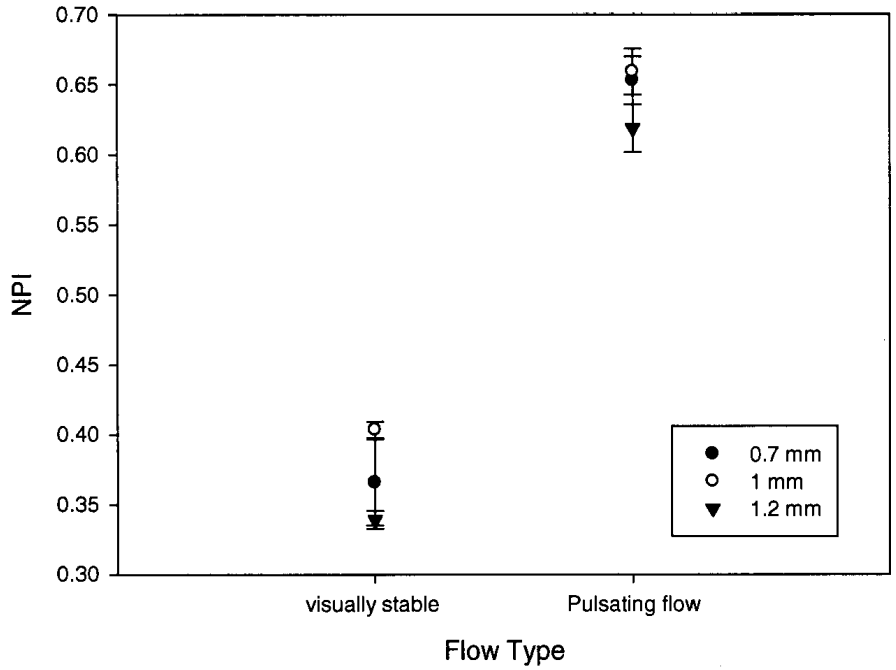

Figure 3.10: NPI vs. gas restriction, 1.2% ALR, F_L= 0.027 kg/s, fully open needle valve, Type I spray nozzle D=1.66 mm

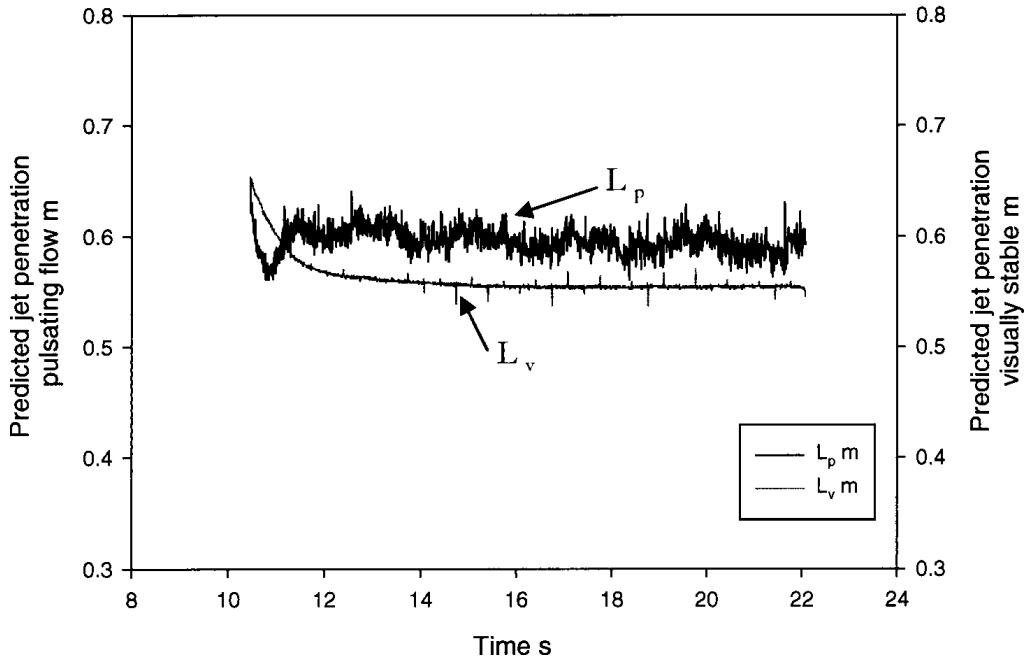

Figure 3.11: Jet penetration vs visually stable flow and non-mechanically pulsating flow, 0.7 mm gas orifice restriction, 1.2% ALR, F_L= 0.027 kg/s, fully open needle valve, type I spray nozzle D=1.66 mm

3.4.3 Effect of liquid restriction

The effect of the liquid restriction of the first water line on the NPI was studied under four positions of the needle valve 1) fully open needle valve corresponds to 0.026 kg/s time averaged liquid flow rate and at P_L= 27 psig (179 KPa), 2) one rotation close needle valve corresponds to 0.021 kg/s and at P_L= 22 psig (152 KPa) , 3) two rotations close needle valve corresponds to 0.019 kg/s and at P_L= 20 psig (137 KPa) 4) three rotations close needle valve corresponds to 0.017 kg/s and at P_L= 18 psig (124 KPa) . The liquid restriction was used to control the liquid flow rate. Figure 3.12 shows that pulsations increase the NPI from 0.3591 for visually stable flow to 0.6676 for non-mechanically pulsating flow when the needle valve is fully open. Figures 3.8 and 3.7 show the liquid and gas flow rates for pulsating and visually stable flows, respectively. To have a clear understanding of the behaviour of the pulsating flow, the jet penetration was calculated for both flows and shown in Figure 3.13. The jet penetrations show that, even with a small jet pulsation amplitude of 5 cm, there is still a remarkable effect of pulsating flow on NPI.

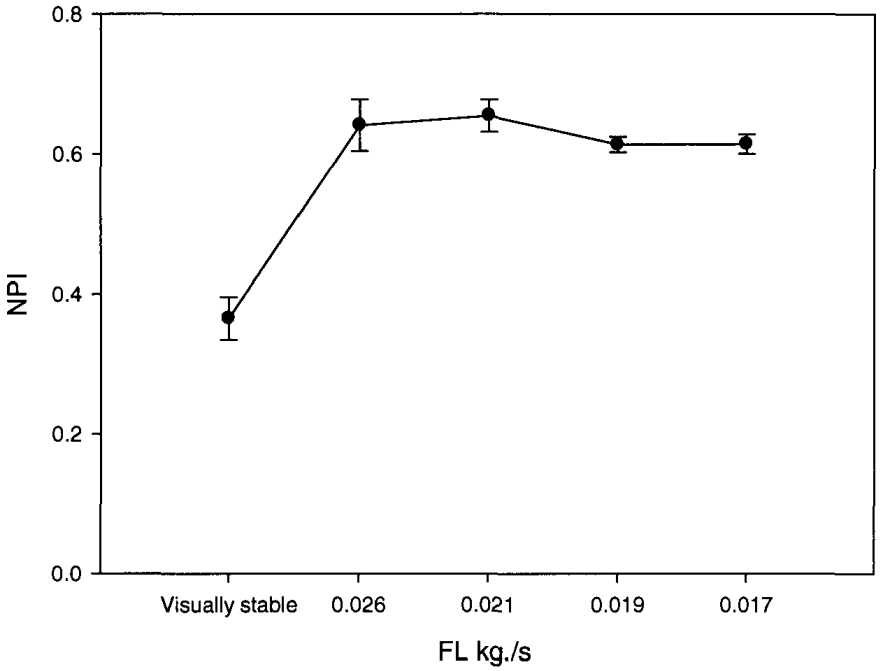

Figure 3.12: NPI vs. liquid restriction, 1.2% ALR, 1 mm gas orifice restriction, type I spray nozzle D=1.66 mm

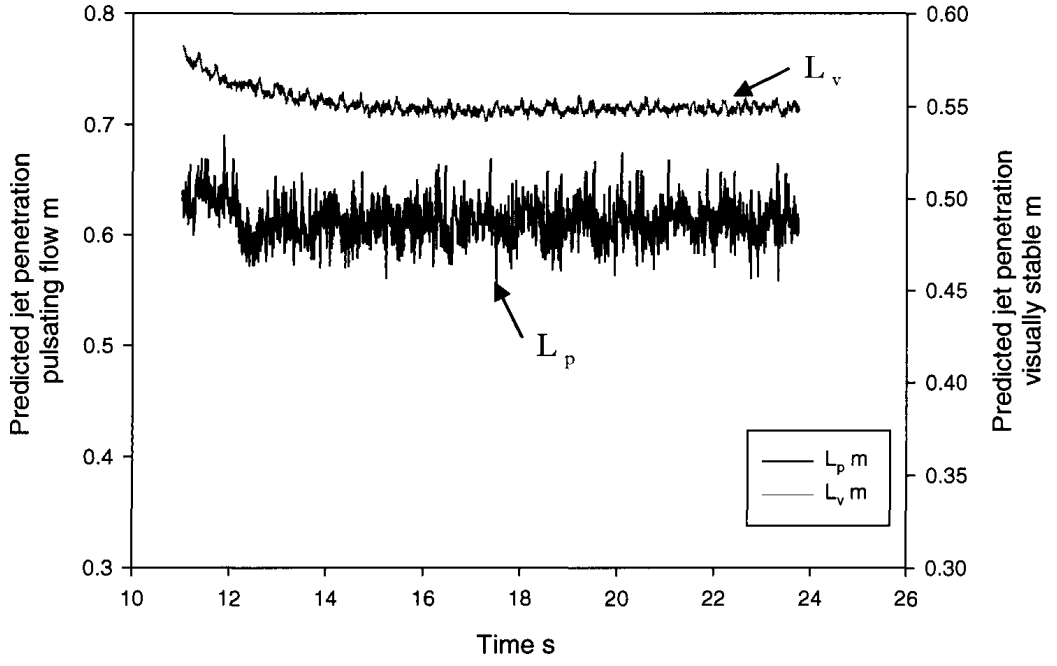

Figure 3.13: jet penetration for visually stable and non-mechanically pulsating flow, one rotation close needle valve, type I spray nozzle D=1.66 mm, 1.2% ALR

3.4.4 Relation between gas, liquid flowrates and predicted jet penetration

It was found that pulsations improved the interactions between gas-liquid jet and fluidized bed particles. Figure 3.14 and 3.15 demonstrate the relationship between the instantaneous gas and liquid flow rates and the jet penetration at a liquid flowrate of 0.027 kg/s and 1.2 % ALR. The jet penetration is predominantly related to the liquid flow rate, as shown in Figure 3.14, and there is a weak relationship between gas flow rate and jet penetration (Figure 3.15). In addition, this finding can be confirmed by the results obtained previously using a solenoid valve to impose pulsations of well-defined frequency and described in Chapter 2. Figure 3.16 shows that, for these earlier experiments, there also was a relationship between instantaneous liquid flow rate and jet penetration.

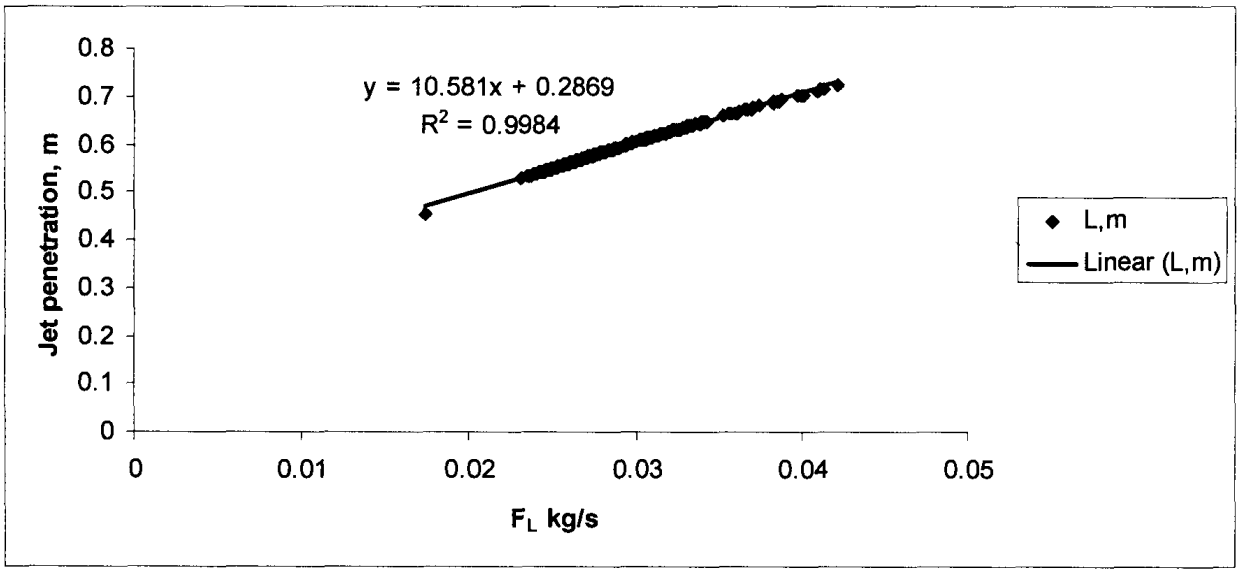

Figure 3.14: Relationship between instantaneous liquid flow rate and jet penetration for non-mechanically pulsating flow, fully open needle valve, Type I spray nozzle D=1.66 mm, 1.2% ALR, F_L=0.027 kg/s

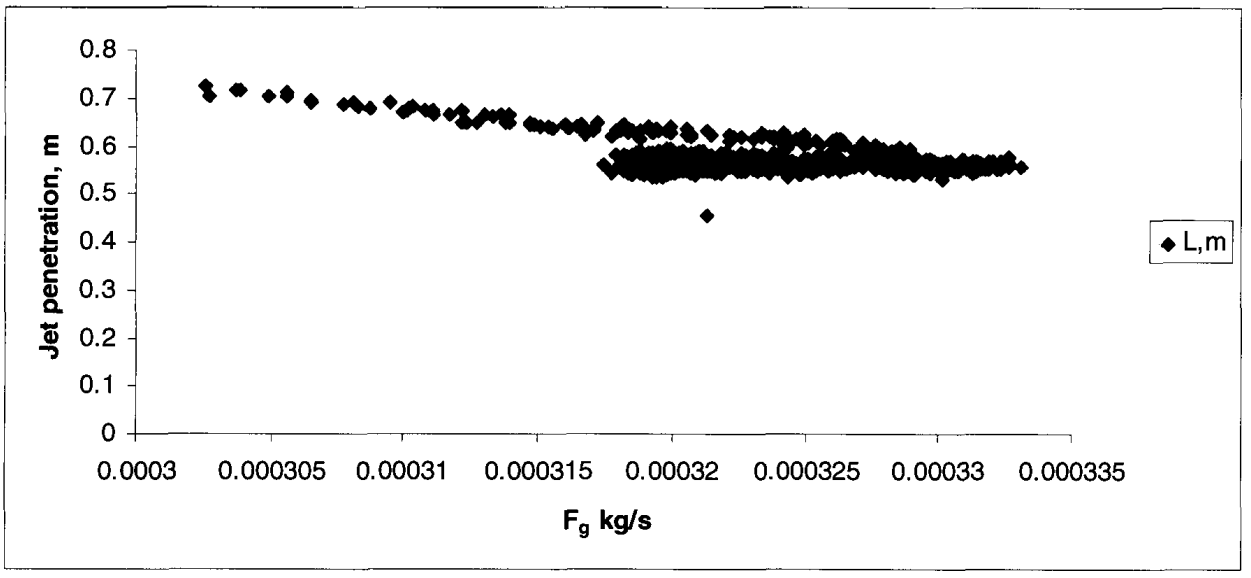

Figure 3.15: Relationship between instantaneous gas flow rate and jet penetration for non-mechanically pulsating flow, fully open needle valve, Type I spray nozzle D=1.66 mm, 1.2% ALR, F_L=0.027 kg/s

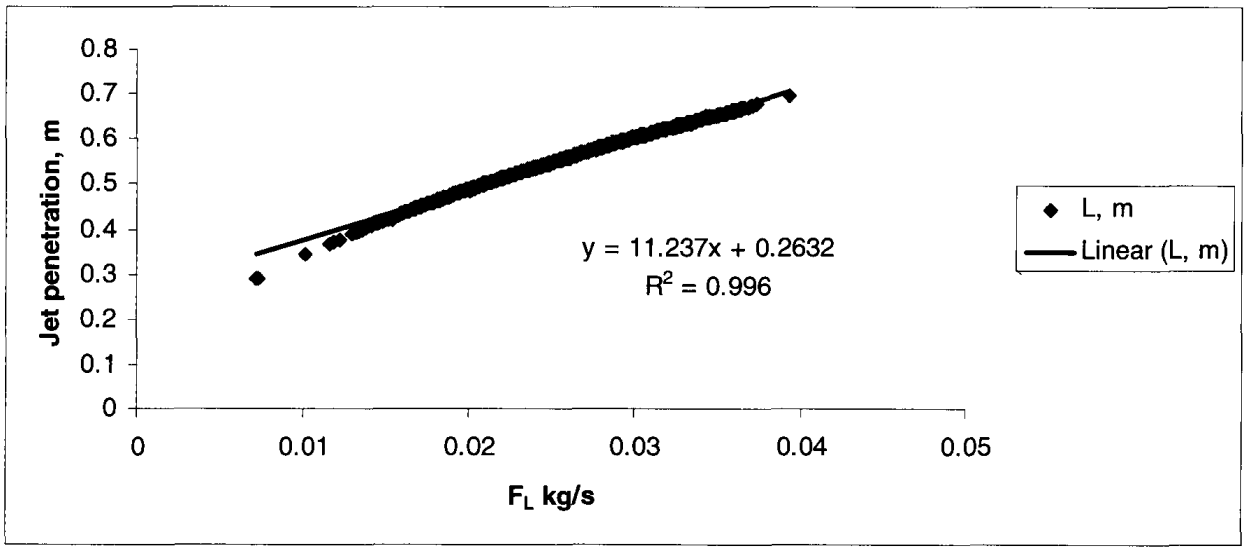

Figure 3.16: Relationship between instantaneous liquid flow rate and jet penetration for imposed pulsation using solenoid valve, fully open needle valve, Type I spray nozzle D=1.66 mm, 1.7% ALR, F_L=0.027 kg/s

3.5 Conclusions:

This study investigated the effect of non-mechanically induced flow pulsations on the interactions between a gas-liquid spray jet and fluidized particles. It was found that pulsations increased the value of a the nozzle performance index (NPI) by 20% to 50%. Jet

penetration calculations showed that small pulsations of the liquid flow can have a dramatic effect on NPI through complex mechanisms that are likely related to the rapid expansion-contraction of the spray jet cavity. Finally, it was found that jet penetration is strongly related to liquid flow rate rather than to the gas flow rate.

3.6 References:

Ariyapadi, S., Berruti, F., Briens, C., McMillan, J. & Zhou, D. 2004, "Horizontal penetration of gas-liquid spray jets in gas-solid fluidized beds", *International Journal of Chemical Reactor Engineering,* vol. 2.

Ariyapadi, S., Berruti, F., Briens, C., Knapper, B., Skwarok, R., Chan, E., 2005 "Stability of horizontal gas–liquid sprays in open air and in a gas–solid fluidized bed", *Powder Technology,* 155 161–174.

Ariyapadi, S., Holdsworth, D., Norley, C., Berruti, F., & Briens, C. 2003, "Digital X-ray imaging technique to study the horizontal injection of gas-liquid jets into fluidized beds", *International Journal of Chemical Reactor Engineering, 1*(A56)

Benjelloun, F., Liegeois, R., Vanderschuren, J. 1995, "Penetration length of horizontal gas jets into atmospheric fluidized beds", Proc. Fluidization-VIII, J-F. Large and C. Laguerie Eds., Engineering Foundation, N.Y., 239-246

Bruhns, S. & Werther, J. 2005, "An investigation of the mechanism of liquid injection into fluidized beds", *AICHE Journal,* vol. 51, no. 3, pp. 766-775.

Chan, E. W., Base, T. E., & McCracken, T. 2001, "Design and development of syncrude coker feed nozzles: A coker 2000 initiative", *Syncrude Canada Technical Report,*

Gray, M.R., Le, T., McCaffre, W.C., Berruti, F., Soundararajan, S., Chan, E., Huq, I. & Thorne, C. 2001, "Coupling of mass transfer and reaction in coking of thin films of an Athabasca vacuum residue", *Industrial and Engineering Chemistry Research,* vol. 40, no. 15, pp. 3317-3324.

House, P.K., Saberian, M., Briens, C.L., Berruti, F. & Chan, E. 2004, "Injection of a liquid spray into a fluidized bed: Particle-liquid mixing and impact on fluid coker yields", *Industrial and Engineering Chemistry Research,* vol. 43, no. 18, pp. 5663-5669.

Knapper, B. A., Gray, M. R., Chan, E. W., & Mikula, R. 2003, "Measurement of efficiency of distribution of liquid feed in a gas-solid fluidized bed reactor", *Int. J. Chem. React. Eng., 1*(A35).

Lamari M.L. 200, "An experimental investigation of two-phase (air– water) flow regimes in a horizontal tube at near atmospheric conditions", PhD. thesis, Carleton University, Ottawa, Canada.

Leach, A., Portoghese, F., Briens, C. & Berruti, F. 2008, "A new and rapid method for the evaluation of the liquid-solid contact resulting from liquid injection into a fluidized bed", *Powder Technology,* vol. 184, no. 1, pp. 44-51.

Leclère, K., Briens, C., Gauthier, T., Bayle, J., Guigon, P. & Bergougnou, M. 2004, "Experimental measurement of droplet vaporization kinetics in a fluidized bed", *Chemical Engineering and Processing: Process Intensification,* vol. 43, no. 6, pp. 693-699.

McDougall, S., Saberian, M., Briens, C., Berruti, F. & Chan, E. 2005, "Effect of liquid properties on the agglomerating tendency of a wet gas–solid fluidized bed", *Powder Technology,* vol. 149, no. 2-3, pp. 61-67.

McDougall, S.L., Saberian, M., Briens, C., Berruti, F. & Chan, E.W. 2004, "Characterization of fluidization quality in fluidized beds of wet particles", *International Journal of Chemical Reactor Engineering,* vol. 2.

Portoghese, F., House, P., Berruti, F., Briens, C., Adamiak, K. & Chan, E. 2008, "Electric conductance method to study the contact of injected liquid with fluidized particles", *AICHE Journal,* vol. 54, no. 7, pp. 1770-1781.

Taitel Y., Dukler A.E.1976, "A model for predicting flow regime transitions in horizontal and near horizontal gas–liquid flow", AIChE J. vol. 22, 47– 55.

Weber, S., Briens, C., Berruti, F., Chan, E. & Gray, M. 2006, "Agglomerate stability in fluidized beds of glass beads and silica sand", *Powder Technology,* vol. 165, no. 3, pp. 115-127.

Chapter 4

COMPARISON OF THE IMPACT OF FLOW PULSATIONS ON THE PERFORMANCE OF VARIOUS LIQUID-GAS INJECTORS IN A GAS-SOLID FLUIDIZED BED

Rana Sabouni [1], Franco Berruti[1], Cedric Briens[1]

[1]Institute for Chemical and Fuels from Alternative Resources (ICFAR),
Engineering, University of Western Ontario
London, ON, Canada N6A 5B9

4.1 Introduction:

Liquid injections into fluidized bed of solid particles are widely engaged in numerous numbers of industrial applications including chemical and petrochemical industries such as fluid catalytic cracking, fluid coking and gas phase polymerization. In such processes, the liquid injection is performed using gas-atomized spray nozzles. In fluid cokers, bitumen is injected into a bed of hot coke particles fluidized with steam, after being mixed with steam in order to improve its atomization. Heat from the hot coke particles thermally cracks the bitumen and converts it into lighter and more valuable hydrocarbon products. The thermal cracking reaction depends on the contact between bitumen and hot coke, which should occur rapidly to increase the yield of valuable condensable products and to avoid poor bed fluidity (House et al., 2004) .

It is of crucial importance to provide rapid and uniform distribution of liquid on the surface of the fluidized particles in order to minimize heat and mass transfer limitations and maximize the thermal cracking reaction yield (House et al., 2004; Bruhns and Werther,

2005). In order to ensure rapid liquid-solid contact the liquid injection should form a thin film on the surface of the solid particles and contact large numbers of solid particles. Ariyapadi et al. (2003) showed that the injected liquid forms agglomerates with the bed particles. These agglomerates either survive for a long time or break up into smaller agglomerates (McDougall et al., 2005; Weber et al., 2006). Moreover, McDougall et al. (2005) found that agglomerate formation is strongly affected by liquid properties such as viscosity and contact angle.

Therefore, studying the interaction between liquid-solid particles in a gas-fluidized bed is important in order to improve the interaction between liquid-solid particles and make the process more efficient and profitable.

Portoghese et al. (2008) investigated the use of conductance probes to evaluate the nozzle performance. The conductance probes were used to measure the electrical conductance of the bed solids after completing the liquid injection and after defluidization of the wetted particles. If most of the injected liquid is concentrated in a few agglomerates, most of the bed is dry and the bed conductance is small. Conversely, if the liquid is well distributed on the particles, forming a liquid film on the particles surface that connects all the particles, the bed conductance is large. Leach et al. (2008) improved this method through the definition of a Nozzle Performance Index (NPI) to rank various nozzles according to their liquid-solid contact performance.

Bruhns and Werther (2005) and Weber et al. (2006) investigated the mechanism of liquid injection into a pilot plant bubbling fluidized bed using different measurement techniques, such as (a) fast response thermocouples, in order to measure the local temperatures near the injection nozzle, (b) gas suction probes, to measure the gas concentration, and (c) capacitance probes, for the detection of liquid in the dense gas solid phase. Knapper et al. (2003) examined the used of copper naphthenate as a tracer to measure the coating of atomized bitumen onto solid coke particles in a fluid coking pilot plant.

Leach et al. (2009) compared the performance of different spray nozzles in gas solid fluidized beds based on a Nozzle Performance Index (NPI), using a conductance probe technique. They compared different commercial nozzle sprays, such as hollow cone, vertical fanjet and wide hollow cone, as well as custom made nozzles designs, such as Type I and Type II (refer to chapter 2 and 3). Their study showed that increasing the liquid flow rate, or reducing the nozzle size, enhanced the liquid distribution in the fluidized bed. In addition, they demonstrated that there was a non-monotonic relationship between the gas to liquid ratio and liquid mixing for all the tested nozzles, and there is an optimal value of the gas-to-liquid ratio for each nozzle. Finally they concluded that nozzle geometry has a significant effect on the contact between sprayed liquid and fluidized bed particles.

In the authors' previous experimental work described in this thesis, it was found that applying pulsation of well defined amplitude using a mechanical method, such as solenoid valve, nearly doubles its nozzle performance index when compared to non-pulsating flow (Chapter 2). Later, in Chapter 3, the authors demonstrated that generating non-

mechanically induced pulsations also improves the nozzle performance index by about 20 to 50% when compared to visually stable flow. All these studies, however, were performed with a single type of spray nozzle. Therefore, it is important to investigate the effect of applying pulsations on liquid-solid contact with other spray nozzle geometries. The objective of the current research was to check the effect of imposing fluctuations of well defined frequency and amplitude on the liquid flow using four different spray nozzles of completely different types, under a variety of operating conditions, and to measure the resulting effects on the interaction between the gas-liquid jet and the fluidized bed particles.

4.2 **Apparatus:**

The experiments were conducted in a fluidized bed column with a rectangular cross section of 1.2 m x 0.15 m, as shown in Figure 4.1. The column walls are made of steel. The column is filled with silica sand with a Sauter mean diameter of 190 μm and an apparent particle density of 2600 kg/m^3 (Group B of the Geldart's powder classification). The bed has a mass of 250 kg and its static height is 0.85 m. The bed was fluidized by air with a constant relative humidity of 12% and a superficial velocity of 0.24 m/s. Three parallel sonic nozzles were used to control the fluidization air flowrate. The outgoing air was sent to two cyclones placed in series to separate the entrained particles and return them back to the bed.

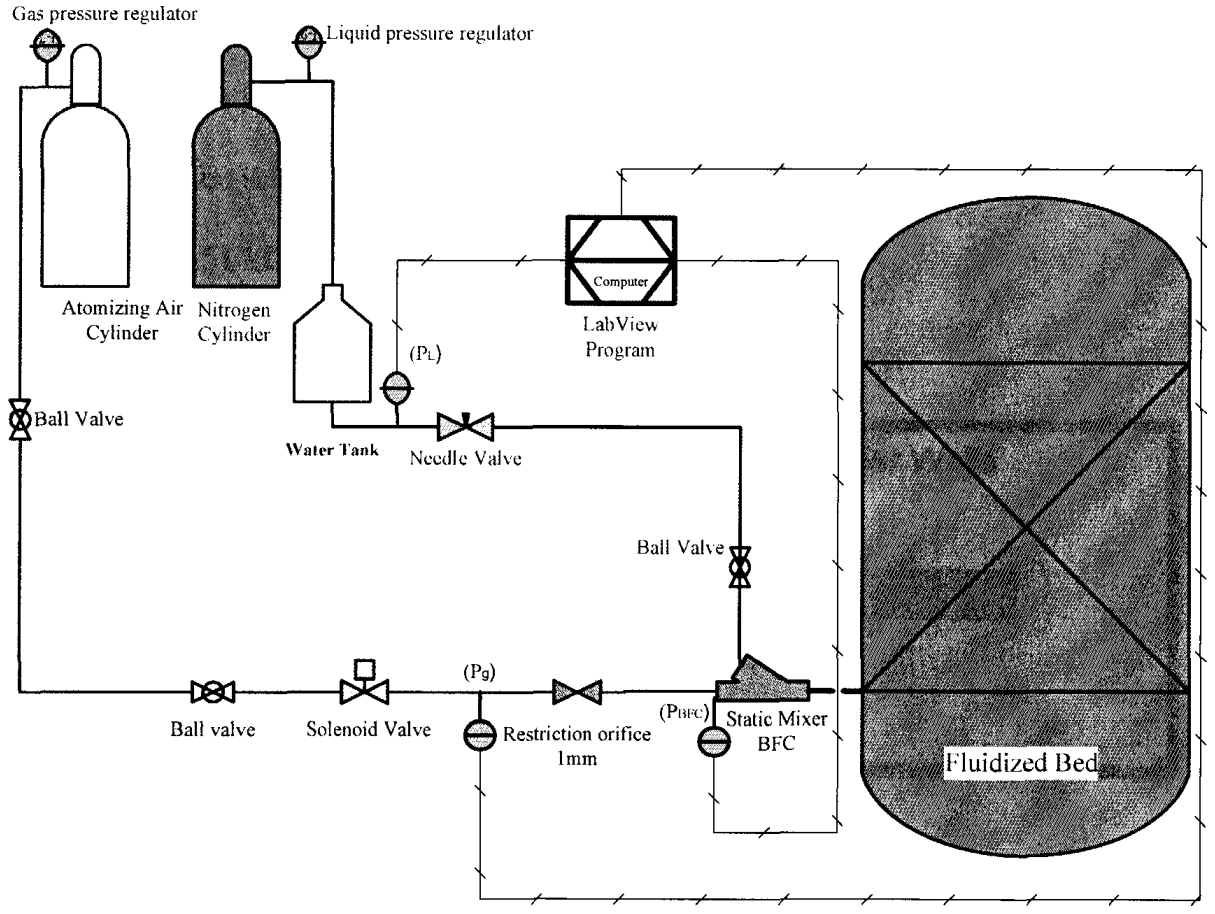

Figure 4.1: Schematic Diagram of Experimental Apparatus.

The bed temperature was monitored using four thermocouples to ensure that the bed temperature was 20°C before each liquid injection. These thermocouples penetrated 2.5 cm into the bed, and were placed at heights of 15, 35, 55, and 75 cm above the gas distributor.

To measure the electrical conductance of the bed, an electrode was located along the center of the bed section, at a height of 0.37 m above the gas distributor. This electrode was used to implement the conductivity technique from Portoghese et al. (2008). Later, the bed conductance measurements were used to calculate the Nozzle Performance Index (NPI). To ensure that the probe was electrically insulated from the bed walls, nylon fittings were used

to hold the probe while the bed was electrically grounded. The probe was made of a stainless steel hollow tube with an outer diameter of 7 mm. Figure 4.2 shows the conductive probe schematic diagram. The electrode penetrated 0.65 m into the bed and was connected to a 51 kΩ resistor.

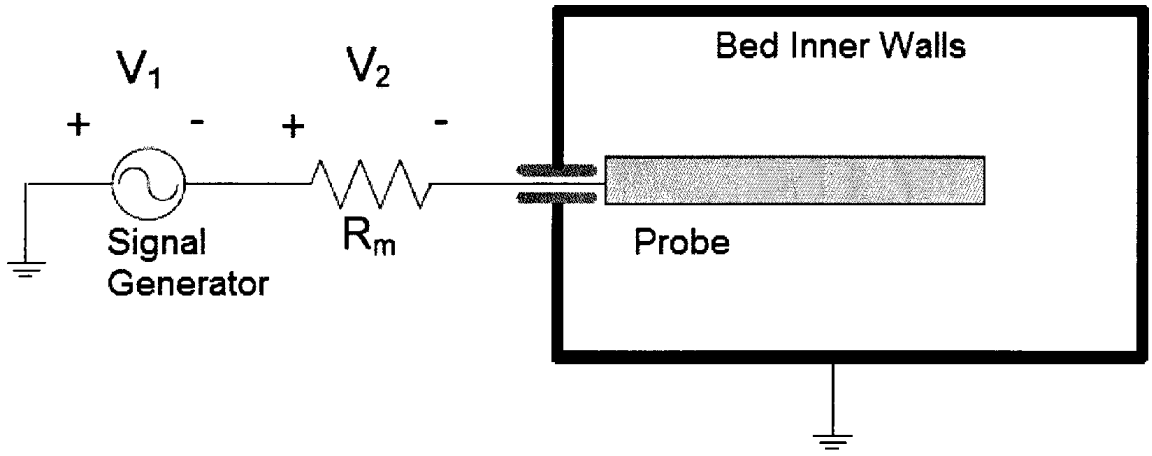

Figure 4.2: Schematic Diagram of Conductive Probe

The conductance of the bed was calculated based on simple application of Ohm's Law:

$$G_{bed} = \frac{1}{R_{bed}} = \frac{1}{R_m} * \left[\frac{V_2}{V_1 - V_2} \right] \tag{4.1}$$

where R_{bed} is the electrical resistance of the bed and R_m is the resistance of the resistor (known value).

A function generator was used to generate an electrical alternating current across the bed. Based on the work of Portoghese et al. (2008), the waveform was set to be sinusoidal with a frequency of 100 Hz, and a voltage of 6.7 V. The voltage imposed by the signal

generator (V_1) was used with the voltage measured across the resistor (V_2) to calculate the bed conductance. A data acquisition system was used to measure the voltage V_1 imposed by the signal generator, the voltage V_2 across the resistor, and the temperature of the four thermocouples, at a frequency of 1000 Hz. Figure 4.3 shows the electrical solenoid valve circuit diagram used in the experiments.

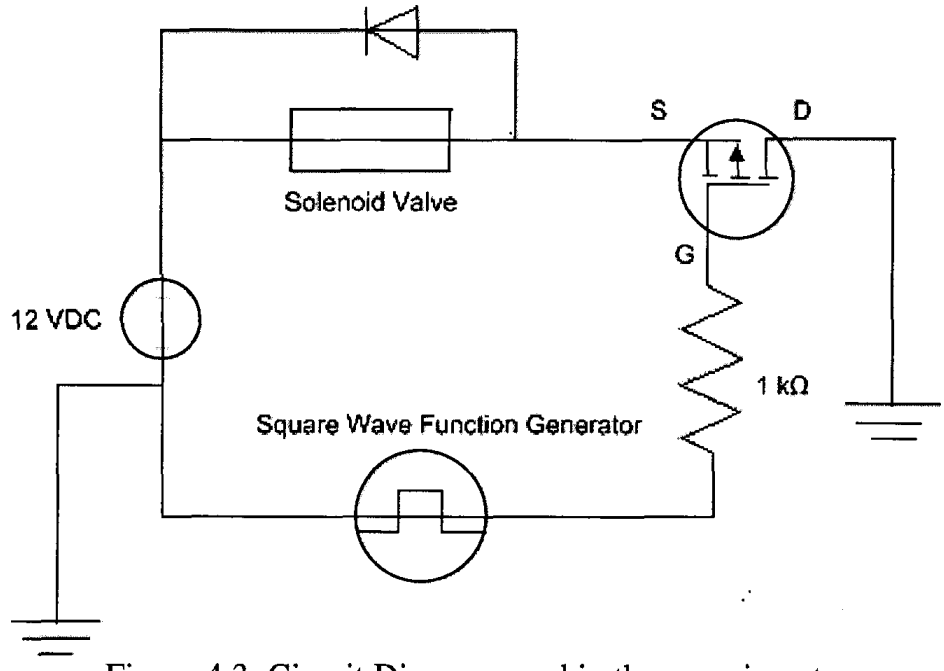

Figure 4.3: Circuit Diagram used in the experiments.

The liquid was injected into the fluidized bed using a gas-atomized nozzle that was located 0.6 m above the gas distributor and protruded into the bed for 0.05 m from the wall. De-ionized water was used as the injection liquid to avoid the accumulation of impurities in the fluidized bed, and air was used as injection gas. Pressure regulators were used to control the air and water flowrates. The water line used a nitrogen cylinder to pressurize the water tank upstream of a needle valve, and the tank pressure was measured with a calibrated pressure transducer (Figure 4.1).

The air line consisted of an air cylinder to pressurize the air upstream of a solenoid valve, a calibrated pressure transducer and a calibrated orifice restriction (Figure 4.1). In order to induce pulsations in the liquid spray, a solenoid valve was introduced in the air stream, just upstream of the restriction orifice (Figure 4.1). This solenoid valve was controlled by a function generator using the circuit shown in Figure 4.3. By opening and closing the gas line (because of the opening and closing of the solenoid valve), the gas-to-liquid ratio is no longer held constant, and the fluctuations in gas pressure in the line cause the water flowrate to also change. This induces the pulsations whose effects were investigated in this study. The frequency of pulsation was fast enough that the gas flowrate never decreased to zero, as there was still a release of gas from the region between the solenoid valve and the restriction orifice governing the gas flowrate.

The air and water lines go to a pre-mixer (BFC) then to the spray nozzle, when using Type I and Type II atomization nozzles, while the other nozzles did not need an external pre-mixer. A calibrated pressure transducer was located on the external pre-mixer or, when there was no external pre-mixer, just upstream of the spray nozzle. All pressure transducers were calibrated and connected to a data acquisition system to measure the pressure drops across the air restriction orifice (P_g-P_{BFC}), and across the liquid needle valve (P_L-P_{BFC}), from which the instantaneous gas and liquid flowrates to the pre-mixer could be determined.

Four different gas atomized spray nozzles were used. The first two nozzles were the custom made types (Type I and Type II) as illustrated in Figure 4.4. The first one had two throats with a diameter of 1.6 mm. The second one had the same internal geometry as Type

I, except for a deviated section located downstream of the second throat. Both types of nozzles were developed by Portoghese et al. (2008). These two types of nozzles required an external static pre-mixer to mix the water and air from different sides (at angle of 30^0 from the nozzle) before reaching the nozzle.

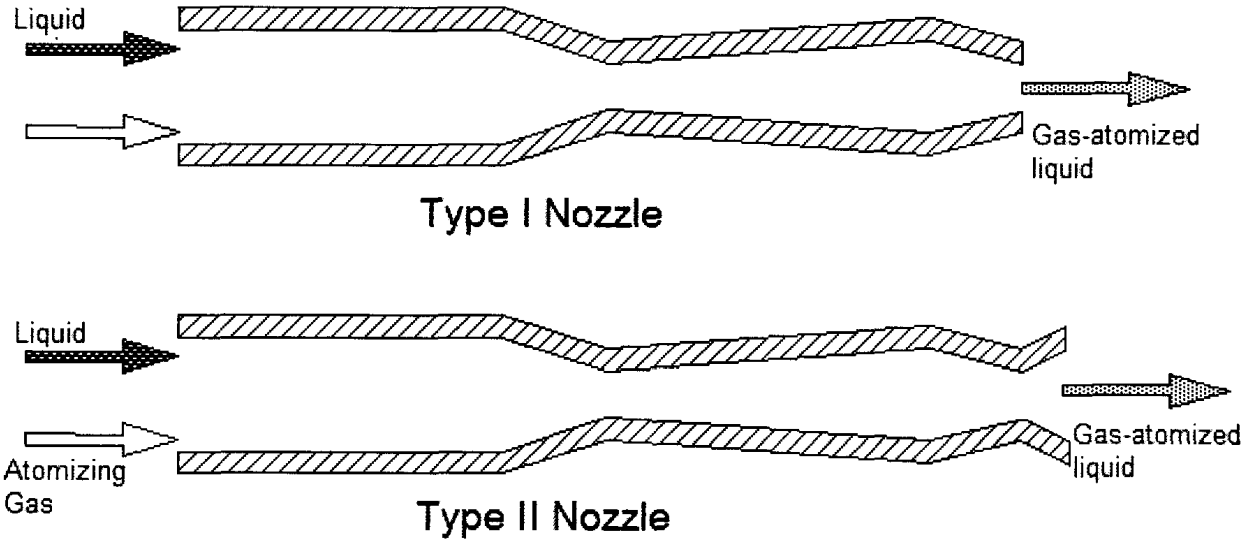

Figure 4.4: Internal Geometry of Type I Nozzle and Type II Nozzle.

This study used hollow cone (XA AD 200) and vertical fanjet (XA PF 200) atomization nozzles, which are commercial nozzles from the BETE Fog Nozzle Co. These two nozzles did not require an external static pre-mixer, because both were designed to mix water and air within the nozzle. The internal geometry of these two nozzles is shown in Figure 4.5, which illustrates that both nozzles have the same internal geometry, but different nozzle tips and conical spray angles. The hollow cone had an angle of $\theta = 60^o$ while vertical fanjet had and angle of $\theta = 85^o$.

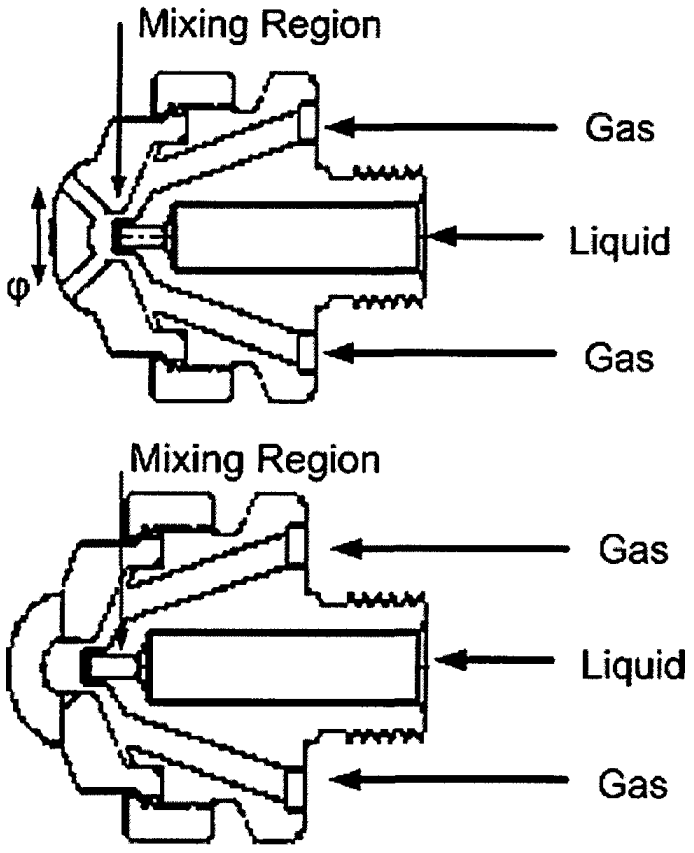

Figure 4.5: Internal geometry of commercial nozzles (BETE Fog Nozzle Co.): hollow cone (XA AD 200, top) and vertical fanjet (XA PF 200, bottom).

4.3 **Experimental Procedures:**

The goal of the experiments performed was to compare the performance of four types of gas-atomized nozzles under pulsating flow for various operating conditions such as three different liquid flowrates, three different air to liquid ratio (ALR), and three different gas orifice restrictions. The comparison between the gas atomized nozzles is based on the Nozzle Performance Index (NPI), which was defined by Leach et al. (2008). The Nozzle Performance Index (NPI) characterizes the quality of the interaction between injected liquid and bed solids, and the calculation procedure for the NPI is provided later in this section.

A common experimental procedure was used for all experiments as follows:

1) The fluidization air velocity was set to 0.25 m/s.

2) The needle valve opening was set fully open in all the experiments.

3) At t=0, the data acquisition was started using the LabView program (version 8, National Instruments)

4) Simultaneously, the solenoid valve was switched on and pulsated at the desired frequency.

5) At t=10 s, water was injected into the bed through the spray nozzle. The duration of the water injection was 15 s.

6) The bed was fluidized for a short time (10 s) after the water injection so that the larger, wetter and heavier liquid-solid agglomerates could settle away from the electrode region. At t = 25 s, the liquid injection, fluidization air, and solenoid valve were stopped, and the bed was defluidized for 7 minutes. Conductance measurements were performed during these 7 minutes. Leach et al. (2008) found that the conductance of the bed was low when the bed is dry and defluidized, because silica sand particles do not conduct electricity. However, when these particles are wetted with water, the bed conductance increases because the water forms high conductivity paths. Therefore, if the water is well distributed over the solid particles, the bed conductance is higher.

7) At t=7 min the bed was refluidized again to dry it by vaporizing the injected water and to ensure that the bed temperature returned to its initial value of 20 ^{0}C before starting a new experiment.

The injection time was kept constant at 15 seconds in all of the experiments to ensure that the mass of injected liquid was always the same, since the liquid mass flowrate was maintained at 0.022 kg/s except for the two experiments which were conducted to check the effect of the liquid flow rate (0.019 kg/s and 0.026 kg/s). The air to liquid ratio (ALR) was maintained constant for each run. The pressure values for the pre-mixer (P_{BFC}), liquid (P_L), and air (P_g) streams were recorded during each experiment.

As the last step, a plot of bed conductance vs. time was used to estimate the Nozzle Performance Index (NPI), which is defined as the slope of the trend-line of that plot, using a logarithmic scale for time. This method was developed by Leach et al. (2008). A high NPI value means that water diffuses quickly through the defluidized bed, increasing the bed conductance quickly. A high NPI therefore corresponds to a good original distribution of the liquid on the bed particles, just before defluidization. To disregard any irregularities in the start-up of the de-fluidization, only data subsequent to t = 50 s were used. Figure 4.6 shows an example of the change with time of the conductance of the defluidized bed, for which the NPI is 0.8637.

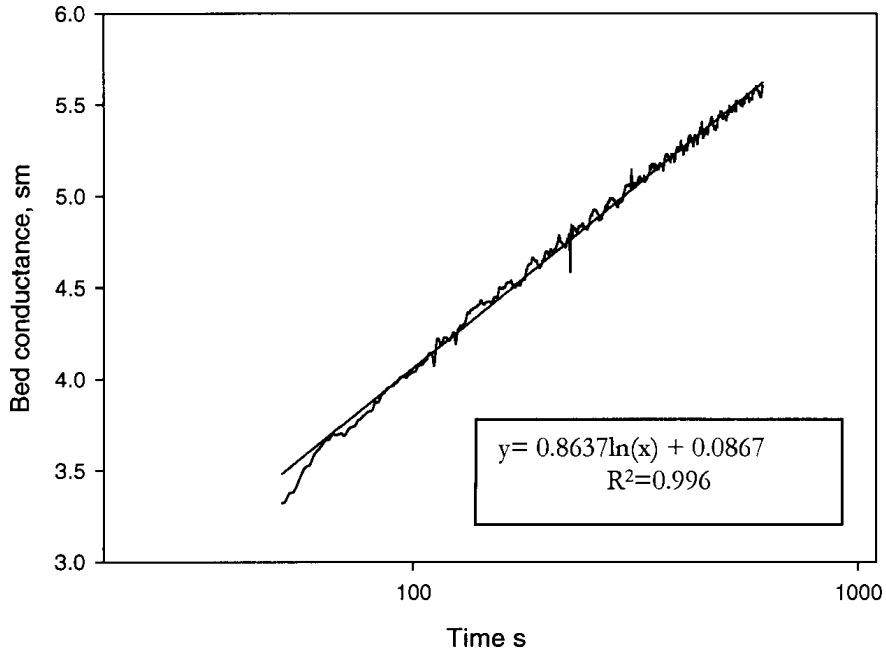

Figure 4.6: Conductance method, 1 Hz, Fully open needle valve, Type I Nozzle D=1.66 mm, F_L=0.022 kg/s, 1 mm restriction orifice, 1.7 ALR%

4.4 Results and discussion:

4.4.1 Liquid flowrate

Figures 4.7, 4.8 and 4.9 illustrate the effect of liquid flowrate on the nozzle performance for the four nozzles investigated in this study for pulsating flow (solenoid valve frequency of 1 Hz) and non-pulsating flow (solenoid valve frequency of 0 Hz). All the tests were performed at the same air to liquid ratio of 1.7wt%. In all cases, imposing artificial pulsations more than doubled the Nozzle Performance Index (NPI) for both custom made air atomized nozzles (Type I and Type II) as well as for the commercial air atomized nozzles (Vertical fanjet and Hollow cone). With pulsating flow, the Type I nozzle performed better than any of the other nozzles for all three liquid flowrates (Figures 4.7, 4.8 and 4.9). With non-pulsating flow, the Type I nozzle performed better, except for the 0.026 kg/s liquid flowrate. The vertical fanjet nozzle had the lowest nozzle performance index

for nearly all conditions, with the exception of pulsating flow at the 0.026 kg/s liquid flowrate. In addition, Figures 4.7, 4.8 and 4.9 show the standard deviation error bars. Although the vertical fanjet nozzle gave the poorest contact under most of the operating conditions while the Type I nozzle performed the best, the error bars are such that one cannot clearly differentiate between nozzles. On the other hand, in all cases it is clear that pulsations always improve the NPI.

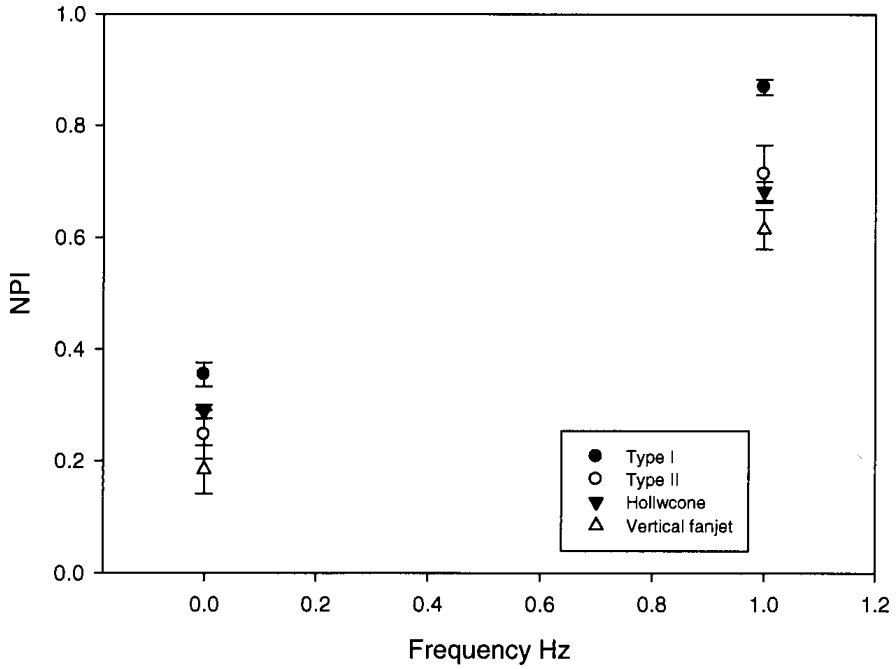

Figure 4.7: Effect of Liquid flowrate, F_L= 0.019 kg/s, fully open needle valve, 1.7% ALR, 1 mm gas orifice restriction. Standard deviation error bars.

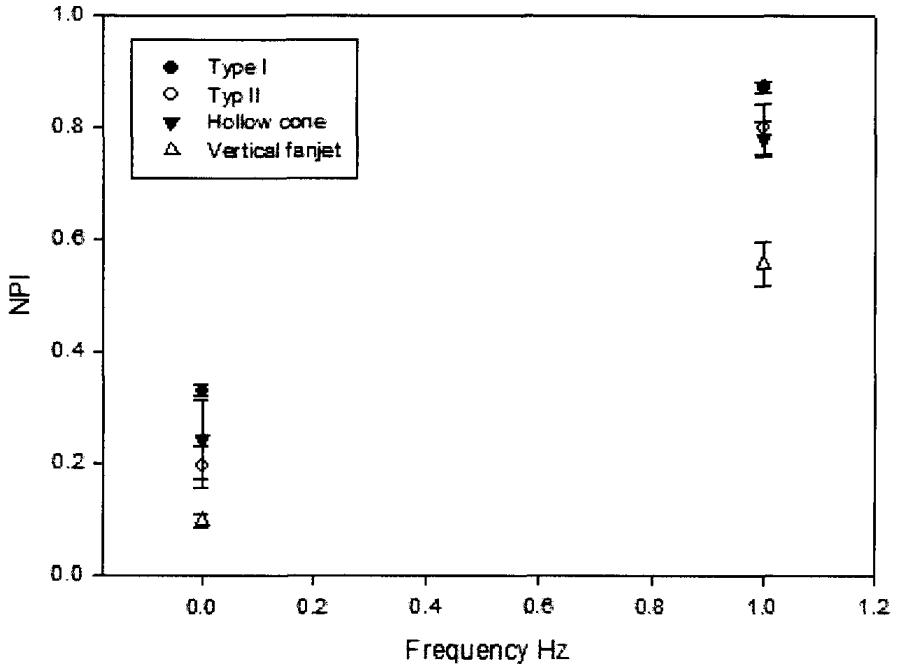

Figure 4.8: Effect of Liquid flowrate, F_L= 0.022 kg/s, fully open needle valve, 1.7% ALR, 1 mm gas orifice restriction. Standard deviation error bars.

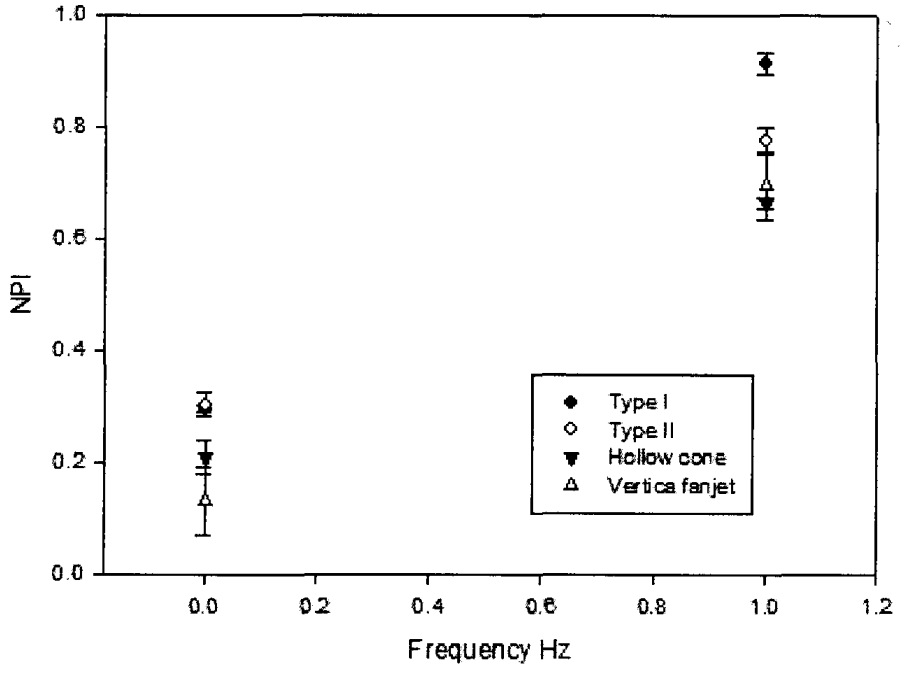

Figure 4.9: Effect of Liquid flowrate, F_L= 0.026 kg/s, fully open needle valve, 1.7% ALR, 1 mm gas orifice restriction, standard deviation error bars.

Figure 4.10 illustrates the comparison between the four different spray nozzles in terms of the NPI ratios ($NPI_{\text{with pulsations}}/NPI_{\text{without pulsations}}$) for the three liquid flowrates investigated. It is clear that, whatever the type of the spray nozzle; the NPI for the pulsating flow is about 2.4 to 8.2 times its value when the spray nozzle flow is not pulsating.

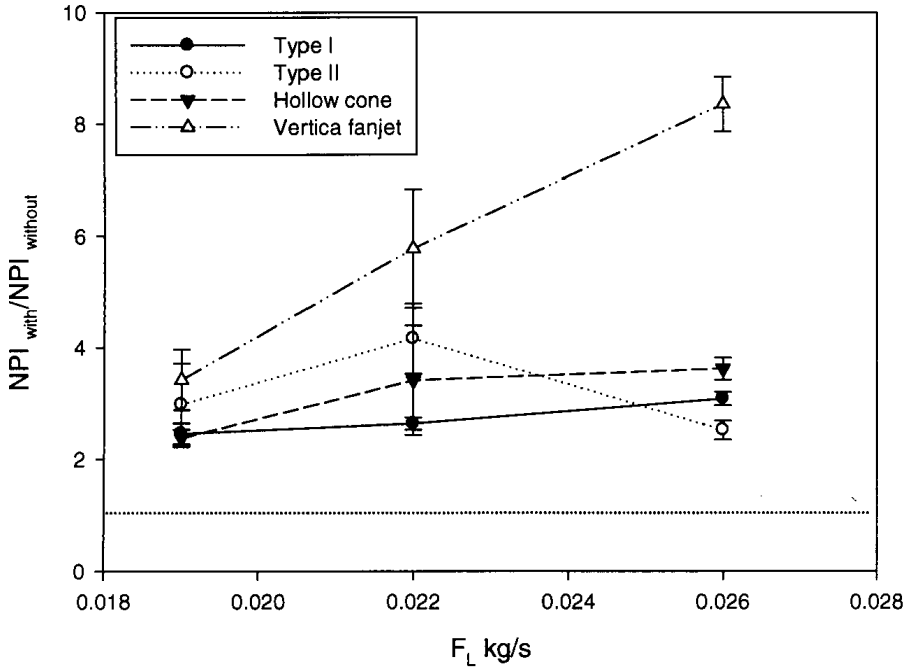

Figure 4.10: NPI with pulsations/ NPI without pulsations vs. liquid flow rate, 1.7%ALR, 1 mm gas orifice restriction, and standard deviation error bars.

Figure 4.11 summarizes the instantaneous water and air flowrates for both pulsating and non-pulsating flow for two nozzles (Type II and Vertical Fanjet) while all other variables were held constant (0.022 kg/s liquid flowrate, 1 mm gas orifice restriction, air to liquid ratio of 1.7%). In all cases, the imposed gas flow pulsations were much larger than

the normal, non-mechanically induced pulsations. The gas pulsations, in turn, induced significant liquid flow pulsations but, as shown in previous studies (chapter 2), the key was that the liquid flow never decreased to 0.

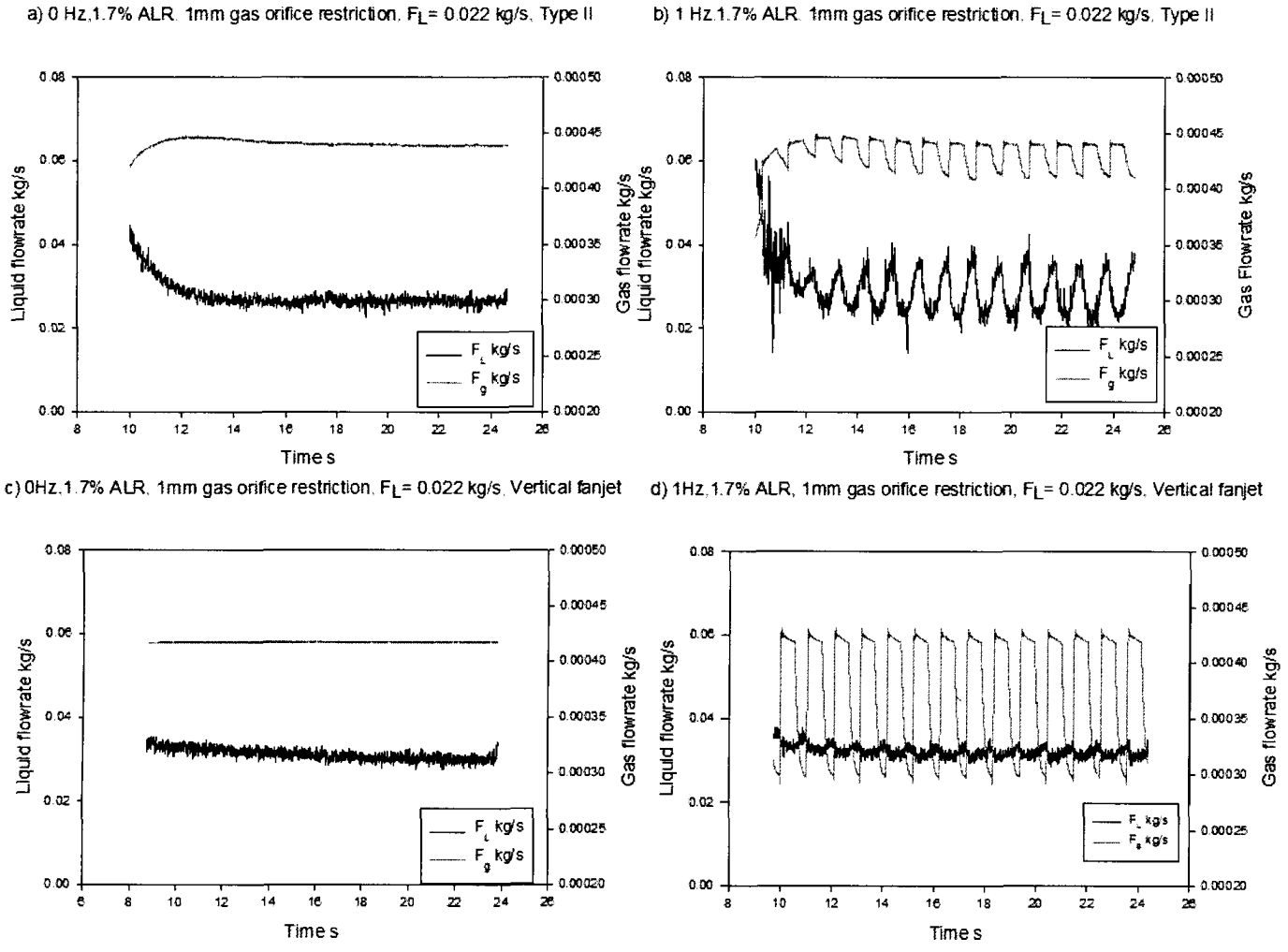

Figure 4.11: instantaneous gas and liquid flowrate for both Type II and Vertical fanjet air atomized nozzles, 1.7%, F_L=0.022kg/s, 1mm gas restriction

4.4.2 Gas orifice restriction

The effect of the variations in the gas orifice restriction on the nozzle performance, shown in Figure 4.1, is shown in Figures 4.12, 4.13 and 4.14 for the four nozzles, with all the other variables kept constant (liquid flowrate of 0.022 kg/s and air to liquid ratio of 1.7%) each point these figures shows an average of three runs at the same conditions. The

custom made air atomized nozzles performed better than the commercial nozzles with the three different gas orifice restrictions. Moreover, Figures 4.12, 4.13 and 4.14 show that the gas orifice restriction affects the performance of the commercial nozzles (Hollow cone and Vertical fanjet) more than the custom made nozzles (Type I and Type II). Hollow cone and Vertical fanjet nozzles provide a higher NPI when using the 0.7 mm orifice size than the other sizes, for the pulsating flow case at 1 Hz frequency.

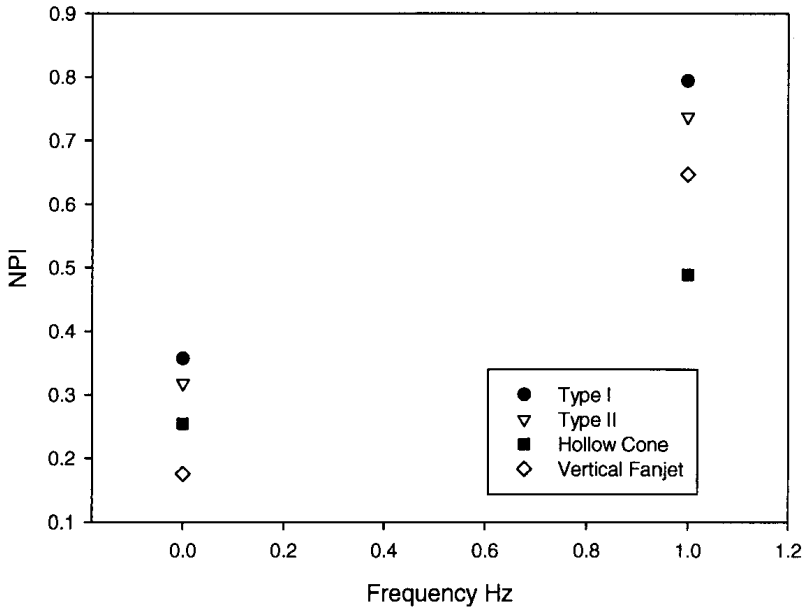

Figure 4.12: Effect of gas orifice restriction, 0.7 mm gas orifice restriction, fully open needle valve, F_L= 0.022 kg/s, 1.7% ALR

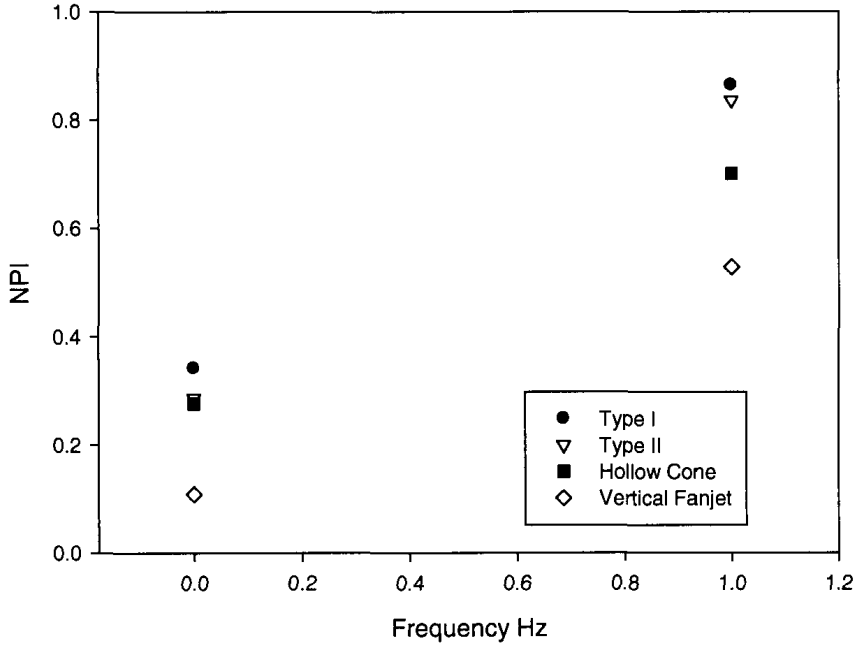

Figure 4.13: Effect of gas orifice restriction, 1 mm gas orifice restriction, fully open needle valve, F_L= 0.022 kg/s, 1.7% ALR

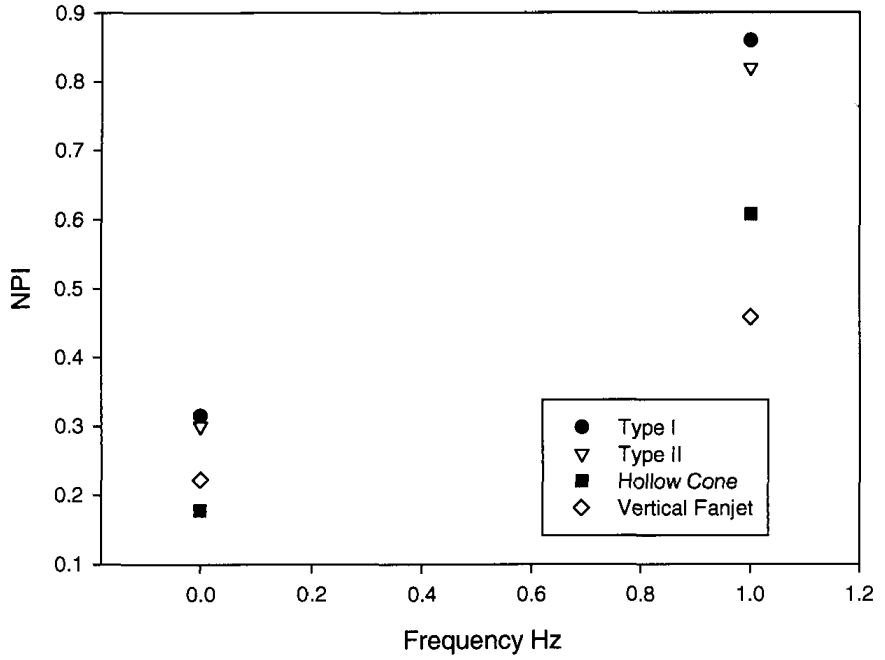

Figure 4.14: Effect of gas orifice restriction, 1.2 mm gas orifice restriction, fully open needle valve, F_L= 0.022 kg/s, 1.7% ALR

Figure 4.15 shows the NPI $_{\text{with pulsations}}$/ NPI $_{\text{without pulsations}}$ as function of gas orifice restriction. Figure 4.15 demonstrated that the NPI for the imposed pulsations flow increases by 2 to 4.8 times its value when using non pulsating flow, regardless of the nozzle type is used. In addition, Figure 4.15 demonstrates different performance trend from one nozzle to another depending on the gas orifice restriction. This can be related to the internal geometry of the nozzle for example vertical fanjet shows a huge decrease on NPI ratio at 1.2 mm gas orifice restriction compare to other nozzles. However, hollow cone spray nozzles shows increase on NPI ratio at 1.2 mm gas orifice restriction.

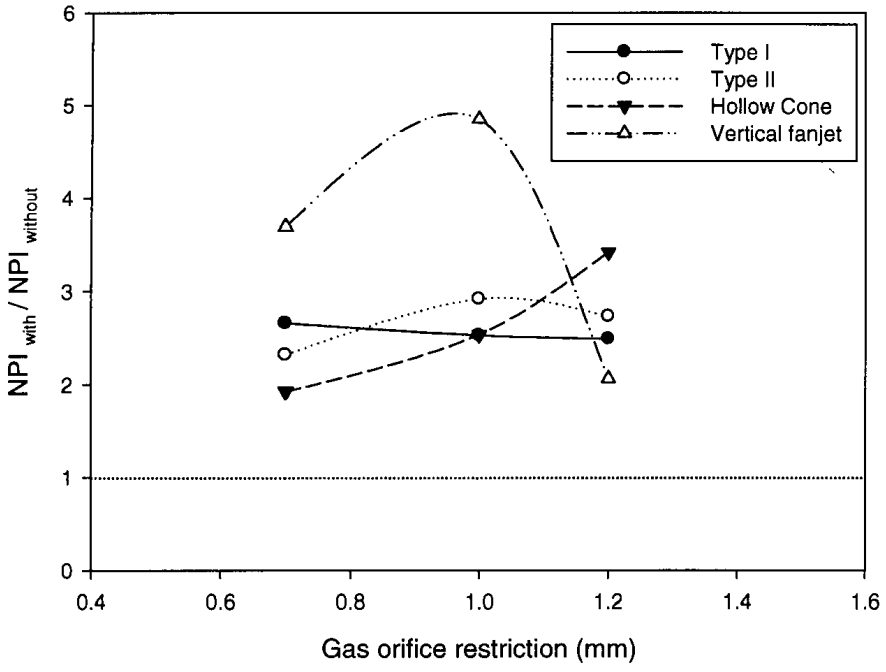

Figure 4.15: NPI $_{\text{with pulsations}}$ / NPI $_{\text{without pulsations}}$ vs. gas orifice restriction. 1.7% ALR, F_L= 0.022 kg/s.

Figure 4.16 shows the instantaneous water and air flowrate for both pulsating flow and non-pulsating flow for Type II and Vertical fanjet nozzles. As shown in Figure 4.16 d, the amplitude of pulsation for the liquid flowrate is very small when using the 1.2 mm gas restriction for the Vertical fanjet nozzle. This can explain the reduction in Nozzle Performance Index (NPI) when compared to the 1 mm gas restriction, for example, for which the liquid pulsations are much stronger (Figure 4.11 b).

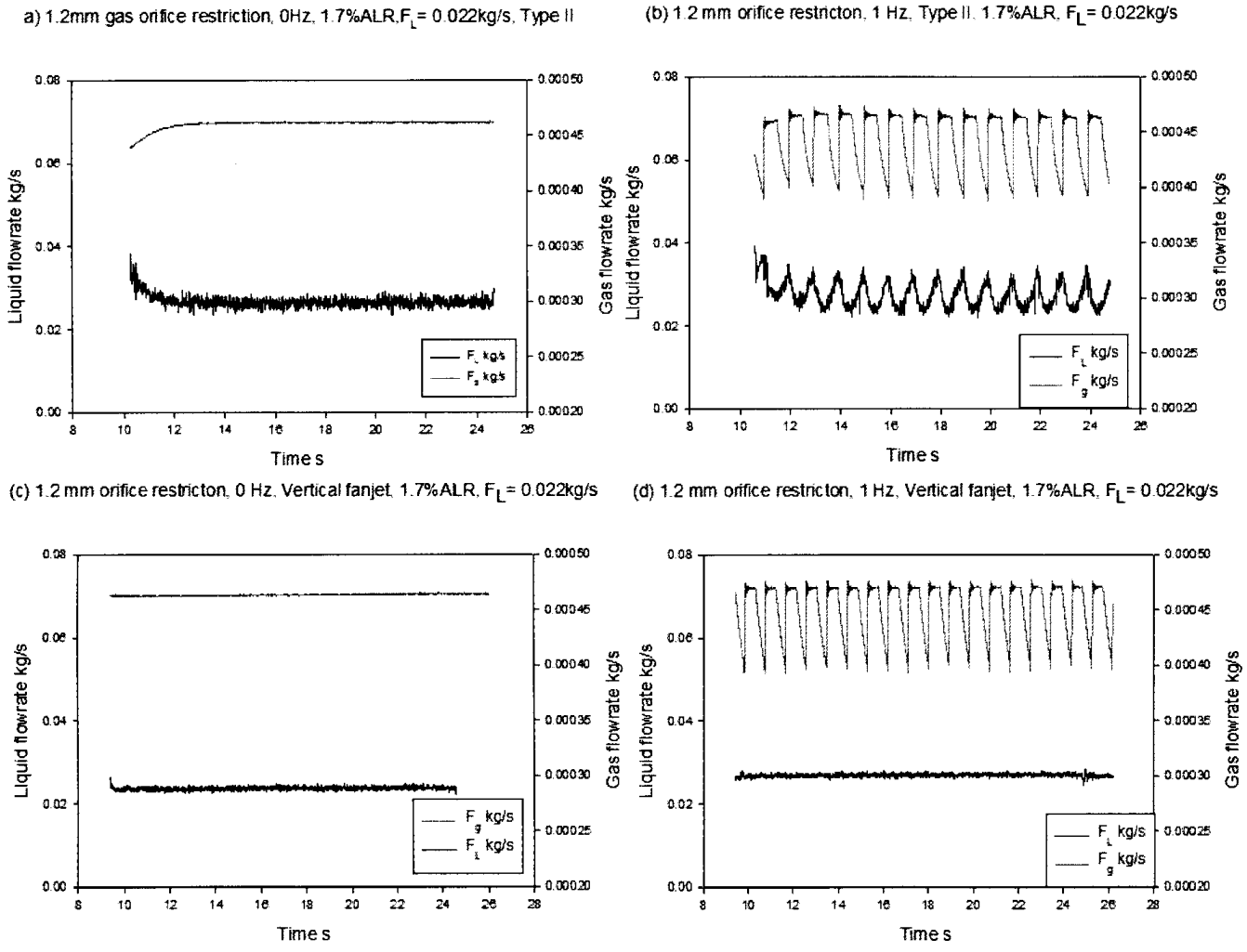

Figure 4.16: Instantaneous gas and liquid flowrate for both Type II and Vertical fanjet air atomized nozzles,1.7%, F_L=0.022kg/s, 1.2 mm gas restriction

4.4.3 Air to liquid ratio (ALR)

Figures 4.17, 4.18 and 4.19 illustrate the effect of air to liquid ratio (ALR %) on the Nozzle Performance Index (NPI), with the other variables held constant (liquid flow rate of 0.022 kg/s and 1 mm gas orifice restriction). It is found that nozzle performance for both custom made and commercial air atomized nozzles are affected by changing the air to liquid ratio. Moreover, pulsating flow provided a better nozzle performance compared to the non pulsating flow at the three different air-to-liquid ratio for the all four nozzles that are investigated. However, Hollow cone nozzles performed the best at 1.7% air to liquid ratio compared to 1.5% and 2.5% air to liquid ratio. On the other hand, Vertical fanjet shows best nozzle performance at 2.5 % among the other air to liquid ratio tested.

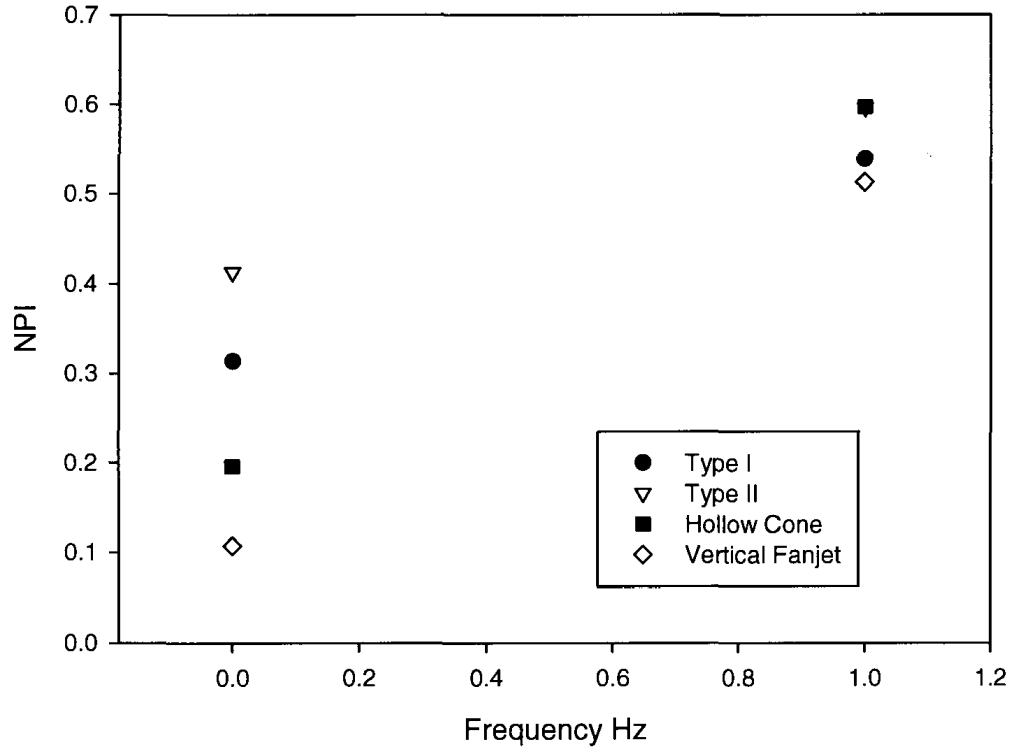

Figure 4.17: Effect of Air to Liquid ratio, F_L= 0.022 kg/s, fully open needle valve, 1.5% ALR, 1 mm gas orifice restriction

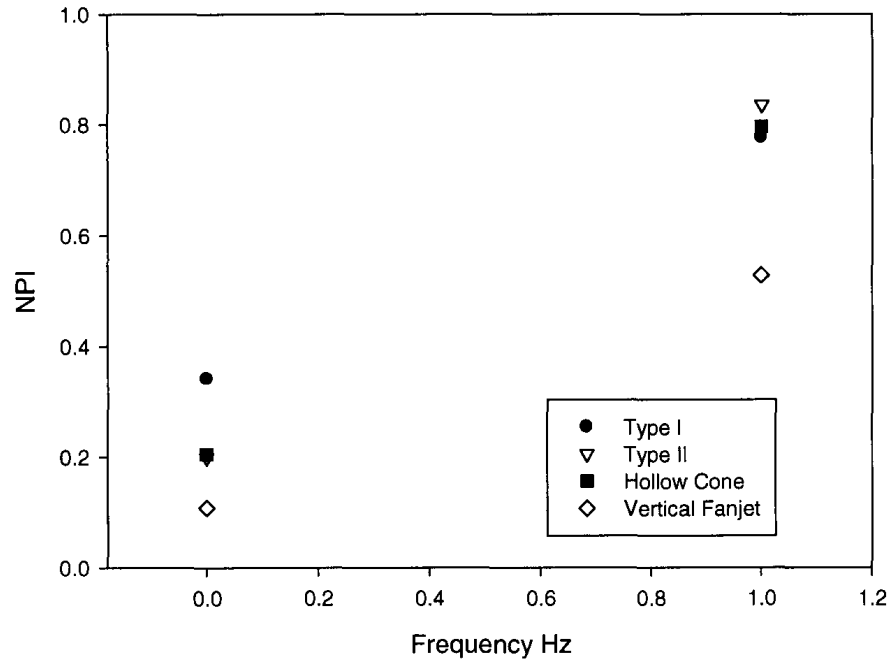

Figure 4.18: Effect of Air to Liquid ratio, F_L= 0.022 kg/s, fully open needle valve, 1.7% ALR, 1 mm gas orifice restriction

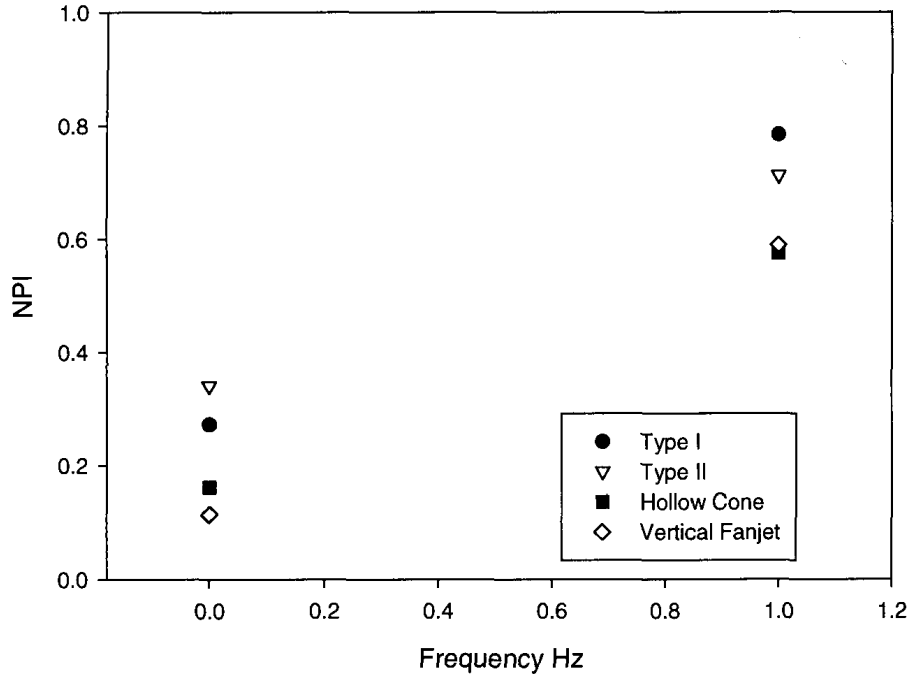

Figure 4.19: Effect of Air to Liquid ratio, F_L= 0.022 kg/s, fully open needle valve, 2.5% ALR, 1 mm gas orifice restriction

Figure 4.20 compares the effect of the ALR % on the ratio NPI $_{\text{with pulsations}}$/ NPI $_{\text{without pulsations}}$ for the four different spray nozzles. In all cases, the flow pulsations greatly increased the NPI from 1.5 to 7 times its value in the absence of pulsations. As discussed before in Figure 4.15 and 4.10 the difference in the performance of the four different spray nozzles can be related to the internal geometry of the spray. Therefore Figure 4.20 demonstrates a different trend between the four spray nozzles. Vertical fanjet shows the most unusual trend compare to the other three nozzles. Because vertical fanjet has wide vertical spray angle creating more larger spray droplets leading to more agglomerates formation Leach et al., (2009).

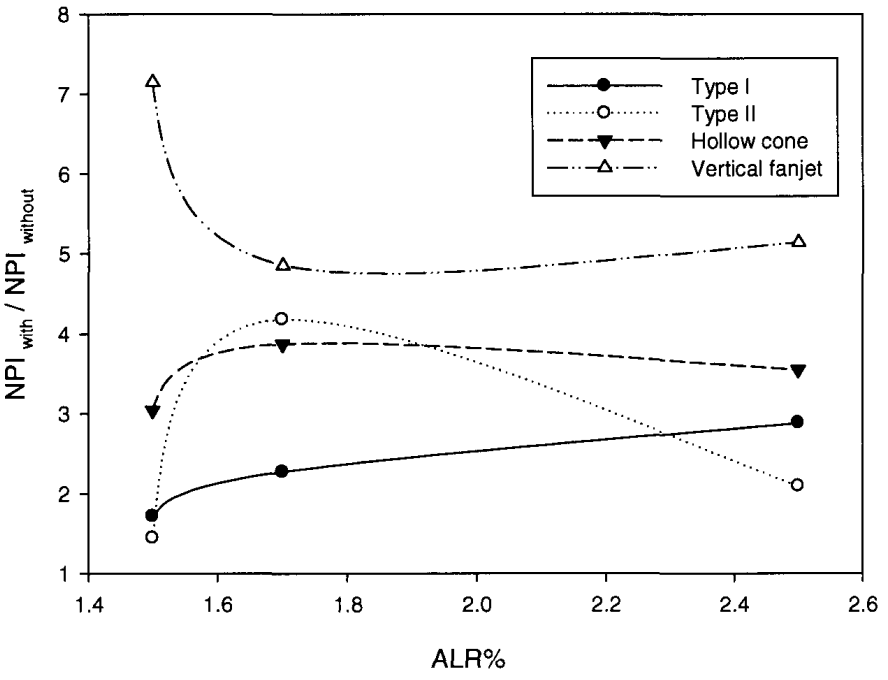

Figure 4.20: NPI $_{\text{with pulsations}}$ / NPI $_{\text{without pulsations}}$ vs. ALR%, F_L= 0.022 kg/s, 1 mm gas orifice restriction

Finally the instantaneous liquid and gas flowrates are presented in Figure 4.21. In general, Vertical fanjet nozzle has responded with the lowest Nozzle Performance Index (NPI) for all three different tested air-to-liquid ratios (ALR) at both pulsating and non pulsating flow. This result can be related to the internal geometry of the Vertical fanjet nozzle, where the liquid spray is not distributed over a large area through the bed of solid particles, resulting in larger liquid solid agglomerates which are more difficult to break up into smaller ones.

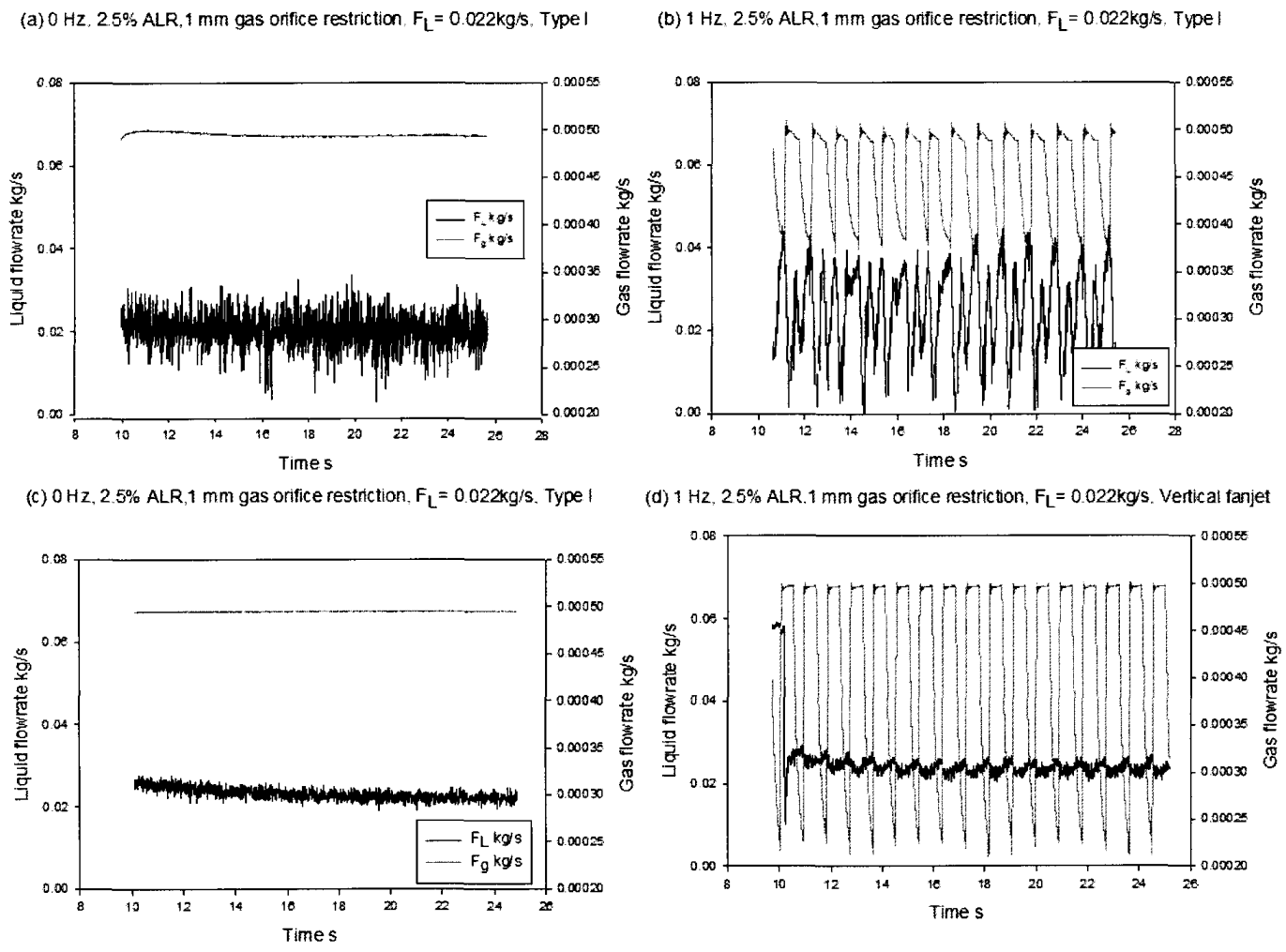

Figure 4.21: Instantaneous gas and liquid flowrate for both Type II and Vertical fanjet air atomized nozzles, 2.5%, FL=0.022kg/s, 1mm gas restriction

4.5 **Conclusions:**

Artificially induced flow pulsations greatly improved the contact between injected liquid and fluidized particles, for four completely different types of spray nozzles. The vertical fanjet nozzle gave the poorest contact under most of the operating conditions while, the Type I nozzle performed the best. The nozzle performance was improved by increasing the amplitude of the liquid flowrate pulsations.

4.6 **References:**

Ariyapadi, S., Holdsworth, D., Norley, C., Berruti, F., & Briens, C. 2003, "Digital X-ray imaging technique to study the horizontal injection of gas-liquid jets into fluidized beds", *International Journal of Chemical Reactor Engineering, 1*(A56)

Bruhns, S. & Werther, J. 2005, "An investigation of the mechanism of liquid injection into fluidized beds", *AICHE Journal,* vol. 51, no. 3, pp. 766-775.

House, P.K., Saberian, M., Briens, C.L., Berruti, F. & Chan, E. 2004, "Injection of a liquid spray into a fluidized bed: Particle-liquid mixing and impact on fluid coker yields", *Industrial and Engineering Chemistry Research,* vol. 43, no. 18, pp. 5663-5669.

Knapper, B. A., Gray, M. R., Chan, E. W., & Mikula, R. 2003, "Measurement of efficiency of distribution of liquid feed in a gas-solid fluidized bed reactor", *Int. J. Chem. React. Eng., 1*(A35)

Leach, A., Chaplin, G., Briens, C. & Berruti, F. 2009, "Comparison of the performance of liquid-gas injection nozzles in a gas-solid fluidized bed", *Chemical Engineering and Processing: Process Intensification,* vol. 48, no. 3, pp. 780-788.

Leach, A., Portoghese, F., Briens, C. & Berruti, F. 2008, "A new and rapid method for the evaluation of the liquid-solid contact resulting from liquid injection into a fluidized bed", *Powder Technology,* vol. 184, no. 1, pp. 44-51.

Leclère, K., Briens, C., Gauthier, T., Bayle, J., Guigon, P. & Bergougnou, M. 2004, "Experimental measurement of droplet vaporization kinetics in a fluidized bed", *Chemical Engineering and Processing: Process Intensification,* vol. 43, no. 6, pp. 693-699.

McDougall, S., Saberian, M., Briens, C., Berruti, F. & Chan, E. 2005, "Effect of liquid properties on the agglomerating tendency of a wet gas–solid fluidized bed", *Powder Technology,* vol. 149, no. 2-3, pp. 61-67.

Portoghese, F., Berruti, F. & Briens, C. 2005, "Use of triboelectric probes for on-line monitoring of liquid concentration in wet gas–solid fluidized beds", *Chemical Engineering Science,* vol. 60, no. 22, pp. 6043-6048.

Portoghese, F., House, P., Berruti, F., Briens, C., Adamiak, K. & Chan, E. 2008, "Electric conductance method to study the contact of injected liquid with fluidized particles", *AICHE Journal,* vol. 54, no. 7, pp. 1770-1781.

Portoghese, F., Berruti, F., Briens, C. & Chan, E. 2007, "Novel triboelectric method for characterizing the performance of nozzles injecting gas-atomized liquid into a

fluidized bed", *Chemical Engineering and Processing: Process Intensification,* vol. 46, no. 10, pp. 924-934.

Weber, S., Briens, C., Berruti, F., Chan, E. & Gray, M. 2006, "Agglomerate stability in fluidized beds of glass beads and silica sand", *Powder Technology,* vol. 165, no. 3, pp. 115-127

Chapter 5

CONCLUSIONS AND RECOMMENDATIONS

This chapter summarizes the main conclusions of this thesis, and presents some recommendations for future research.

5.1 Conclusions:

Several experiments were conducted under various operating conditions to investigate the beneficial effects of imposing fluctuations of well-defined frequency and amplitude on the liquid spray in gas-solid fluidized beds. The following are the main conclusions of the research:

1) Pulsating spray nozzle flow creates jet fluctuations as a result, the jet penetration moves rapidly back and forth. Since the wet agglomerates form at the jet tip, this back and forth motion has two impacts: it distributes the liquid over more bed solids, thus creating dryier and weaker agglomerates than with a stable jet, and it disrupts the agglomerates. This implies that the smaller and weaker wet agglomerates are more likely to break up, which promotes further dispersion of the liquid on the bed particles. Thus, applying artificial pulsations to the gas line using a solenoid valve and non-mechanically induced pulsations resulted in impressive improvements of the nozzle performance.

2) The greatly beneficial effect of artificially induced pulsations on the distribution of a liquid spray in gas solid fluidized beds was established under a variety of operating conditions such as air-to-liquid ratio (ALR), liquid flow rate, gas properties and nozzle geometry. It can be concluded that in general, pulsations have a huge positive effect on increasing the nozzle performance under all the previous operating conditions. However, the relative effect of pulsations is highest for 2.5% ALR and smallest for 1.5% ALR. Furthermore, pulsations greatly improved the nozzle performance with different gas properties (Air and mixed gas of 18 mole% helium and 82 mole% nitrogen). Moreover, it has been found that the greatly beneficial effect of the pulsations was obtained over a wide range of pulsations characteristics, as was observed by varying their frequency and amplitude.

3) Pulsations were also induced without using any source of mechanical pulsations such as a solenoid valve that may not be viewed as reliable for long-term, industrial use. Therefore, a new method has been developed to create pulsations by inducing slug flow for a fraction of the total gas-liquid flow going to the spray nozzle. The remarkable results demonstrated that such pulsations also have a positive impact on nozzle performance under a variety of operating conditions. Moreover the relationship between liquid, gas flowrates and predicted jet penetration was developed. It was found that predicted jet penetration is much more strongly related to the liquid flow pulsations than to the gas flow pulsations.

4) Several gas atomized nozzles including two custom made nozzles (Type I and Type II nozzles) and two commercial nozzles (Hollow cone and Vertical fanjet nozzles) were

investigated using pulsating flow, over a wide range of operating conditions. In all cases, pulsations greatly improved the liquid-solid contact. Although, under standard conditions, the vertical fanjet air atomized nozzle always performed much more poorly than the other nozzles, induced pulsations were able to bring its performance to a higher level than achieved by the best nozzle in the absence of pulsations.

5.2 Recommendations:

1) In this present dissertation, some operating conditions were considered to check the effect of pulsating liquid spray in a gas solid fluidized bed, including liquid flowrate, gas restriction, air to liquid ratio (ALR) and frequency (chapters 2 and 4). However, there are many other variables that can be addressed in future work such as fluidizing gas velocity, different fluidized bed particles, different liquid spray properties such as density and temperature. These studies are needed to check if the pulsations of liquid spray are beneficial over an even wider range of operating conditions.

2) The non-mechanical means of inducing spray pulsations were investigated experimentally in this present study (chapter 3), in a laboratory gas-solid fluidized bed and their results on improving the nozzle performance and distribution on liquid over fluidized bed particles were impressive. Therefore, applying non-mechanically induced pulsations to a large scale fluidized bed is crucial to ensure that such pulsations can be useful in industrial applications such as fluid coking and fluid catalytic cracking.

3) The predicted jet penetration was calculated in the present research (Chapter 2 and 3) using the model from Ariyapadi et al. (2004). In order to, gain a better understanding of the behaviour of pulsating liquid sprays and to characterize the effect of pulsations on

the liquid distribution in gas-solid fluidized beds, it is important to measure the fluctuating horizontal jet penetration experimentally. There are several ways to do that such as using triboelectric probes. This method is based on measuring the difference in the electrical charge between wetted and dry solid fluidized bed particles. Another method is to use thermocouples, while imposing a significant temperature difference between the injected liquid and the fluidized bed particles. Also the jet penetration can be measured using X-ray visualization techniques similar to the work done by Ariyapadi et al. (2003). Finally, an infra red (night vision) camera can be used as new method to film the pulsating jet penetration.

4) House et al. (2004) used a unique technique to characterize the initial liquid-solid contact between the sprayed liquid droplets and the fluidized bed particles. This technique employed binding solutions to trap the initial-liquid solid mixture. It could be used to performed a detailed study of the effect of pulsating flow on agglomerate characteristics. Another way to characterize the pulsating liquid injections is to take samples (agglomerates) after de-fluidizing the bed and run an avalanche test for to check the moisture content of these agglomerates.

5) In all the experiments conducted in this present work (chapters 2, 3 and 4), one type of pre-mixer was used. Therefore, future work can focus on investigating the effect of different pre-mixer geometries for both pulsating and non pulsating liquid sprays in order to understand the mechanism of liquid spray distribution in gas solid fluidized beds.

6) Future work is needed to characterize the droplet size distribution and to understand how the pulsating liquid spray works in a fluidized bed at different operating conditions and compare these results to non pulsating sprays.

7) Another important parameter that can be studied in future research is the effect of pulsating sprays on the entrainment of solid particles into the jet cavity created in a gas-solid fluidized bed by the spray, at different operating conditions. Results need to be compared to non pulsating sprays.

By studying other parameters such as jet penetration, liquid droplet size, entrainment of solid particles and pre-mixer geometry one can better understand the beneficial effect of pulsating liquid sprays on the jet bed interaction in gas solid fluidized beds.

5.3 **References:**

Ariyapadi, S., Berruti, F., Briens, C., McMillan, J. & Zhou, D. 2004, "Horizontal penetration of gas-liquid spray jets in gas-solid fluidized beds", *International Journal of Chemical Reactor Engineering,* vol. 2.

Ariyapadi, S., Holdsworth, D., Norley, C., Berruti, F., & Briens, C. 2003, "Digital X-ray imaging technique to study the horizontal injection of gas-liquid jets into fluidized beds", *International Journal of Chemical Reactor Engineering, 1*(A56)

House, P.K., Saberian, M., Briens, C.L., Berruti, F. & Chan, E. 2004, "Injection of a liquid spray into a fluidized bed: Particle-liquid mixing and impact on fluid coker yields", *Industrial and Engineering Chemistry Research,* vol. 43, no. 18, pp. 5663-5669.

APPENDIX A

USE OF PULSATIONS TO ENHANCE THE DISTRIBUTION OF LIQUID INJECTED INTO FLUIDIZED PARTICLES WITH COMMERCIAL-SCALE NOZZLES

Aidan Leach, Rana Sabouni [1], Franco Berruti[1], Cedric Briens[1]

[1]Institute for Chemical and Fuels from Alternative Resources (ICFAR),
Engineering, University of Western Ontario
London, ON, Canada N6A 5B9

A.1 Introduction

Gas-atomized liquid feeds are used in many industrial gas-solid fluidized bed reactors. These injections are used to either introduce feedstocks or coolants into a wide variety of chemical reactors. Some examples include fluid cokers, fluid catalytic cracker (FCC) and gas-phase polymerization reactors. In the fluid coker units, such as the ones used to produce synthetic crude from the Athabasca oil sands of Northern Alberta, heavy bitumen is mixed with steam, and then injected into a fluidized bed of coke particles. The steam helps break the bitumen into droplets, and then helps disperse it into the bed. This reaction takes place at approximately 530 °C (Song et al., 2004). Bitumen is heated on contact with the coke and, after achieving sufficiently high temperatures, its large hydrocarbon molecules are thermally cracked into smaller, more valuable products. The efficiency and product yields of this reactor system are highly dependent on the effectiveness of the liquid-solid contact that occurs immediately after the liquid injection (House et al., 2004).

While maximizing solid-liquid contact is critical in processes where most of the liquid vaporizes immediately after the injection (Leclère et al., 2003), such as FCC or polymerization reactors, it is even more important in processes where the injected liquid does not evaporate quickly, and the main reactions occur in the liquid-phase, such as fluid coking. In addition, fluid coking is endothermic. In these situations, it is of great importance to maximize the performance of the injection nozzle, in order to spread the liquid as efficiently as possible and minimize mass and heat transfer limitations, in order to allow the reactions to proceed quickly and efficiently (Bruhns et al., 2005). In fluid coking, it has been seen that a more uniform distribution of liquid, on the largest possible number of particles, results in higher yields of valuable products, making the unit more efficient and profitable (Knapper et al., 2003). Previous studies have shown that the ideal liquid distribution is achieved when the liquid forms a thin uniform film over the solid particles (House et al, 2004). This ideal case is not feasible in large industrial units, where the injected liquid does not evenly coat the solid particles (Knapper et al., 2003). What happens in reality is that liquid-solid agglomerates form upon the injection, trapping the liquid feed. This trapped liquid reacts slowly, hindering the kinetics of the cracking reactions. While many of the agglomerates break apart quickly as a result of rigorous mixing in the fluidized bed, hastening the reaction, stronger agglomerates will persist, continue to limit the reaction, and could negatively affect the quality of fluidization (Weber et al., 2003). These agglomerates were detected using X-ray analysis in a previous work by Ariyapadi et al. (2003a). In a more recent study by House et al. (2004), a sucrose solution was used in the injection, in order to recover the agglomerates and determine their strength and other properties.

One potential factor which could influence the quality of the performance of injection nozzles is the presence of fluctuations in the injection flowrate. Several studies have investigated the effects of nozzle pulsations on the quality of liquid-solid contact efficiency. Hulet et al. (2003) used local triboelectric probes placed throughout a liquid jet to determine the consistency of the liquid spray over the course of an injection. These small probes measured the electrical signal produced by the physical contact between moving particles (through the triboelectric effect). The presence of liquid changed the amount of electricity produced. The study found that pulsations in the gas-liquid spray jet are caused by unstable flow through the nozzle, and these pulsations tend to reduce the quality of the liquid-solid contact. A further study by Ariyapadi et al. (2003b) found that these pulsations occur in the same fashion in open-air tests as they do in a fluidized bed. As such, the pulsations are not caused by the turbulence or chaotic flow within the fluidized bed, but, rather, primarily by the conditions upstream as well as the tip of the nozzle. Also, this allowed for calibrations of future pulsation systems, such as the ones presented in this study, to be performed in open-air.

A study by Chan et al. (2001) assumed that stable, non-pulsating sprays are required for optimal reactor operation. It was then shown in a fluid coking unit, that a stable spray provided higher liquid yields and lower sulphur dioxide and coke formation than a strongly pulsating spray. A limitation of this study is that it only attempted very severe pulsations, when the spray alternated between well-atomized liquid droplets, and a liquid-only injection. McDougall et al. (2005) then used several techniques to measure the quality of fluidization in a fluidized bed, such as measuring the bubble size at the transport disengaging height (TDH) in the bed, dropping a ball through the fluid bed and measuring

the settling velocity, and determining the micro-agglomerate (liquid-solid agglomerates that maintain fluidization) content in the bed by measuring the fines leaving the bed. It was found that pulsating sprays reduced the bed fluidization quality and promoted agglomerate formation. That study did not directly measure liquid-solid contact.

Sabouni et al. (2009) used the active conductance technique from a previous study by Portoghese et al. (2008), as well as in Chapter 3, to study the effect of nozzle pulsations on the quality of liquid-solid contact in a laboratory scale fluidized bed. The study focussed on gas-line pulsations that were milder than those of previous studies and where the instantaneous gas to liquid ratio in the nozzle was never reduced all of the way to 0 wt%. These pulsations led to a dramatic increase in nozzle performance. The purpose of the current study is to build on this study, and to test it with commercial scale nozzles in a large scale fluidized bed, under a wide variety of operating conditions.

A.2 Experimental Apparatus

Experiments were performed in a wedge-shaped fluidized bed. The bed had two parallel sides with lengths of 0.2 m and 1.2 m, spaced 3.5 m apart (Figures A.1 and A.2). The walls of the bed were made of steel and were electrically grounded. Air was used as a fluidizing gas, and was controlled with a system of 4 parallel sonic nozzles. The relative humidity of the fluidization air was held constant at approximately 12% at the compressor outlet, and entered the system at a constant temperature of 20 °C.

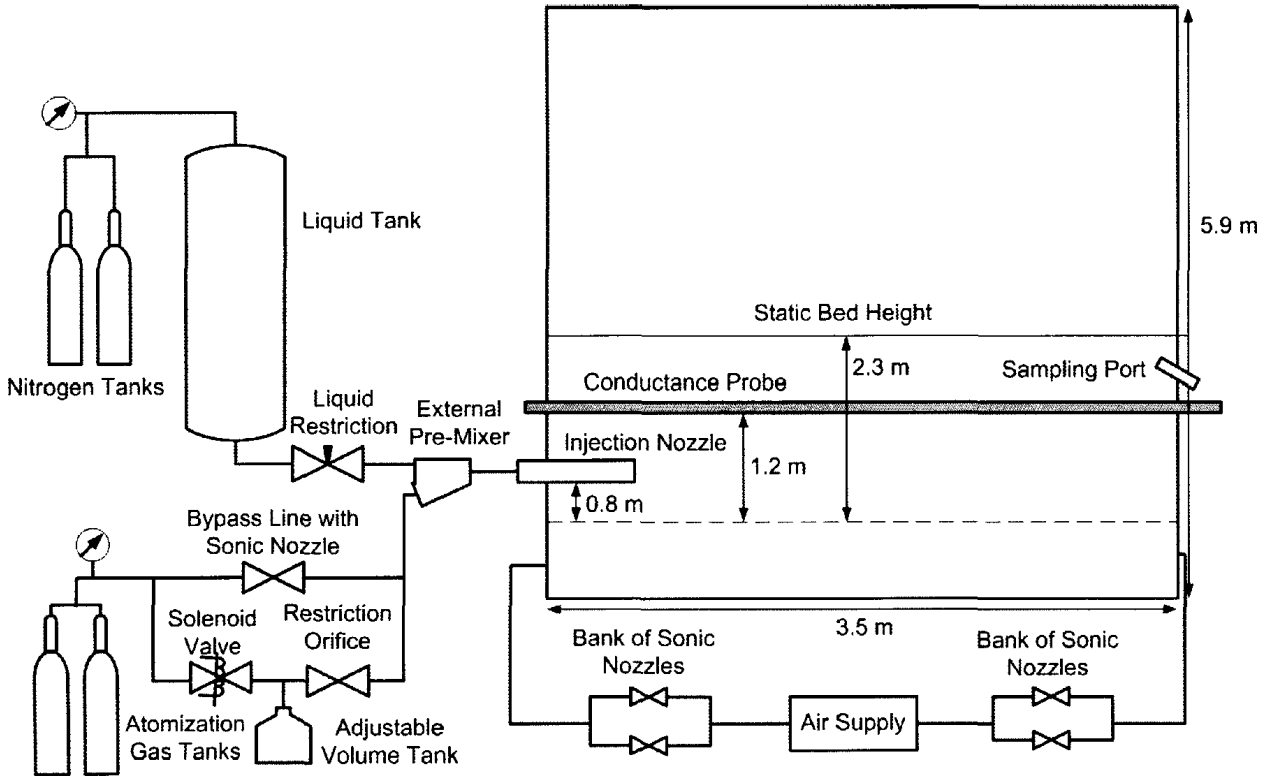

Figure A.1: Schematic diagram of experimental apparatus

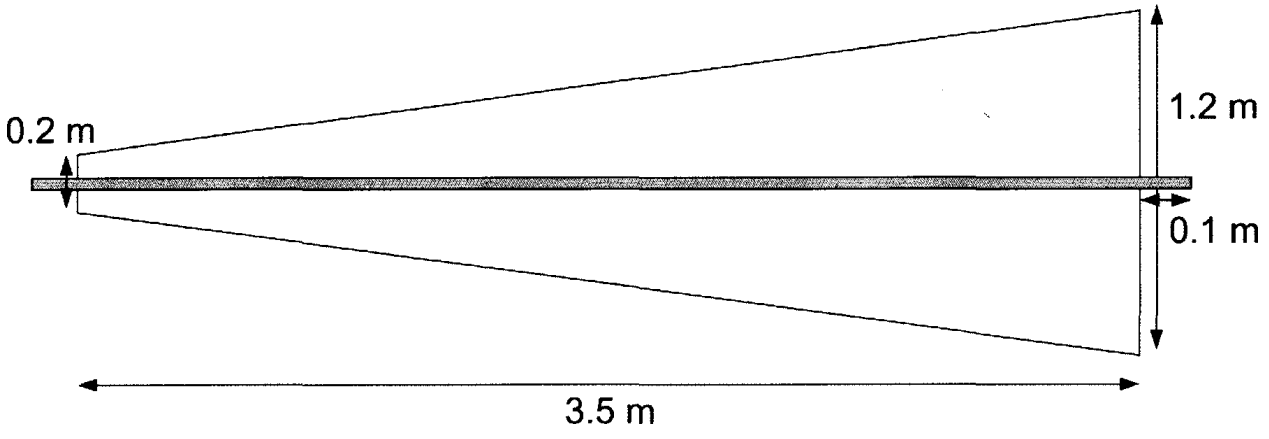

Figure A.2: Dimensions of experimental apparatus (top view) with placement of conductance probe in grey

The fluidized bed was filled with silica sand particles with a Sauter mean diameter of 190 μm and a particle density of 2600 kg/m3. These particles are Group B particles when considering Geldart's powder classification system. They are not porous particles. These

are both characteristics shared with coke particles, making silica sand a good choice for an industrial comparison. The bed had a static height of 2.3 m and contained 8800 kg of sand.

A.1.1 Probes and Data Acquisition

Type J thermocouples were used in the bed to monitor the temperature of the air entering and leaving the system, as well as the temperature of the bed itself. To ensure accurate data, 18 thermocouples were used in total, in various locations in the bed. The thermocouples had a penetration depth of 2.5 cm.

The electrode used as the conductance probe was a stainless steel tube with an outer diameter of 7 mm and a thickness of 1 mm. It was placed 1.2 m above the distributor grid in the fluidized bed and ran through the long side of the bed, hanging out 10 cm on each side (as shown in Figure A.1). A similar probe was used in previous studies [13, 15], but in this study a probe was used that was large enough to run throughout he entire unit. This was necessary due to the high forces present in a larger fluidized bed. The tube was held in place with nylon fittings so that it was electrically insulated from the grounded bed walls. The probe was connected to a 51 kΩ resistor. Figure A.3 shows a schematic diagram of the conductance probe.

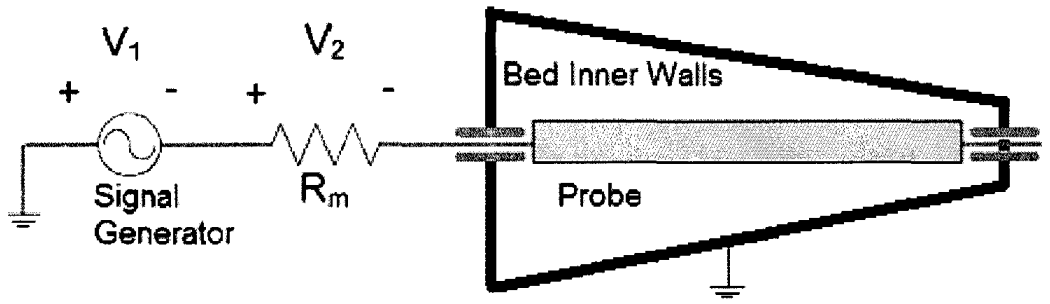

Figure A.3: Placement and corresponding circuit for the conductance probe.

A.1.2 Active Conductance Technique

A function generator was used to apply a sinusoidal electrical signal to the conductance probe. Its sinusoidal signal had an RMS voltage of 6.7 V. With reference to Figure A.3, the conductance of the bed could be determined by using the ratio of the voltage across the resistor (V_2) and the voltage produced by the function generator (V_1), by using Ohm's Law:

$$R_{bed} = 1/\Gamma_{bed} = R_m*(V_1/V_2-1) \quad (A.1)$$

where R_{bed} is the electrical resistance of the bed and Γ_{bed} is the electrical conductance. R_m is the known resistance of the resistor in the system (51 kΩ).

A data acquisition system recorded the voltages V_1 and V_2, the thermocouple readings, and the signals from the pressure transducers measuring the gas and liquid pressures in the injection and the differential across the bed, from which the bed height

could be estimated. The data was sampled at 1000 Hz during the injection and defluidization, but the sampling frequency was reduced to 100 Hz during drying.

The liquid was injected through a commercial scale nozzle illustrated in Figure A.4 (similar in geometry to the Type I nozzle used in previous chapters), which was placed 1 m above the gas distributor, in the centre of the smaller (0.2 m) wall of the bed (see Figure A.1). This nozzle has been patented for fluid coking applications (Base et al., 1999), and was used in previous studies, presented in Chapters 2 and 3.

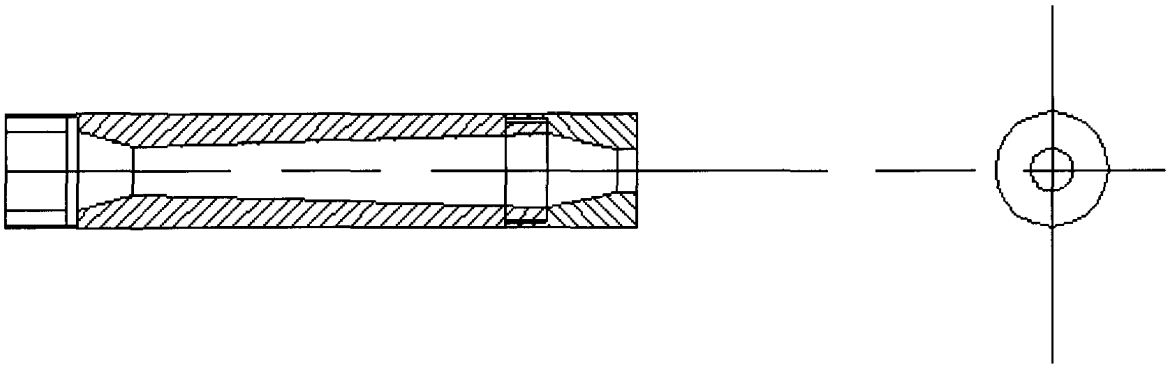

Figure A.4: Diagram of the nozzle used in this study

De-ionized water was used as the liquid for the injections, due to its high purity. This purity was required to prevent an accumulation of impurities over the course of several experiments. The liquid flowrate was controlled by regulating the nitrogen pressure applied to the liquid feed tank. The time-averaged liquid flowrate was 2.2 kg/s for all the experiments of this study. A gas mixture of 18% nitrogen and 82% helium by mass was used for the atomizing gas. This was chosen because the combination of these mixed gas, de-ionized water and silica sand provides a realistic approximation of the steam, bitumen and coke system used in industrial fluid coking units. The gas flowrate was controlled

using a restriction orifice. Pressure transducers were used to measure the pressure on both sides of the orifice, and, using calibration data, the instantaneous flowrate could be determined from the instantaneous pressures.

The gas and liquid were mixed in an external pre-mixer upstream of the spray nozzle. Two types of pre-mixer were utilized: a bilateral flow conditioner (BFC) and a Venturi pre-mixer. In the BFC, the water and gas enter from different sides, both at an angle of 30° with respect to the axis of the nozzle. In the Venturi, the gas enters at a right angle to the liquid flow in the Venturi throat. The pressure in the pre-mixer was monitored with a pressure transducer.

A.1.3 Solenoid Valve

In order to induce pulsations in the liquid spray, a solenoid valve was introduced in the atomizing gas line, just upstream of the restriction orifice (Figure A.1). The volume between the solenoid valve and the restriction orifice was varied in the experiments to change the pulsations amplitude. This solenoid valve was controlled by a function generator using the circuit shown in Figure A.5. The function generator produced a square-wave electrical voltage. Due to the nature of the transistor in the circuit, the solenoid valve is opened when the signal is at its high setting and closed when the signal is low. The high and low periods have an equal period, which can be controlled by changing the frequency of the square-wave signal. By opening and closing the gas line, the gas-to-liquid ratio is no longer held constant, and the fluctuations in gas pressure in the line cause the water flowrate to also change. This induces the pulsations whose effects were investigated in this study. The frequency of pulsation was fast enough that the gas flowrate never decreased to

zero, as there was still a release of gas from the region between the solenoid valve and the restriction orifice governing the gas flowrate.

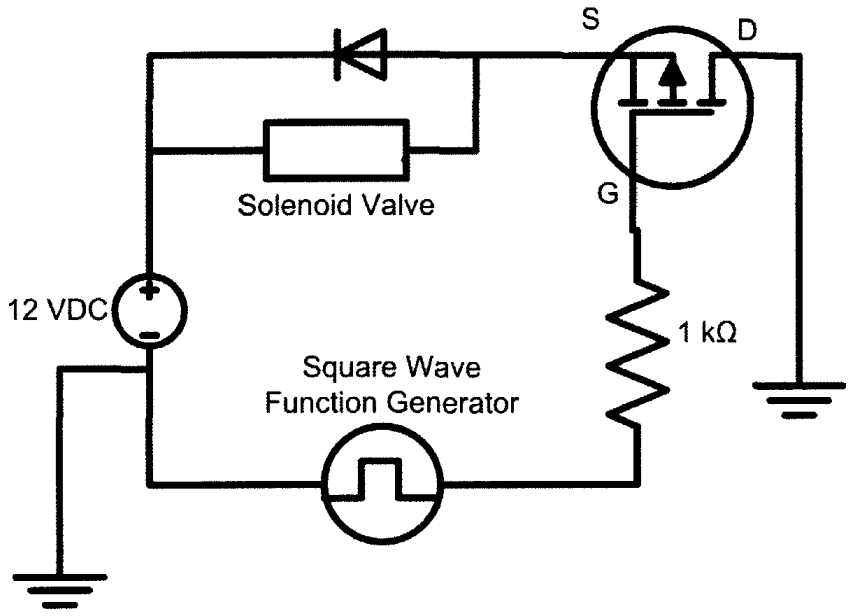

Figure A.5: Circuit diagram of solenoid valve-based pulsation technique

A.1.4 Sampling Port

Samples of the bed material were taken from the bed after the atomized liquid injection using a sampling port 1.5 m above the distributor grid, on the opposite side of the bed from the nozzle (Figure A.1). Each sample had an approximate mass of 500 g. These samples were then tested in two pieces of equipment: an avalanche machine and a moisture balance. The avalanche testing equipment consists of a rotating drum with a rotational speed of 0.3 rpm, which uses image recognition software to calculate how often the sample slips ("avalanches") during the rotation. When the force of gravity overcomes the cohesive forces between the particles, the avalanche occurs; as such, the mean avalanche time (t_{av}) characterizes the powder cohesiveness (Lavoie et al., 2002; Lee et al., 2000). In the

moisture test, approximately 10 g of sample is introduced in the moisture balance, weighed, and then heated at 105 degrees Celsius until the weight is no longer changing.

A.3 **Experimental Procedure**

This section describes the methodology of the experiments that examined the effect of nozzle pulsations on the quality of a gas-atomized liquid injection. Several measurements were taken to determine the liquid-solid contact efficiency in the bed. Bed conductance measurements were collected, using the conductance probe. This conductance has been found to be proportional to the quality of liquid-solid mixing (Portoghese, 2008).

The silica sand used in this study is a low-conductance particulate material, and does not conduct electricity at a significant level when it is dry. However, when water is added, the wetted sand becomes relatively conductive. Wetted regions can become high conductance paths, which allows for the transmission of electrical current. When the water is distributed well throughout the system, there are more conductive paths for the electricity to flow, which results in an increased bed conductance. (Portoghese, 2008)

Before the start of each experiment, the superficial gas velocity of the fluidization air was set to 0.15 m/s. The solenoid valve circuit was completed, creating artificial fluctuations in the injection gas flowrate.

At the start of the experiment (t = 0 s), the water-mixed gas mixture was injected into the bed. The injection lasted for 10 s. The liquid and gas flowrates were set to the desired levels by adjusting the upstream pressure in the gas cylinders. The liquid flowrate was set

so that the averaged flowrate was 2.2 kg/s, and so that 22 kg of water was injected in total. Since there was 8800 kg of silica sand in the bed, the maximum liquid-to-solid (L/S) ratio in the bed was 0.25 wt%. An average gas-to-liquid ratio (GLR) of 0.8% was achieved, resulting in a gas flowrate of 0.176 kg/s.

At t = 15 s, the fluidization gas velocity was reduced to 0.075 m/s. The liquid was then allowed to mix for an additional 45 s. At t = 1 min, the fluidization gas was stopped, thus immediately defluidizing the bed. During this time, conductance measurements were taken, measuring how well the liquid was spread throughout the bed.

At t = 10 min, the bed was refluidized, at a superficial fluidization gas velocity of 0.12 m/s. It was then allowed to dry for two hours, such that the bed would be completely dry and ready for the next experiment. Online measurements of bed temperature and conductance were used to ensure the bed was completely dry before each experiment, and that each experiment started at a constant temperature of 20 °C.

A.3.1 Agglomerate Sampling

Three 500 g samples of the sand within the bed were taken from a sampling port above the fluidized bed, at times t = 11 min, 15 min and 20 min. These samples were then tested for free moisture content (the amount of liquid present in the sand that is not trapped in agglomerates) and for the presence of agglomerates in the sample.

In the evaporation test, a small amount (10 g or so) of each sample is weighed, and then heated at 105 degrees Celsius, until the weight stops changing. The percentage change in mass is then recorded, as this is approximately the amount of total moisture (the sum of

the amount of free moisture, micro agglomerates and macro agglomerates) present in the sample. This test is repeated 3 times for each sample.

In the avalanche test, about 300 g of a sample is placed in a rotating drum, and rotated at 0.3 rpm. Image recognition software detects when the sample slides ("avalanches") during the rotation. The test continues until the sample rotates 128 times, and the average avalanche time and the standard deviation of the avalanche time are recorded. This data can then be used to determine the micro agglomerate, macro agglomerate and free moisture content of the fluidized bed, as demonstrated in the next section.

A.3.2 Micro-agglomerate and Macro-agglomerate Calculations

During the fluidized bed injection, much of the liquid gets trapped in liquid-solid agglomerates. In a reactor, these agglomerates restrict mass and hear transfer, and negatively affect the reactions in fluid cokers (Weber et al., 2006). These agglomerates can be further divided into two subcategories: agglomerates that are small enough to fluidize together with the rest of the bed material (called micro-agglomerates), and agglomerates that are too large and heavy and sink to the bottom of the fluidized bed (called macro-agglomerates). Any injected liquid that does not agglomerate is known as free moisture. The free moisture and moisture in the agglomerates could then be expressed using a liquid-to-solid ratio (L/S), which is a ratio between the mass of liquid present in the bed in the form described (free moisture, micro-agglomerate or macro-agglomerate), and the total mass of solids of the bed. As such, the sum of the 3 (L/S) ratios should equal the overall liquid-solid ratio in the bed.

A correlation between the average time between avalanches and the content of free moisture in the sample was derived from calibration data with mechanically mixed samples of known free moisture contents. This correlation is as follows:

$$\ln (L/S)_{\text{free moisture}} = 3.046 - 0.004626(t_{av})^{2.5} + 0.00148763(t_{av})^{3} \quad \text{(A.2)}$$

From this correlation, the free moisture content of the sample can be determined. Since macro-agglomerates are by definition not fluidized, there are no macro-agglomerates present in the sample. As such, the amount of micro-agglomerates present in the sample can be determined by subtracting the free moisture content from the total moisture content of the sample.

$$(L/S)_{\text{micro}} = (L/S)_{\text{total moisture, sample}} - (L/S)_{\text{free moisture}} \quad \text{(A.3)}$$

The bed is vigorously mixed when samples are taken, and it can be assumed that samples are representative of the material that is fluidized in the bed. The mass of solids trapped in the micro-agglomerates is considered insignificant, and the total solid content is assumed to be constant. As such, one can determine the macro-agglomerate content in the bed from:

$$(L/S)_{\text{macro}} = (L/S)_{\text{total moisture, mass balance}} - (L/S)_{\text{total moisture, sample}} \quad \text{(A.4)}$$

This equation assumes a negligible amount of solids is trapped in macro-agglomerates, compared to the total mass of solids in the bed. This assumption can be justified in view of the very large mass of solids in the bed and the relatively small mass of macro-agglomerates. Therefore, the total moisture content of the bed can be calculated with

a simple mass balance. The mass of liquid originally injected into the initially dry bed is known. The evaporation rate of liquid from the bed can be estimated by considering the following points:

Fluidization air enters the system at a constant relative humidity of 12% as experimentally measured. Air is assumed to leave the fluidized bed saturated with water. Except for a short time during the initial injection, this is an accurate assumption as verified by humidity measurements of the air leaving the column.

It is assumed that there is no drying during defluidization, when no air is flowing through the system.

First, the saturation pressure and saturation humidity were determined, using Antoine's equation.

$$P_{sat} = e^{\left(23.44 - \frac{3965}{T + 232.8}\right)} \tag{A.5}$$

$$h_{sat} = 0.6219\left(\frac{\frac{P_{sat}}{101325\ Pa}}{1 - \frac{P_{sat}}{101325\ Pa}}\right) \tag{A.6}$$

Since the data acquisition also monitors the fluidization gas flowrate, one can use the difference between the saturation humidity and the inlet humidity to determine the rate of evaporation:

$$\text{Evaporation Rate} = F_g(h_{sat} - h_{in}) \tag{A.7}$$

$$\left(\frac{L}{S}\right)_{\text{total moisture mass balance}}(t) = \frac{m_{liq.\ injected} - \int_0^t (Evaporation\ rate)\,dt}{m_{solids}} \quad \text{(A.8)}$$

A.4 Results

Figure A.6 shows the effect of the pulsations on the liquid and gas flowrates during the injection. The pulsations are not shaped perfectly like the square waveform that is applied to the solenoid valve. This irregularity is caused by two factors. There is a volume between the solenoid valve and the restriction orifice and, when the solenoid valve is closed, the gas in this volume is gradually released through the orifice, causing the flowrate to decrease over time. This creates a capacitance effect, and it explains the reason for the residual gas flow when the solenoid valve is closed.

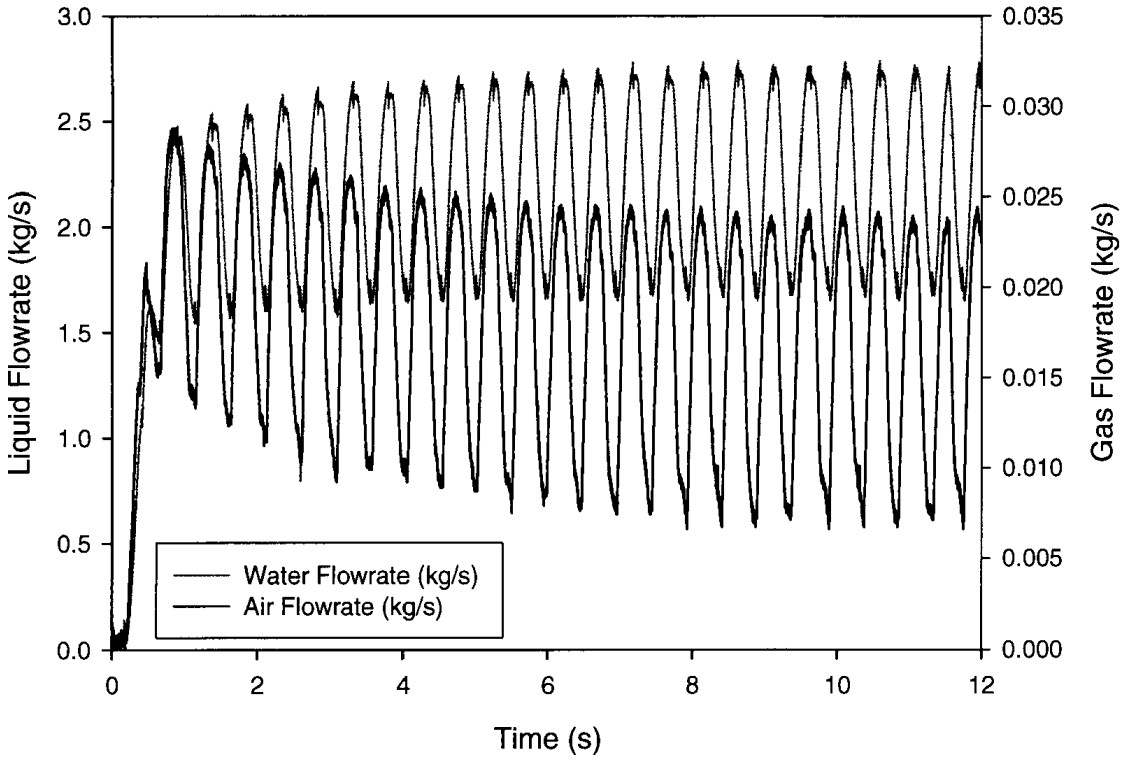

Figure A.6: Liquid and Gas Flowrates during Injection with 2 Hz Pulsations with the BFC Pre-mixer and a volume of 12.5 mL between Solenoid Valve and Restriction Orifice

As expected, although the pulsations are applied only to the gas line, they greatly affect the liquid flowrate, as shown by Figure A.6. A lower gas flowrate results in a smaller pressure drop through the spry nozzle, and, consequently, a lower pressure upstream of the premixer. Since the pressure of the liquid tank is held constant, this change in downstream pressure changes (increases) the liquid flowrate.

The results shown in Figure A.6 were obtained with the smallest volume between the solenoid valve and the restriction orifice (known as the "dead volume" or "capacitance"), which resulted in large pulsations. The gradual, slow decrease in the average gas flowrate, and conversely the increase in the liquid flowrate, is due to irregularities with the start-up of the injection. The injection length was 10 s so that the irregularities of the initial start-up could be considered insignificant relative to the steady-state flowrate (which started at about t = 2 s).

Increasing the dead volume in the injection line led to a significant decrease in the amplitude of the pulsations. This can be seen in Figure A.7, which illustrates the flow rates found in a test where the spacing volume is increased from 34 mL to 500 mL. With this change, the pulsation amplitude decrease to approximately a third of the value seen with the smallest dead volume, as shown in Figure A.6. The time averaged flowrates of liquid and gas are held constant, so that a good comparison can be made between different tests.

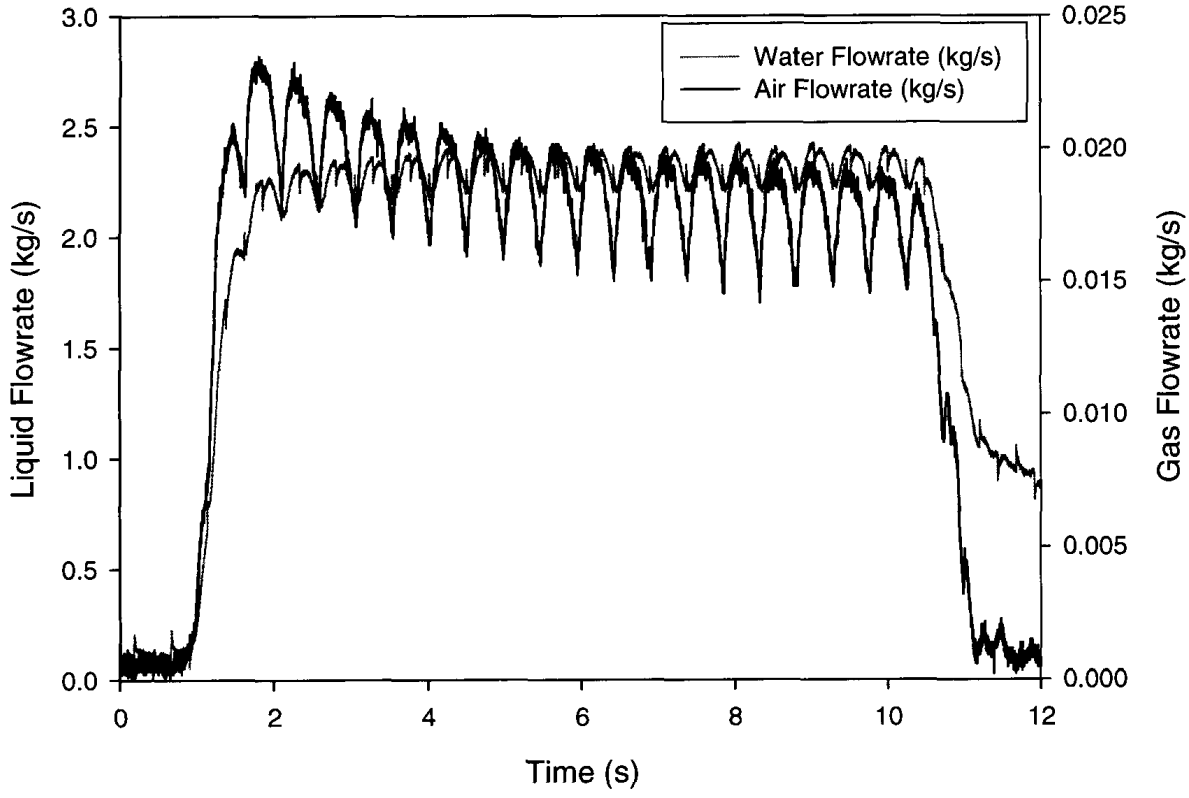

Figure A.7: Liquid and Gas Flowrates during Injection with 2 Hz Pulsations in Type I Nozzle with BFC Pre-mixer and a volume of 500 mL between Solenoid Valve and Restriction Orifice.

The effect of changing the dead volume on the amplitude of the nozzle pulsations is shown in Figure A.8. Varying dead volumes show different levels of variance in the gas to liquid (GLR) ratios. In Figure A.9, the effect of changing the dead volume was plotted against the average amplitude of the pulsations for each experiment. The amplitude of pulsation was calculated as the distance between the extremes in the flowrate, and the time-averaged flowrate. It was found that a strong logarithmic correlation was found between the two variables, with an R2 value of 0.9862. Eventually, if the dead volume is sufficiently large, the amplitude of the pulsations will be insignificant enough that the system will resemble the case in which no pulsations are used.

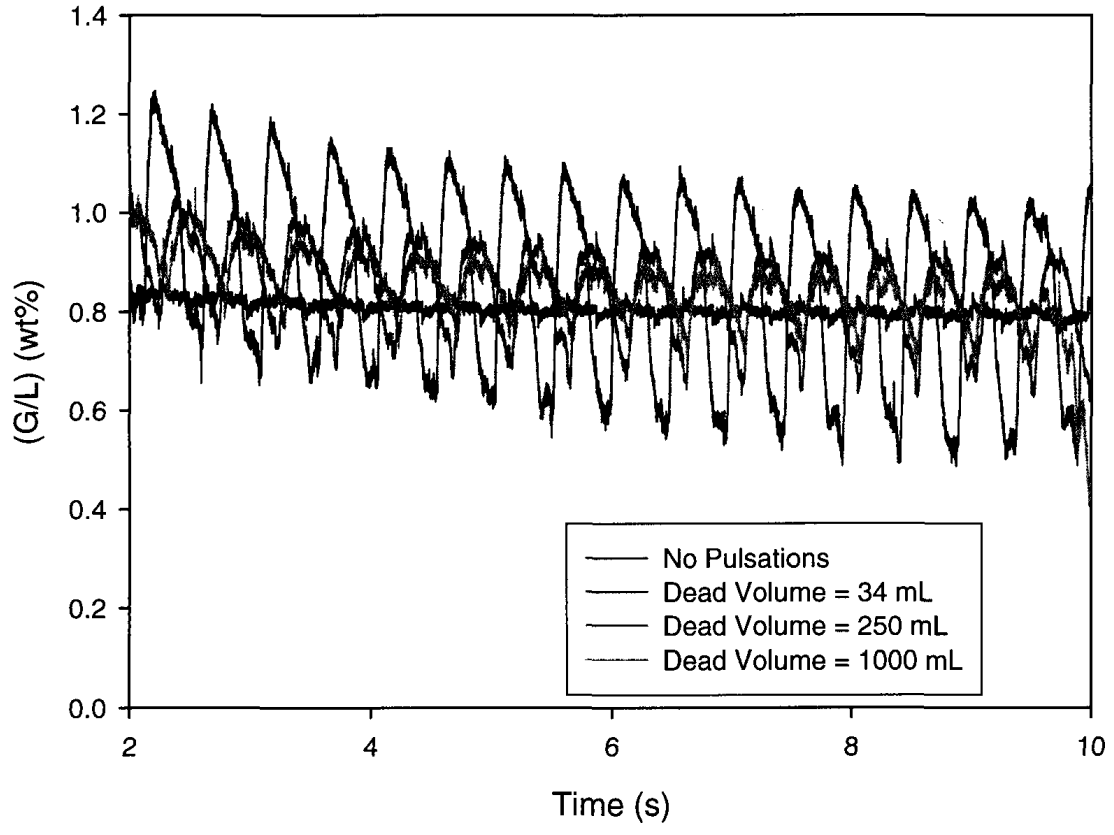

Figure A.8: Gas-to-Liquid Ratios (GLR) at various spacing volumes between the solenoid valve and the sonic nozzle. 2 Hz Pulsations in Type I Nozzle with BFC Pre-mixer, average (GLR) of 0.8 wt%.

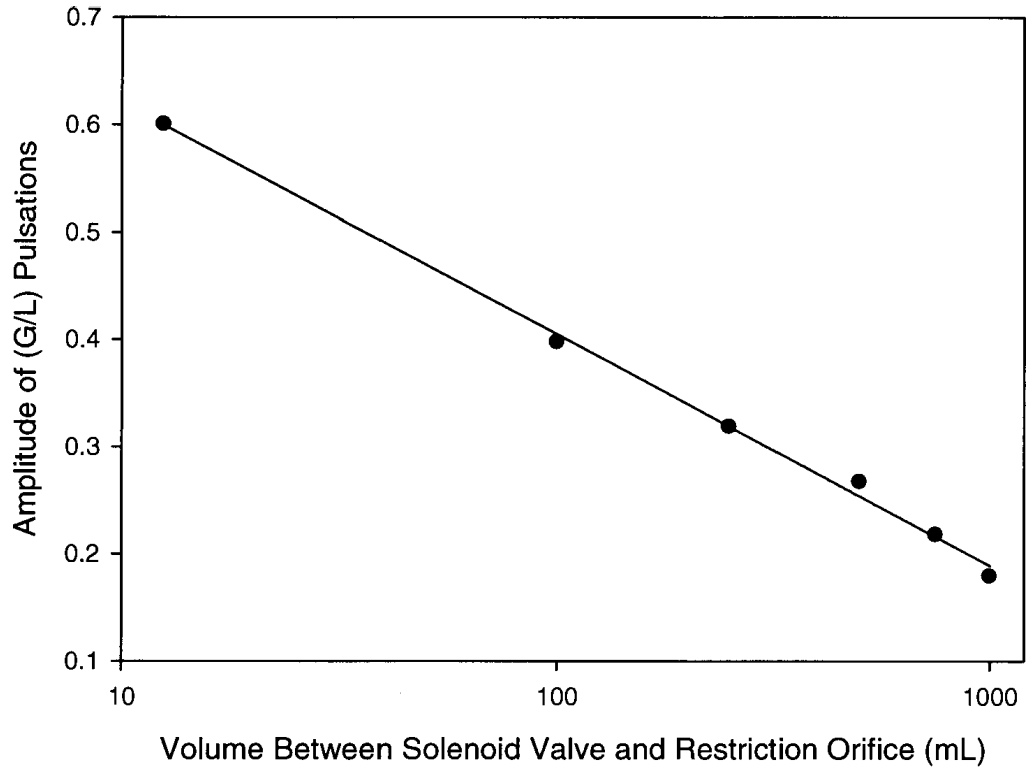

Figure A.9: The effect of changing the volume between the solenoid valve and restriction orifice on the amplitude of the nozzle pulsations. 2 Hz Pulsations in Type I Nozzle with BFC Pre-mixer, average (GLR) of 0.8 wt%.

The conductance of the fluidized bed solids over the course of an experimental run, as measured by the conductance probe is displayed in Figure A.10. For the first 10 minutes of the experiment, the bed is defluidized, and the bed conductance, as measured by the probe, increases logarithmically. The Nozzle Performance Index (NPI), used in a previous work by the authors (Chapter 3), is defined as the slope of this logarithmic curve. This slope measures the rate that the liquid can spread throughout the bed, which roughly translates to the amount of free moisture present. After this point, the bed is refluidized, allowing the agglomerates to break, and the bed solids to dry. As seen in the graph, the

defluidization technique is used because there is much less noise in the probe signal than when the bed is fluidized. Samples are taken 10 minutes after the bed is refluidized, because the liquid and agglomerates have not moved through the unit sufficiently at the time of refluidization for accurate sampling.

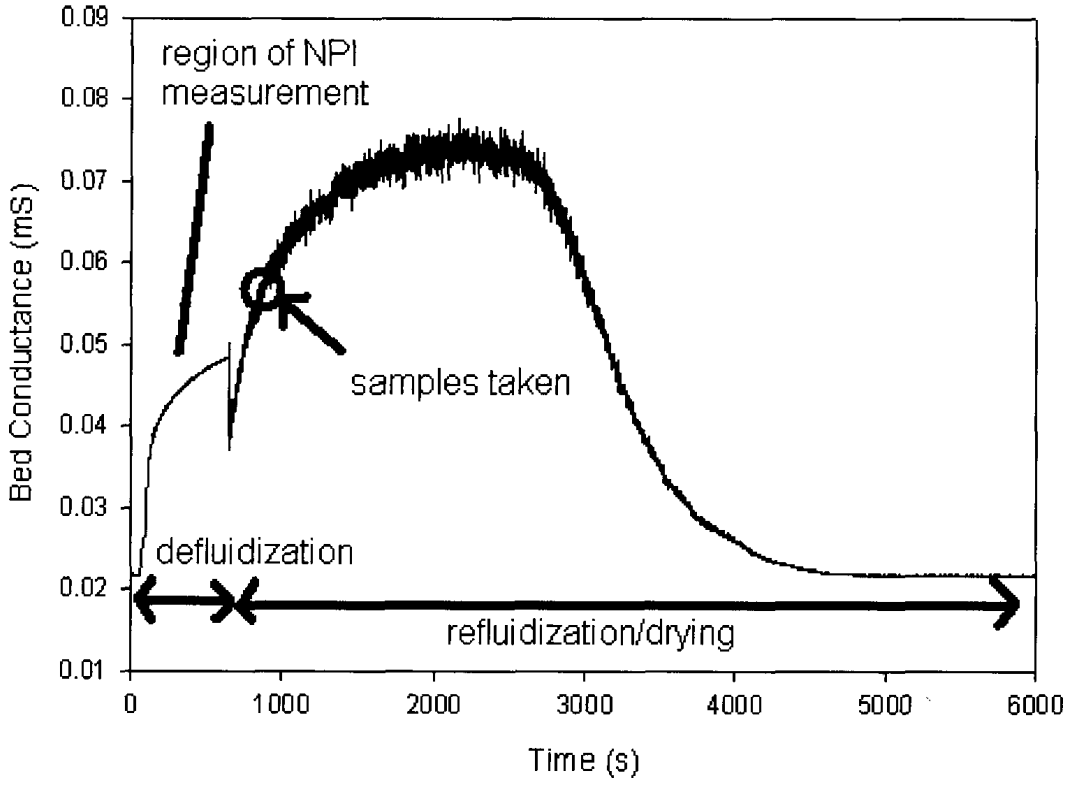

Figure A.10: Conductance Probe signal, including defluidization and refluidization (drying) zones.

A.4.1 Effect of Pulsation Amplitude

The effects of the variation in the amplitude of the pulsations on the quality of the injection and the spreading of liquid, as characterized by the NPI, are displayed in Figure A.11. The amplitude is plotted against both the NPI and the free moisture content (which is calculated using Equation 4.2). Both sets of data show that the nozzle performance is maximized for the largest of the tested pulsation amplitudes. The data where no pulsations

are applied are displayed on the far left of the plot. This corresponds to a pulsation amplitude of about 0.1 wt% (GLR), as there are still small natural fluctuations in the gas flowrate, even when artificial pulsations are not applied. When the amplitude of the pulsations becomes small, the nozzle performance decreases to the same level as a test with no pulsations.

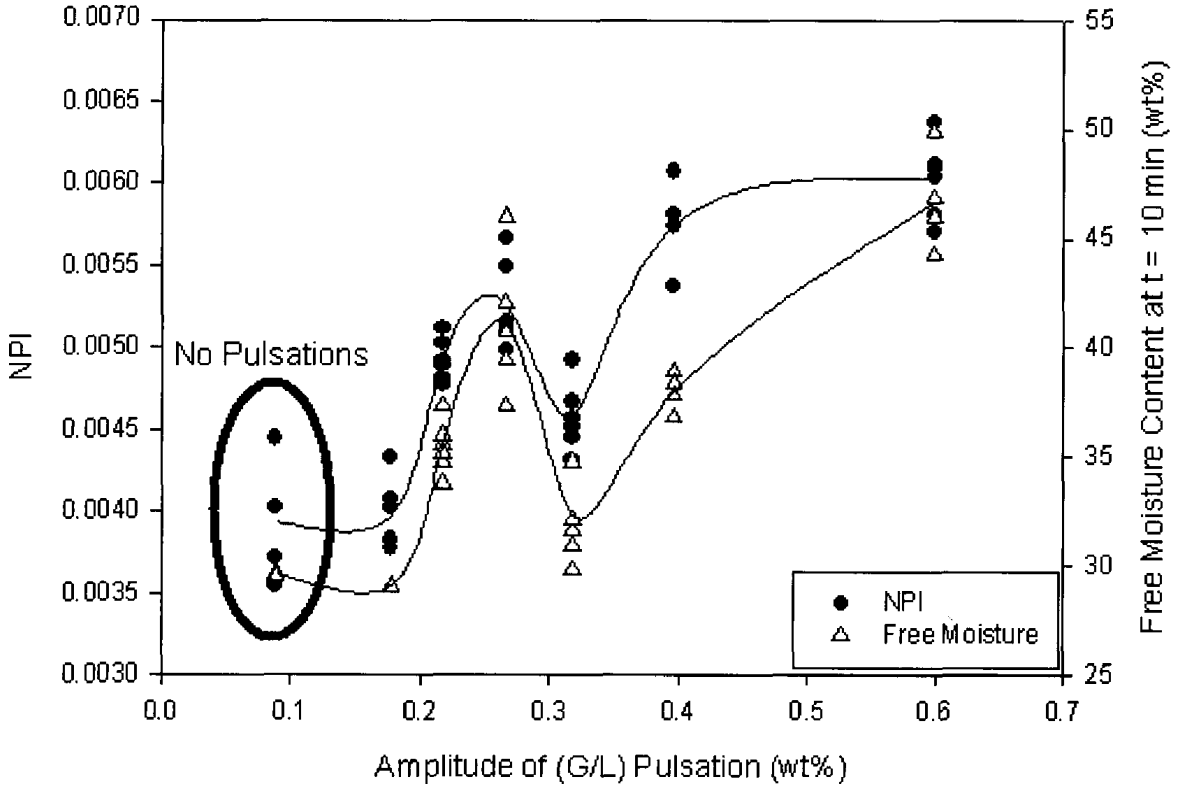

Figure A.11: Effect of changing the amplitude of the nozzle pulsation on the nozzle performance. 2 Hz Pulsations in Type I Nozzle with BFC Pre-mixer, average (GLR) of 0.8 wt%.

One possible explanation for the beneficial impact of the pulsations is that changing (GLR) ratio also changes the jet penetration depth of the injection, as seen in a study by Ariyapadi (2004). Since most of the liquid from the injection is deposited at the end of the jet cavity (House et al., 2004), changing the jet penetration depth would lead to a greater

spread of liquid throughout the fluidized bed, leading to less agglomerate formation, and a higher free moisture content. The pulsations also affect the liquid droplet size: as a result of the pulsations, more liquid is injected in the form of larger droplets: as demonstrated in a previous work by the authors (Chapter 3), small (GLR) ratios result in larger droplets, which is not beneficial to the liquid distribution. There are, therefore, two opposing results of the pulsations: the beneficial variation in jet penetration, and the larger droplet size. This may explain the complex and unexpected behaviour shown in Figure A.11. As such, there is a balance to be found when choosing the optimal pulsation amplitude.

Very similar trends in the effects of the amplitude of the pulsations on NPI and free moisture content have been observed and illustrated in Figure A.11. To further compare these two variables, a plot was constructed comparing these two characteristic parameters (Figure A.12). This plot used the data points from all the experiments used in this work, including the tests varying the amplitude, frequency and (GLR), as well different nozzle configurations. It was found that a fairly strong linear correlation was found between the two variables (R^2 = 0.8032). This shows some evidence that the NPI is an indication of how well moisture is spread throughout the unit, as it was hypothesized in the previous chapters This seems to confirm that the NPI is a very useful tool for determining the quality of an injection, since the free moisture content of the bed leads to increased liquid-solid contact within the bed, which is critical for important industrial processes, such as fluid coking and fluid catalytic cracking (FCC).

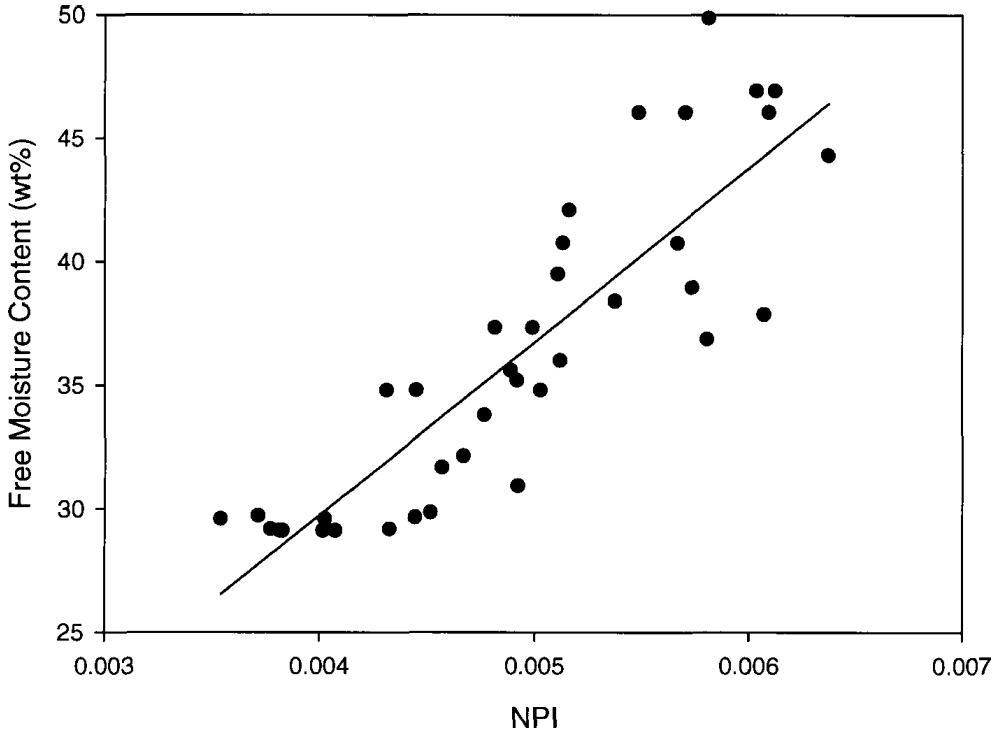

Figure A.12: Correlation between free moisture content in fluidized bed and NPI. R2 = 0.8032.

The concentration of micro-agglomerates (the agglomerates that remain fluidized, as defined in equation (4.3) found in the fluidized bed at different pulsation amplitudes is presented in Figure A.13. Once again, the points on the far left represent the base case, for which no pulsations were applied. Micro-agglomerates are small agglomerates that can still be fluidized, and cause a much less significant mass transfer limitation than the larger macro-agglomerates. The micro-agglomerate content decreases greatly in the mid-range amplitudes of about 0.2-0.3 wt% (GLR). This corresponds to the sudden increase in free moisture and NPI found in Figure A.11. With the exception of these mid-range amplitudes, the micro-agglomerate content displays a steady decrease with increasing nozzle fluctuations, displaying the benefits of larger pulsations.

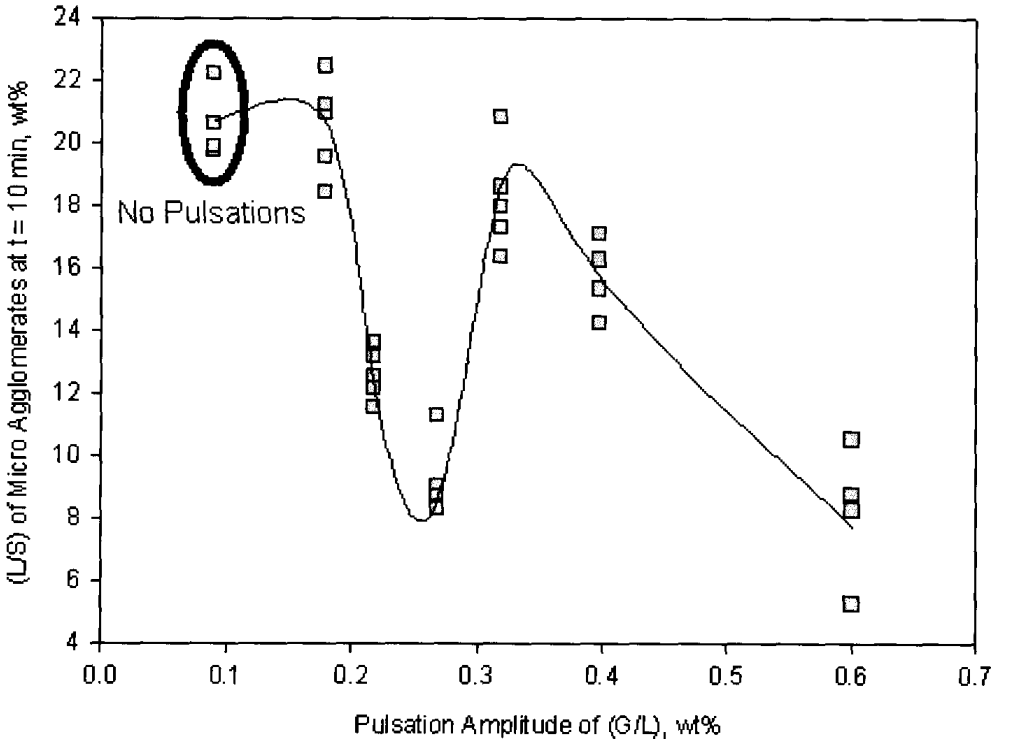

Figure A.13: Micro Agglomerate (Equation 3) Content of Bed after 10 minutes of refluidization. 2 Hz Pulsations in Type I Nozzle with BFC Pre-mixer, average (GLR) of 0.8 wt%.

In Figure A.13, the micro-agglomerate content (agglomerates that remain fluidized, as calculated in equation (4.4) at amplitudes of 0.6 wt% (GLR) and 0.3 wt% (GLR) are approximately identical. However, the nozzle performance and free moisture contents are much higher in the case of the larger pulsations. This is due to the higher macro-agglomerate content at the lower pulsation amplitude, as seen in Figure A.14. At the same point where the micro-agglomerate content suddenly decreases, the macro-agglomerate content increases. At this point, while the free moisture content (and as such, liquid-solid contact efficiency) are increasing, these extra macro agglomerates are also limiting the mass transfer in the bed, as well as potentially causing unwanted defluidized areas of the bed. This increase in macro-agglomerates could be what was detected in previous studies

that led to identifying the negative consequences of the pulsations (Chan et al., 2001; McDougall et al., 2005). However, when the amplitude of the pulsations increases, the macro-agglomerate and micro-agglomerate contents decrease, leading to higher free moisture content. Consequently, the largest pulsations are the most beneficial, as compared to the mid-range pulsations that show high free moisture content but also high macro-agglomerate counts, as well.

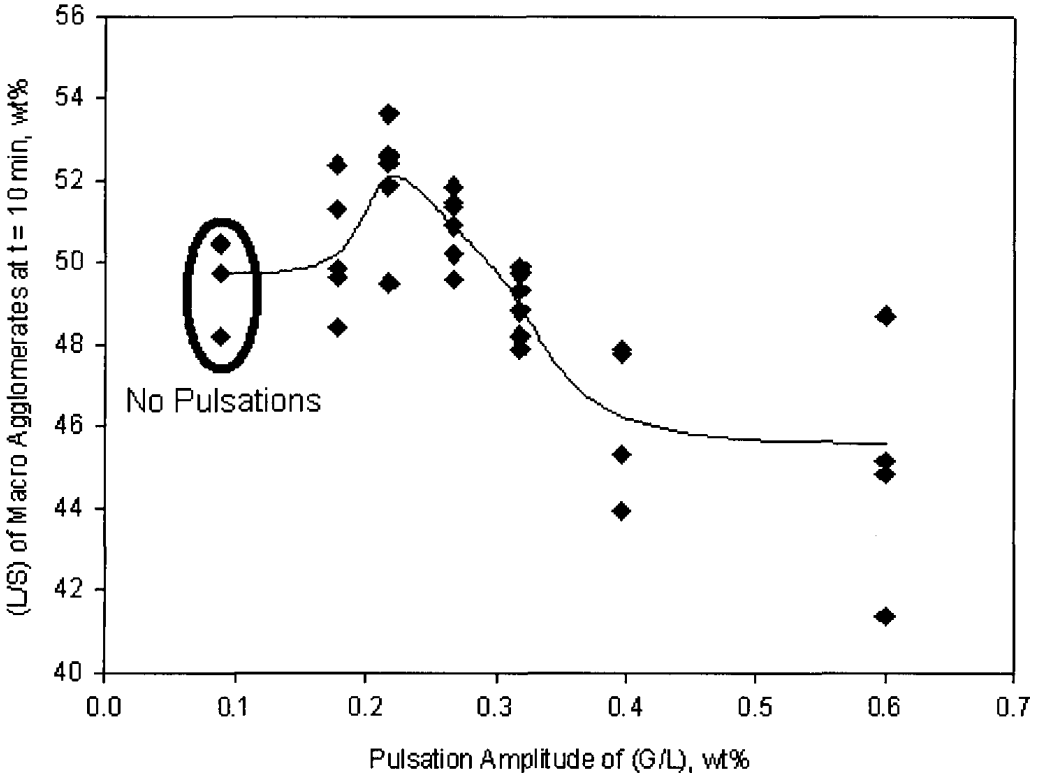

Figure A.14: Macro Agglomerate (Equation 4) Content of Bed after 10 minutes of refluidization. 2 Hz Pulsations in Type I Nozzle with BFC Pre-mixer, average (GLR) of 0.8 wt%.

In Figure A.15, the results presented in the previous figures, which represent data from the pilot-scale unit, are compared to results from a smaller scale unit, as presented in Appendix A. Similar nozzle and pre-mixer geometries are used in both cases, with a

scaling factor of 8 (the internal diameters of the nozzles are 8 times larger on the large scale than the small scale). The same (GLR) ratio is used, even though the individual gas and liquid flowrates, as well as the bed mass, are much smaller. As one can see, a similar trend is apparent in both cases, although the small scale tests exhibit a higher NPI. However, both sets of experiments show that the nozzle performance increases as the gas pulsations become more pronounced.

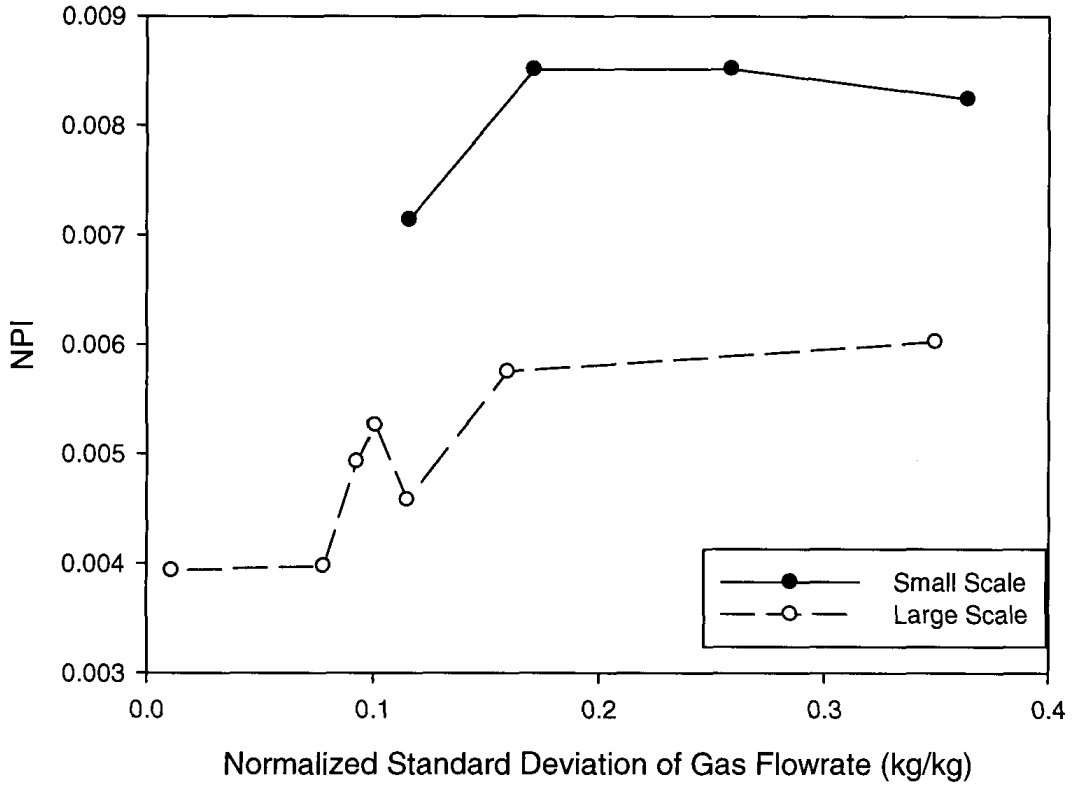

Figure A.15: Comparison Amplitude Tests in Small and Large Scale units. Type I nozzle and BFC pre-mixer used in both cases, with an average (GLR) ratio of 0.8%. Scaling Factor of 8 between large and small scale nozzles

A.4.2 Effect of Pulsation Frequency

The effect of changing the pulsation frequency on the nozzle performance is illustrated in Figure A.16. A frequency of 0 Hz represents the case where no pulsations are applied to the

gas line. The graph shows that a great improvement in nozzle performance occurs when pulsations are applied to the apparatus, but the quality of the jet-bed interaction seems mostly unaffected by the change in the pulsation frequency. Performance at a frequency of 0.5 Hz is slightly poorer than at higher frequencies. This is consistent with attribution of the beneficial effect of pulsations to variations in jet penetration. At 0.5 Hz, the jet remains stationary for a longer period of time and too much liquid is therefore deposited in one limited area. At frequencies ranging from 1 to 5 Hz, the NPI and free moisture content show a tremendous increase, nearly doubling in magnitude when pulsations are applied.

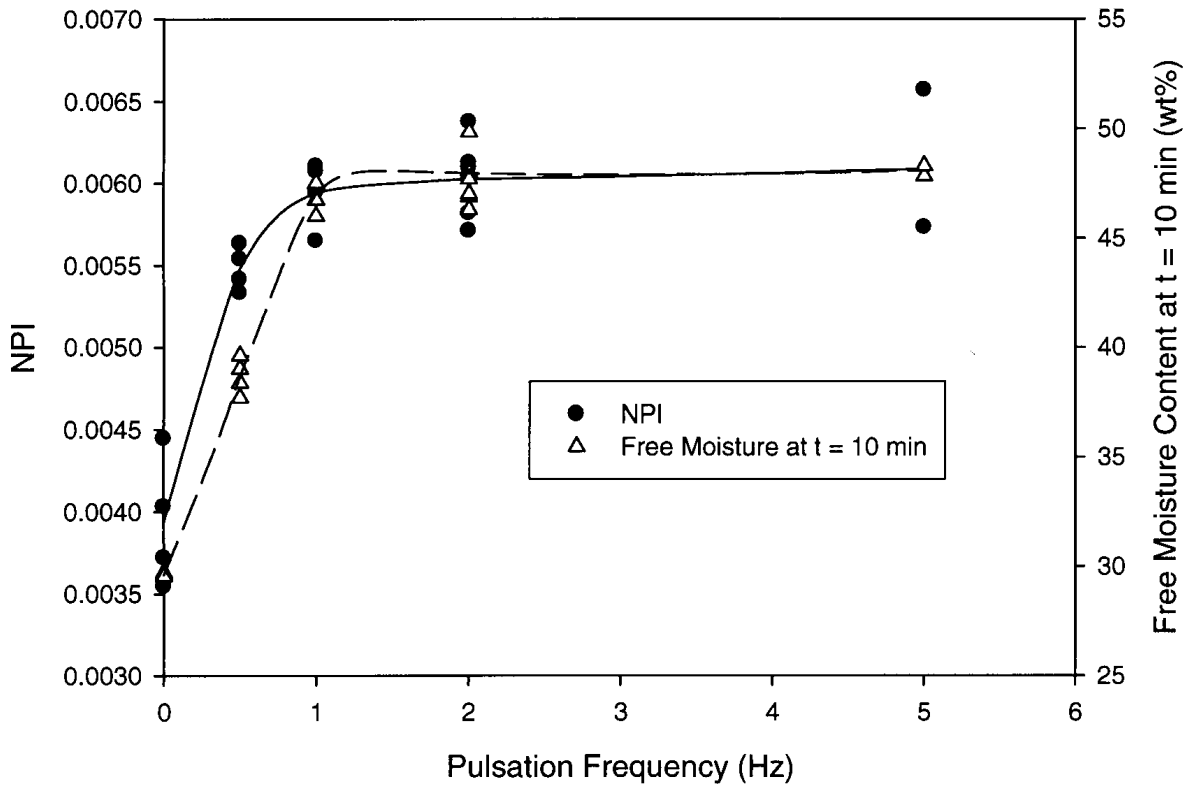

Figure A.16: The Effect of Pulsation Frequency on Nozzle Performance. Average (GLR) Ratio of 0.8 wt%, Pulsation Amplitude of 0.6 wt% (GLR).

Figure A.17 summarizes the effect of different pulsation frequencies on liquid-solid agglomeration, for a pulsation amplitude of 0.6 wt%. The increase in free moisture caused

by inducing pulsations seems to have a close, inverse relationship with the decrease in unwanted macro-agglomerates under the same conditions. There is also a decrease in micro-agglomerates at the same point.

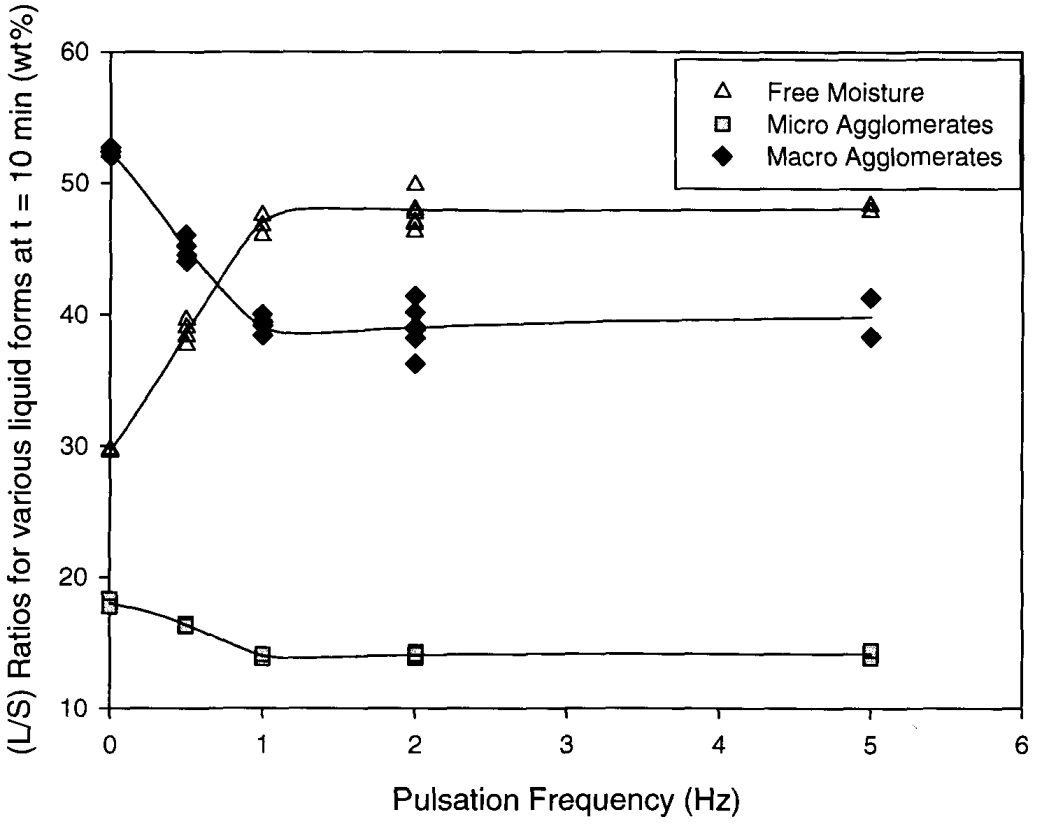

Figure A.17: Agglomeration occurring after 10 minutes refluidization, with various pulsation frequencies. Average (GLR) ratio of 0.8 wt%, pulsation amplitude of 0.6 wt% (GLR).

The effect of frequency is similar in both the small scale and large scale units, as seen in Figure A.18. In both units the pulsation frequency does not seem to matter, as long as it is higher than 1 Hz.

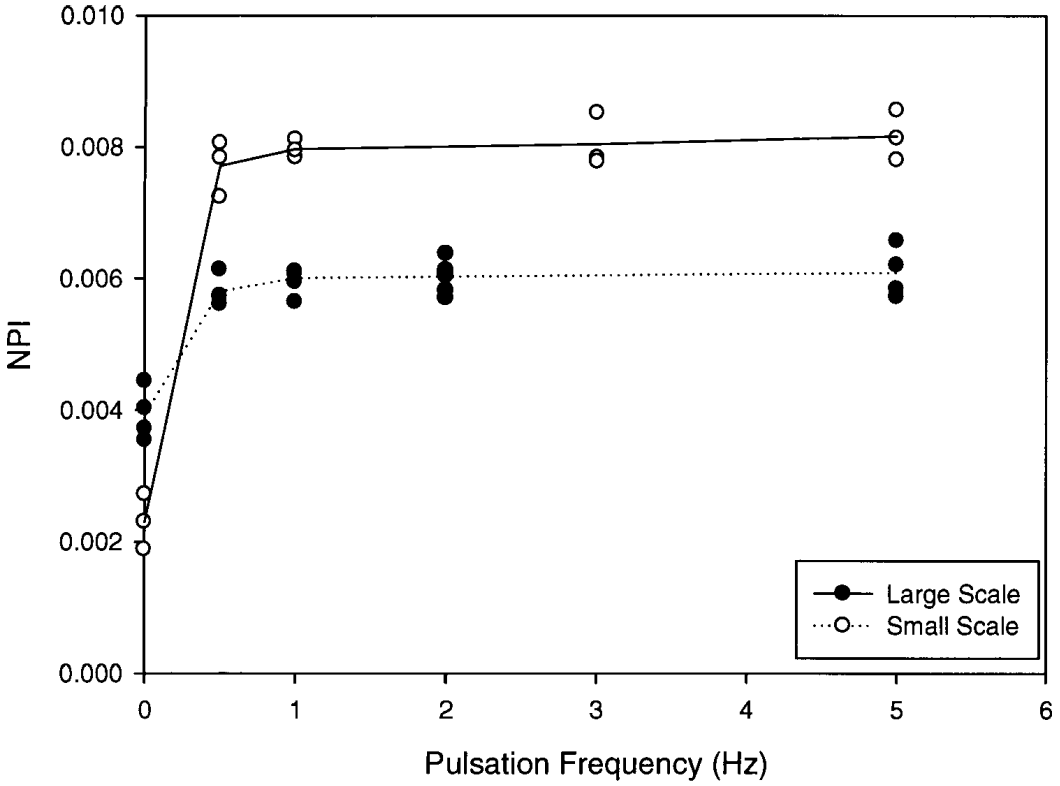

Figure A.18: A comparison of the effect of pulsation frequency on small and large-scale fluidized beds. Type I nozzle and BFC pre-mixer, average (GLR) of 0.8 wt% used.

A.4.3 Effect of Different Pre-mixers

To test the versatility of the pulsation technique, a different type of pre-mixer, the Venturi pre-mixer, was used. These results can be seen in Figure A.19. It shows a similar increase in nozzle performance when pulsations are applied as in the case of the BFC pre-mixer. The Venturi seems to operate slightly better at low frequencies, such as 0.5 Hz. Under the current operating conditions, the BFC shows a slightly improved nozzle performance over the Venturi pre-mixer, both with and without pulsations. The difference between the NPI when pulsations are applied shows that the conductance probe signal does not saturate, even at these high conductance levels. Once again, the Venturi is insensitive to

frequency changes at the high frequencies, showing that the transient periods in between pulsations are unimportant.

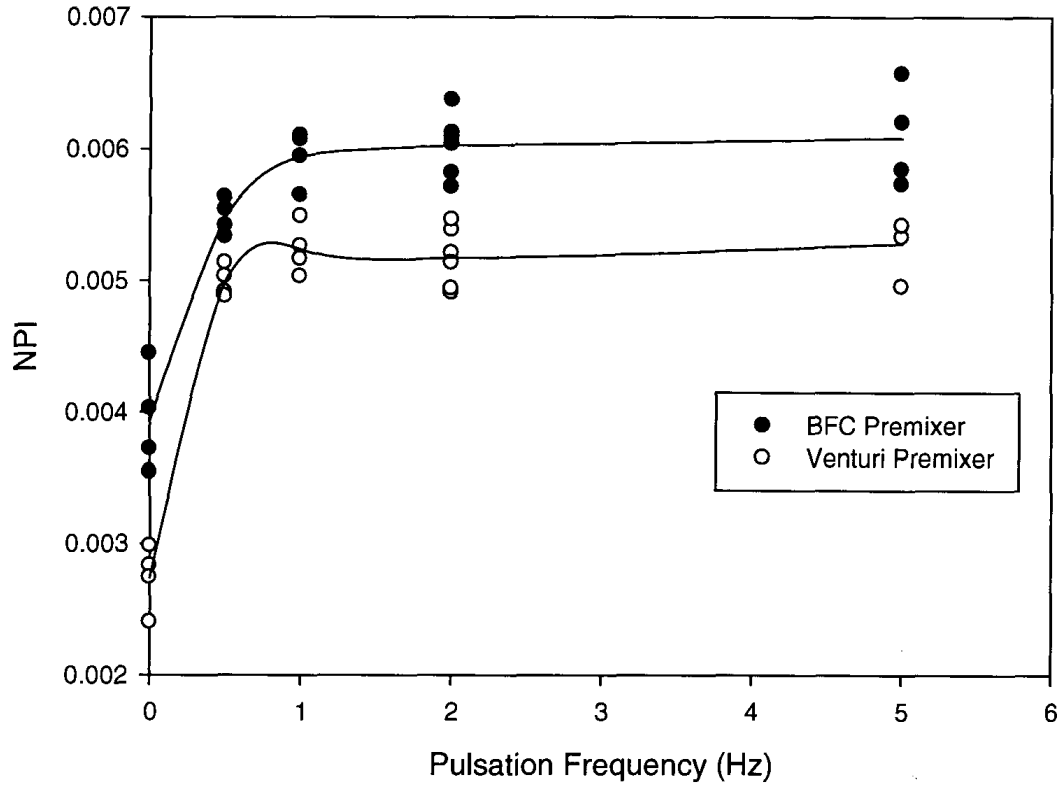

Figure A.19: Comparison of BFC and Venturi Pre-mixers. Type I Nozzle, 12.5 mL dead volume, 0.8% Average (GLR), 2 Hz Pulsation Frequency

There are limitations that prevent the current technique from being used in an industrial setting. However, there are several options on how to implement artificial pulsations in an industrially viable fashion. Technology similar to that used in modern diesel fuel injectors could be used. These techniques include the use of piezo-actuated control valves, in which an applied electrical field causes a material to expand, opening a valve (Suh et al., 2007). It has also been found (Chung et al., 2008) that similar sprays

patterns, if not better spray patterns, can be formed from a piezo-actuated valve as compared to a solenoid-induced control valve. A similar waveform could be applied to the one used in this study, to induce pulsations. This technique would be less prone to breaking than a solenoid valve setup, as there are less delicate parts, such as the spring and solenoid coil.

A.5 Conclusions

Pulsations can be used to dramatically improve the distribution of liquid sprayed in a large-scale fluidized bed unit. The small-scale pulsations experiments were successfully scaled up to a larger scale, showing the industrial viability of applying pulsations, as well as the versatility of this method.

Pulsations frequencies ranging from 1 to 5 Hz are highly beneficial and there is little effect of frequency in this range. Large pulsation amplitudes led to less agglomerate formation and better liquid-solid contact throughout the fluidized bed.

Two types of pre-mixers were tested, and it was found that the effects of pulsations on nozzle performance were similar with both configurations. This helped to demonstrate the versatility of the pulsation technique as a method to improve gas-liquid injections.

Lastly, using analysis of bed samples, it was found that there was a strong correlation between the nozzle performance index used in previous studies and the free moisture content found in the bed, shortly after refluidization. As free moisture is the most beneficial form of liquid within the fluidized bed, this correlation shows that the NPI is a useful tool is determining the quality of liquid spreading throughout the bed solids.

A.6 References

Ariyapadi, S., Holdsworth, D., Norley, C., Berruti, F., & Briens, C. (2003a). Digital X-ray imaging technique to study the horizontal injection of gas-liquid jets into fluidized beds. *International Journal of Chemical Reactor Engineering, 1*(A56)

Ariyapadi, S., Berruti, F., Briens, C., Griffith, P., Hulet, C. (2003b), "Modeling the injection of gas-liquid jets into fluidized beds of fine particles", Can. J. Chem. Eng. **81**, 891.

Ariyapadi, S., Berruti, F., Briens, C., McMillan, J., Zhou, D. (2004), *Horizontal penetration of gas-liquid spray jets in gas-solid fluidized beds*, International Journal of Chemical Reactor Engineering. Volume 2, Article A22.

Base et. al.. (1999). *U.S. Patent No. 6,003,789.* Washington, D.C.: U.S. Patent and Trademark Office.

Bruhns, S. Werther, J. (2005). An Investigation of the Mechanism of Liquid Injection into Fluidized Beds. AIChE Journal Vol. 51, p. 766-775.

Chan, E., Base, T., & McCracken, T. (2001). Design and development of Syncrude coker feed nozzles: A coker 2000 initiative. *Syncrude Canada Technical Report.*

Chung, N. H., Oh, B. G., Sunwoo, M. H. (2008). *Modelling and injection rate estimation of common-rail injectors for direct-injection diesel engines.* Journal of Automobile Engineering, Vol, 222, Part D. p. 1089-1101.

House, P., Saberian, M., Briens, C., Berruti, F., Chan, E. *Injection of a Liquid Spray into a Fluidized Bed: Particle-Liquid Mixing and Impact on Fluid Coker Yields.* Ind. Eng. Chem. Res. 43 (2004) 5663-5669.

Hulet, C., Briens, C., Berruti, F., Chan, E.W., Ariyapadi, S. (2003)., "Entrainment and stability of a horizontal gas-liquid jet in a fluidized bed", Int. J. Chem. Reactor Eng. 1, Article A60

Knapper, B., Gray, M., Chan, E., Mikula, R. (2003). *Measurement of Efficiency of Distribution of Liquid Feed in a Gas-Solid Fluidized Bed Reactor.* International Journal of Chemical Reactor Engineering, Vol. 1.

Lavoie, F., Cartillier, L., Thibert, R. (2002). *New Methods Characterizing Avalanche Behavior to Determine Powder Flow.* Pharmaceutical Research, Vol. 19, No. 6, p. 887-893.

Leclère, K., Briens, C., Gauthier, T., Bayle, J., Guigon, P., Bergougnou, M. (2003). *Experimental study of the vaporization of liquid droplets injected into a gas-solid fluidized bed*, GLS'6, Vancouver, 2003.

Lee, Y., Poynter, R., Podczeck, F., Newton, J. (2000). *Development of Dual Approach to Assess Powder Flow from Avalanching Behavior.* AAPS PharmSciTech, Vol. 1, Issue 3. Article 21.

McDougall, S., Saberian, M., Briens, C., Berruti, F., Chan, E. (2005), *Effect of liquid properties on the agglomerating tendency of a wet gas-solid fluidized bed*, Powder Technology. Volume 149, p. 61-67.

Portoghese, F., House, P., Berruti, F. Briens, C., Adamiak, K., Chan, E. (2008). *Electric conductance method to study the contact of injected liquid with fluidized particles.* AIChE Journal, Vol 54, Issue 7, p 1770-1781.

Song, X., Bi, H., Jim Lim, C. , Grace, J., Chan, E., Knapper, B., McKnight, C. (2004). *Hydrodynamics of the reactor section in fluid cokers*, Powder Technology, **147,** 126-136.

Suh, H. K., Park, S. W., Lee, C. S. (2007). *Effect of piezo-driven injection system on the macroscopic and microscopic atomization characteristics of diesel fuel spray.* Fuel, Vol. 86, p. 2833-2845.

Weber, S., Briens, C., Berruti, F., Chan, E., Gray, M., "Agglomerate stability in fluidized beds of glass beads and silica sand", Powder Technology, Vol. 165, p 115-127, 2006.